FACULTY OF TECHNOLOGY

Geochemical characterization of felsic metavolcanic rocks hosting the Archean Taivaljärvi Ag-Zn-Pb-Au deposit in the Tipasjärvi greenstone belt, eastern Finland

Axel Cima

DEGREE PROGRAMME IN GEOSCIENCES

Master's thesis

May 2019

Supervisors: Eero Hanski, Erkki Kuronen, Tapio Halkoaho

ABSTRACT University of Oulu Faculty of Technology

Degree programme (Master's Thesis) Degree programme in geosciences		Major Subject (Licentiate Thesis)	
Author Cima, Axel		Thesis Supervisors Hanski Eero, Kuronen Erkki, Halkoaho Tapio	
Title of Thesis Geochemical characterization of felsic metavolcanic rocks hosting the Archean Taivaljärvi Ag-Zn-Pb-Au deposit in the Tipasjärvi greenstone belt, eastern Finland.			
Major Subject Geosciences	Type of Thesis Master's thesis	Submission Date May, 2019	Number of Pages 63 p, 2 appendices

The Taivaljärvi Ag-Zn-Pb-Au deposit is located in the Archean Tipasjärvi greenstone belt (TGB) in eastern Finland, which is part of the Tipasjärvi-Kuhmo-Suomussalmi greenstone complex. The deposit is hosted by strongly altered felsic meta-volcanic rocks and has silver as its main commodity.

Geochemical characterization of the host unit of the Taivaljärvi deposit, the Koivumäki Formation, was carried out along the entire TGB. Samples of metavolcanics rocks from different profiles across the TGB were analyzed for whole-rock major and trace element chemistry, including hanging-wall, ore zone and footwall samples from the silver mine. Detailed lithogeochemical exploration techniques were applied in order to identify potential areas for new discoveries in the belt.
Once fertile areas were delineated, they were contrasted with other areas of so far unproven fertility using lithogeochemical data coupled with normative mineral plots, mass-balance calculations, alteration indexes and petrographic observations. Areas of lesser and greater potential for mineralization styles similar as those of the Taivaljärvi deposit were subsequently identified.

There are two main groups of felsic metavolcanic rocks. Those from the mine and the Kivisuo-Talassuo, Lapasuo and South Jäkäläsuo profiles are mainly rhyolites whereas those from the Palovaara, Katajasuo profiles and most of Koraminvaara profiles range from rhyodacites to dacites. All the rocks show a calcalkaline to transitional trend and a trace element signature of a continental arc geological setting.

The main alteration processes are sericitization, chloritization and silicification. Felsic metavolcanic rocks from the mine area are of FII affinities, and show gently sloping REE patterns with La/Yb_N ratios of 5.5-8, moderately high Zr/Y ratios, intermediate HFSE concentrations, and negative Eu anomalies (Eu/Eu* 0.35-0.55). They indicate mass gains in K_2O, SiO_2, MgO and several metals (Ag, Pb, Zn, Au), moderate mass gains in FeO as well as depletion in Na_2O and CaO. The areas that show similar trace element signatures and mass-transfer patterns together with petrographic and geochemical evidence for alteration are Lapasuo and Kivisuo-Talassuo, followed less clearly by Koraminvaara. On the other hand, the Koivumäki, South Jäkäläsuo and Palovaara areas have different characteristics, being less favorable as exploration targets.

Additional Information

Table of contents

1 INTRODUCTION

The Taivaljärvi Ag-Zn-Pb-Au deposit is located in the Archean Tipasjärvi greenstone belt, which is part of the N-S-trending Tipasjärvi-Kuhmo-Suomussalmi (TKS) greenstone complex in eastern Finland. The deposit is hosted by strongly altered felsic metavolcanic rocks and has silver as its main commodity. It is characterized by a low content of sulfide minerals (<5%), disseminated and vein-type ore textures, and well-defined alteration zones (Papunen et al., 1989). Two models have been proposed for the genesis of the Taivaljärvi deposit. Kopperoinen and Tuokko (1988) describe the deposit as a volcanic hosted exhalative (VMS) type, whereas Papunen et al. (1989) and Lindborg et al. (2015) suggested to be a low-sulfidation epithermal deposit. Both models emphasize the role of hydrothermal fluids in the metal enrichment and mineralization processes.

The Nimbus Ag-Zn-(Au) VHSM deposit in the Yilgarn Craton of Western Australia shares many features with the Taivaljärvi deposit, such as a quartz-carbonate-sericite dominated alteration assemblages, the presence of pyrite, sphalerite and galena as well as some Ag-Sb-Pb-Bi sulfosalts in the sulfide mineralization and a similar geotectonic setting. This deposit has been interpreted as a hybrid VHMS-epithermal deposit resulting from low temperature and shallow water conditions (Hollis et al., 2017; Caruso et al., 2018).

Volcanic lithogeochemistry is a powerful tool in the exploration for volcanic-hosted massive sulfide (VHMS) deposits (e.g., Piercey, 2009). Utilization of lithogeochemical data together with mass balance calculations, normative mineral plots, alteration indexes, and geological and geophysical data can allow one to identify which part of the VHMS alteration system one is dealing with.

The purpose of this study was to carry out a geochemical characterization of the host rock unit of the Taivaljärvi Ag-Zn-Pb-Au deposit across several areas of the Tipasjärvi greenstone belt (TGB) in order to identify potential areas for new discoveries in the belt. The study began with an extensive sampling campaign performed during the summer of 2018 as part of Sotkamo Silver's brownfield exploration program.

Alteration observations were made by studying thin sections under polarized optical microscope and calculating normative alteration mineralogy based on whole-rock

geochemical analyses. Trace element analyses and fertility plots for VHMS deposits in rhyolites were applied as well as mass-balance calculations. Samples from different parts of the Taivaljärvi mine were used as a frame of reference for fertile areas. Their compositions were compared with those of samples from other profiles in an attempt to delineate areas of potential new silver ore discoveries.

2 ARCHEAN FELSIC METAVOLCANIC ROCKS HOSTING MASSIVE SULFIDE MINERAL DEPOSITS AND GEOCHEMICAL EXPLORATION TECHNIQUES

The Vihanti-Pyhäsalmi belt contains the most important volcanogenic massive-sulfide (VMS) deposits in Finland. These volcano-sedimentary host rocks belong to a 1.93-1.92 Ga island arc along the northwestern parts of the Raahe-Ladoga shear complex (Mäki et al., 2015). The Taivaljärvi Ag-Zn-Pb-Au deposit in the Tipasjärvi greenstone belt (TGB) is currently the only economic mineralization found in the Archean bedrock in Finland. However, the TGB is highly prospective for Ag-Zn-Pb-Au deposits hosted by acid volcanic rocks, such as represented by the Taivaljärvi deposit (Sotkamo Silver Annual report, 2017). Even though Taivaljärvi is the single deposit of its kind in the Fennoscandian Shield, mining districts with similar geological characteristics are reported in other regions, of which the Abitibi Belt (Fig. 1) in the Superior Province of the Canadian Shield is probably the best known and studied one (Gaboury and Pearson, 2008). Volcanogenic massive sulfide deposits in the Abitibi subprovince are preferentially associated with volcanic successions containing >150 m thicknesses of felsic metavolcanic rocks (almost 50% of the area of volcanic terranes) (Barrie et al., 1993).

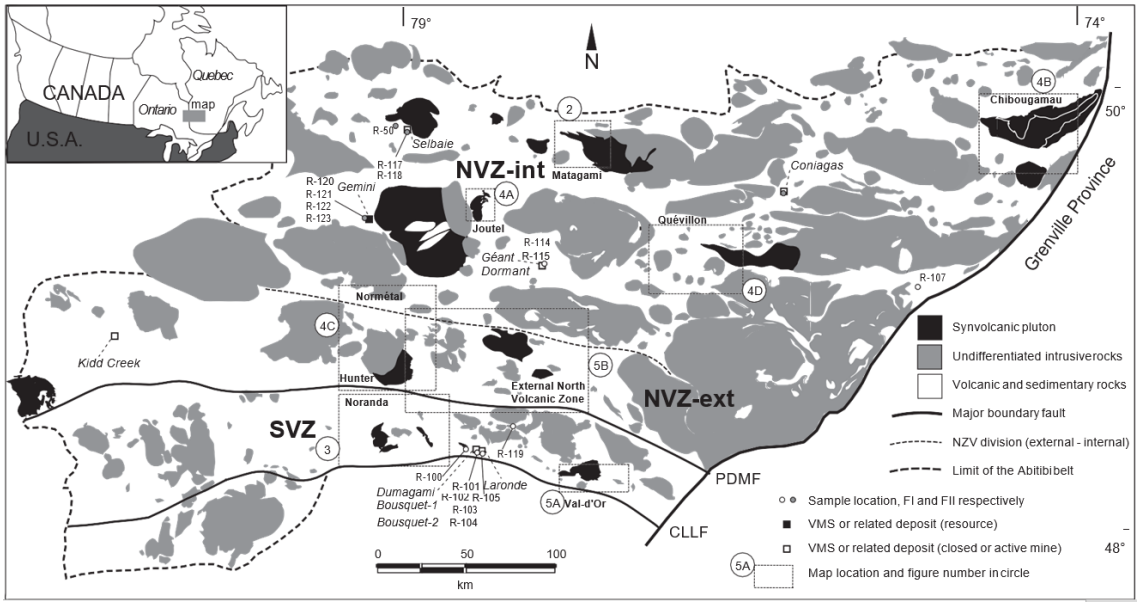

Figure 1. Simplified geologic map of the Abitibi belt, showing the locations of VMS and volcanogenic deposits after Gaboury (2006). Major subdivisions are the Southern Volcanic zone (SVZ), the external North Volcanic zone (NVZ-ext), and internal North Volcanic zone (NVZ-int). Major faults are the Porcupine-Destor-Manneville fault (PDMF) and the Cadillac-Larder Lake fault (CLLF). Published with permission of Taylor & Francis.

Lesher et al. (1986) characterized the felsic units of the Abitibi Belt in four categories and later Hart et al. (2004) added one more category based on REE, HFSE, LILE and Eu/Eu* compositions. (Table 1). FI category includes dacites and rhyodacites characterized by steep REE patterns with weakly negative to moderately positive Eu anomalies, high Zr/Y, low abundances of HFSE and high abundances of Sr. Currently there have not been any base-metal sulfide deposits discoveries in rocks of this category. Examples of this category can be found in the Bowman Subgroup and Skear Group in the Abitibi Belt, in the Kakagi Lake, Lake of the Woods, Shoal Lake, and Sturgeon Lake areas of the Wabigoon Belt and in the Confederation Lake area of the Uchi Belt.

Category FII felsic metavolcanic rocks are rhyodacites and rhyolites characterized by gently sloping REE patterns with variable Eu anomalies, moderate Zr/Y, and intermediate abundances of HFSE elements and Sr. The best examples of this category are known to occur in the Misema Subgroup of the Abitibi Belt, in the Wabigoon Lake and Sturgeon Lake areas in the Abitibi Belt. Of these, the Sturgeon Lake area hosts base-metal sulfide deposits, and its felsic metavolcanic rocks exhibit the most pronounced negative Eu anomalies of this group (Campbell et al., 1981). Although considered less prospective, some districts dominated by FII rhyolites account for about 70% of rhyolites in the Abitibi belt, with important mines such as Horne, Kidd Creek and Laronde in Val d'Or and Selbaie mining districts (Barrie et al., 1993; Gaboury, 2008). Non-Archean examples of this category are seen in Kuroko (LaPierre et al., 1985; Ohmoto, 1996), Rio Tinto (Mitjavila et al., 1997), Bathurst (Lentz, 1996) and Boliden (Weihed et al., 1996).

Felsic metavolcanic rocks of the FIII category, which comprise rhyolites and high-silica rhyolites of the FIII category, have turned out to be the most prospectable among felsic metavolcanic rocks in Abitibi Belt (e.g., Selbaie), showing relatively flat REE patterns with two subcategories: FIIIa exhibits variable negative Eu anomalies, low Zr/Y, and intermediate abundances of HFSE (Hart et al., 2004). The Doyon-Bousquet-Laronde mining camp in Noranda exhibits one of the best examples of this category (Wright-Holfeld et al., 2011). The late Precambrian Parys Mountain deposit also fits with this category (Barrett et al., 2001). Category FIIIb rhyolites exhibit pronounced negative Eu anomalies, low Zr/Y, and high abundances of HFSE. These rocks are not restricted to the Archean although many of the large-tonnage and high grade VMS deposits, such as Kidd Creek, can

be found in the Archean (Prior et al., 1999).

As previously mentioned, Hart et al. (2004) refined Lesher et al. (1986) classification and added the FIV category, which comprises rhyolites and high silica rhyolites characterized by flat to slightly LREE-depleted REE patterns and low REE and HFSE abundances. A good example of this category is found in the Paleoproterozoic Flin Flon deposit (Syme, 1998).

Table 1: Geochemical classification of felsic volcanic rocks as an exploration guide defined by Lesher et al. (1986) and modified by Hart et al. (2004). Also shown are Archean and Paleoproterozoic examples.

Category	FI	FII	FIIIa	FIIIb	FIV
Lithology	Dacite-rhyolite	Dacite-rhyolite	Rhyodacite-high silica rhyolite	Rhyodacite-high silica rhyolite	Rhyolite-high silica rhyolite
$[La/Yb]_N$	5.8-34	1.7-8.8	1.5-3.5	1.1-4.9	0.22-2.1
REE Pattern	Steep	Gently sloping	Relatively flat	Relatively flat	Flat to LREE depleted
Zr/Y	High	Moderate	Low	Low	Very low
Eu/Eu*	Weakly negative to moderately positive	Variable	Variable negative	Pronounced negative	Variable negative
HFSE and Sr	Low HFSE, high Sr	Intermediate	Intermediate	High	Low
Archean examples		Sturgeon Lake, Batthurst, Val d'Or, Selbaie, Taivaljärvi	Noranda	Kidd Creek	Flin Flon (Paleoproterozoic)

Barrie et al. (1993) identified three subgroups related to their geochemical signatures in felsic metavolcanic rocks from the Abitibi Belt. Group I is host to more than 50% of the VMS deposits by total ore tonnage and only represents 10% of the area of volcanic terranes. This group comprises MORB-like tholeiitic basalts, incompatible element-enriched basaltic andesites and geochemically distinctive high-silica rhyolites, with the latter representing the most prospective exploration target. Group II is host to one-third of the volcanogenic massive sulfide deposits by tonnage, and also comprises around 10% of the area of volcanic terranes. It is characterized by bimodal, transitional, tholeiitic to calc-

alkalic volcanic rocks. Group III is host to only one known deposit, Selbaie, which is atypical of volcanogenic massive sulfide deposits in that most of its mineralization is not stratiform. The associated volcanic sequence consists of calc-alkalic volcanic rocks of intermediate to felsic composition. Moreover, the Abitibi Belt komatiite-hosted Ni-Cu-PGE deposits are found exclusively in LILE- and LREE-depleted peridotitic komatiites with no signs of continental crustal contamination (Barrie et al., 1993).

Australian examples of fertile felsic metavolcanic rocks are also found in the Panorama District of the Pilbara Craton, where some of the oldest Archean rocks are found, hosting Zn-Cu deposits with similar alteration styles, tonnages and grades (Brauhart et al., 2001). These authors focused on mass balance calculations, getting similar results to those from the Abitibi Belt in terms of mass transfer of K, Mg and Fe (Larson and Hutchinson, 1993), shown later in this work.

With certain limitations, the classification of Lesher et al. (1986) and Hart et al. (2004), which is based on the geochemistry of felsic metavolcanic rocks, has been used in the Superior Province as a guide to identify prospective horizons for massive base metal sulfide mineralization and it was also tried to be implemented in this study for the Tipasjärvi area.

3 GEOLOGICAL SETTING

3.1 The Tipasjärvi-Kuhmo-Suomussalmi greenstone complex

The Archean Tipasjärvi-Kuhmo-Suomussalmi (TKS) greenstone complex is located in eastern Finland and forms an elongated, N-S-trending complex with a length of about 200 km and width of 3-5 km (Fig. 2). The three greenstone belts that form the STK complex display similar rock associations and stratigraphy, suggesting that they originally belonged to the same volcanic complex. This complex is surrounded by heterogeneous variation of Archean granitoids, varying from stromatitic to nebulitic migmatitic gneisses to discrete felsic plutons from tonalite to trondhjemite and monzogranite in composition (Sorjonen-Ward and Luukkonen, 2005).

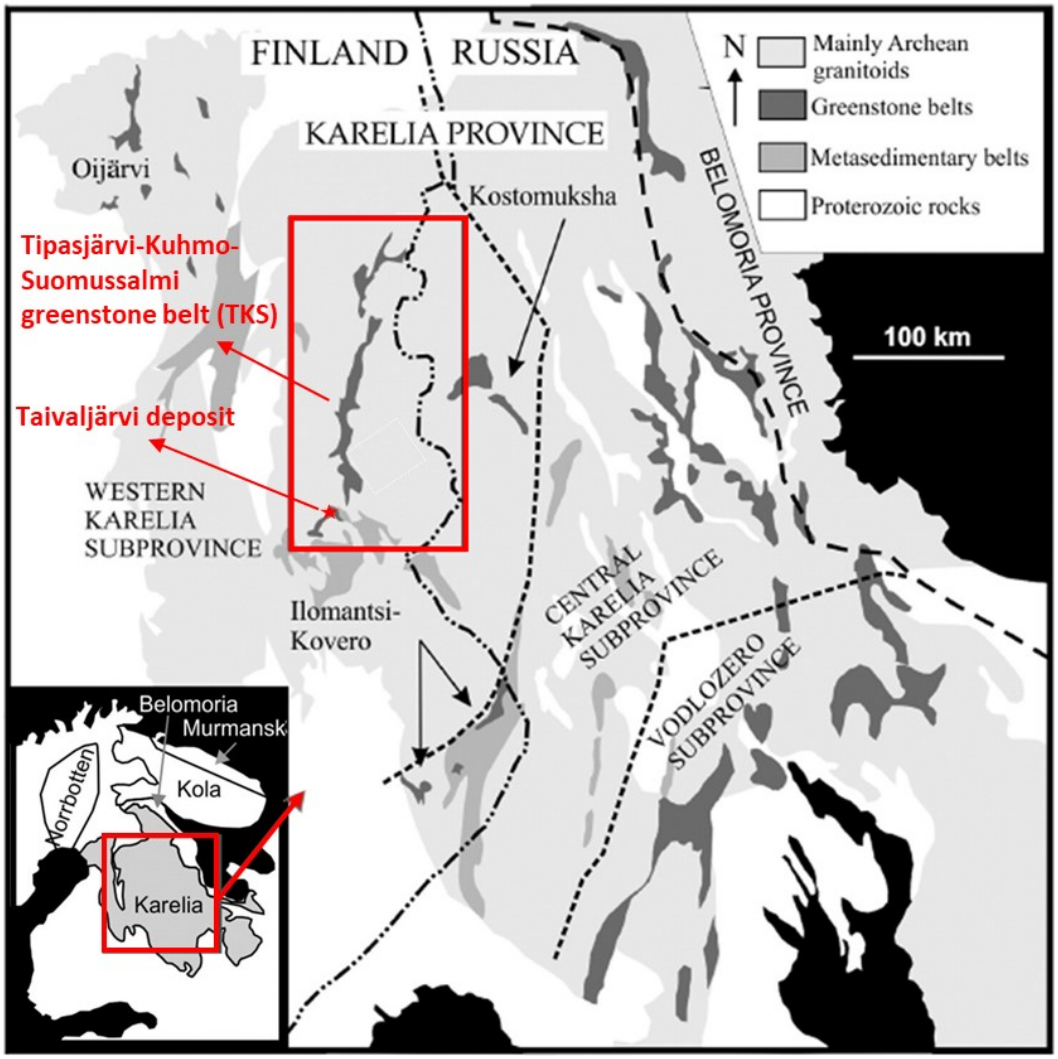

Figure 2. Location map of the Tipasjärvi-Suomussalmi-Kuhmo (TKS) greenstone complex, (modified after Lehtonen, 2016).

Several stratigraphic interpretations have been suggested for the STK complex (Taipale, 1983; Piirainen, 1988; Papunen et al., 2009; Huhma et al., 2012; Lehtonen, 2016). 80% of the STK complex is composed of mafic, ultramafic and felsic volcanic rocks. The last 20% include metasediments, such as mica gneisses, banded iron formations, black schists, and mafic to ultramafic intrusions (Fig. 3).

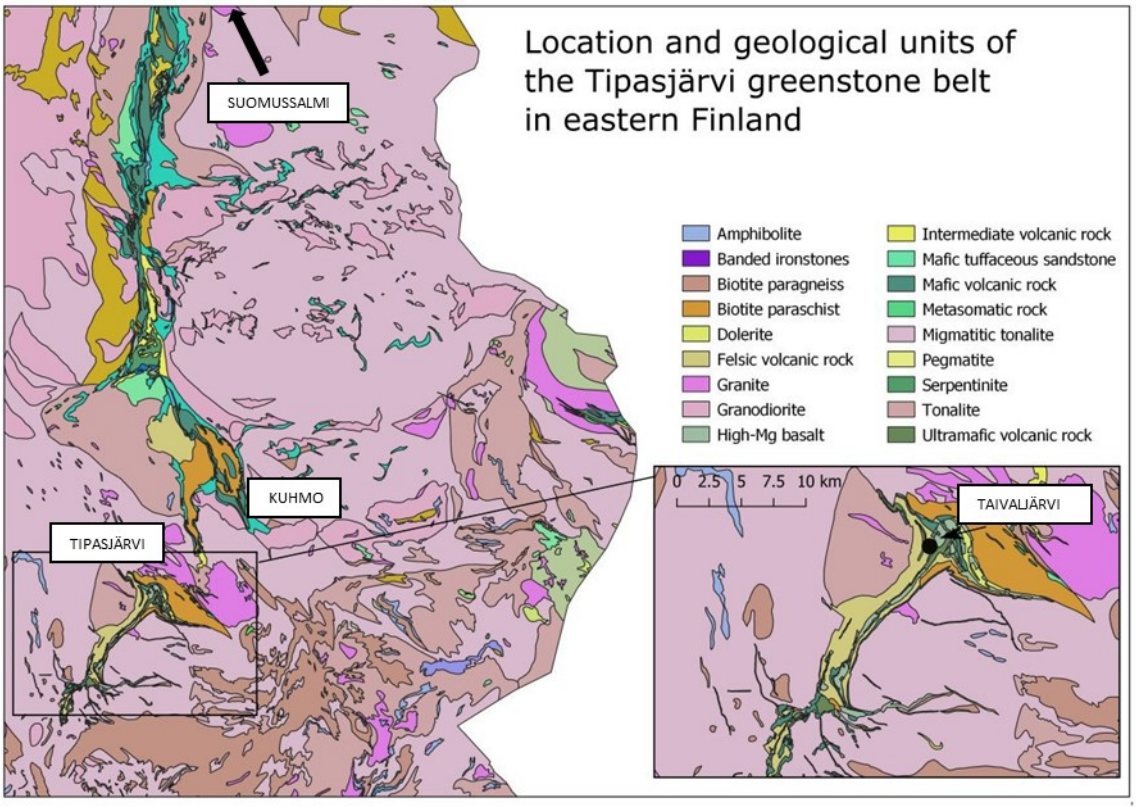

Figure 3. Location and main geological units of the Tipasjärvi greenstone belt in eastern Finland. (modified after the DigiKP version 2.1. Digital map database for bedrock geology of Finland [electronic resource], Geological Survey of Finland; referred on 10.11.2018 and after Ikäheimo, 2018).

Luukkonen (1991) stated that the STK greenstone complex represents a northerly trending synclinorium with oldest units at the margins and younging directions pointing to the center. The complex went through several metamorphic and deformation phases, of which the youngest deformation phase has been dated at Paleoproterozoic (Huhma et al., 2012). Luukkonen (1988) subdivided the deformation of the complex into six phases (D_{1-6}) of which D3 is the main deformation stage of the greenstone belt; and phases D_{1-2} are not visible inside the greenstone belts. Regional metamorphism peaked during D_3. The presence of Al

saturated silicate mineral assemblages (kyanite, sillimanite) and staurolite, cordierite and (Mn-rich) garnet indicates metamorphic P-T conditions of medium- to high amphibolite facies (Kopperoinen and Tuokko, 1988).

Granodiorite-granite and tonalite-trondhjemite-granodiorite (TTG) associations surround the STK belt and were previously thought to work as a basement for the greenstone belts (Papunen et al., 2009). However, it has been observed that granitoids in the vicinity of the greenstone belt cut volcanic rocks and suggest a possible role of these intrusions in the deformation of the belt (Pietikäinen et al., 2008). Geochronological studies (e.g., Huhma et al., 2012), have also confirmed that most of the granitoids surrounding the belt are younger than the greenstone belt. In the latest geochronological study, Lehtonen (2016) concluded that the felsic and intermediate volcanic rocks in the STK complex can be divided into four age groups: 2.94 Ga, 2.84 Ga, 2.82 Ga, and 2.80-2.79 Ga, with the oldest phase (ca. 2.94 Ga) being restricted in the Suomussalmi greenstone belt and the youngest (2.80-2.79 Ga) in the Tipasjärvi and Kuhmo greenstone belts.

The commonly observed pillow structures and the Zr/Nb and Nb/Th ratios in komatiitic rocks suggest that the Tipasjärvi and Kuhmo greenstone belts were erupted in an oceanic plateau setting (Maier et al., 2013). Some authors have also suggested continental rift setting (Luukkonen, 1991; Papunen et al., 2009). Lehtonen (2016) concluded that the most probable setting for the formation of the volcanic rocks with ages of ca. 2.84-2.79 Ga was a intra-continental rift environment or setting with continental and oceanic lithosphere. Older, >2.94 Ga magmatic rocks were formed in a yet unknown tectonic environment, representing an older continent. The preserved primary volcanic textures of these rocks indicate shallow water or subaerial conditions of deposition (Papunen et al., 2009).

3.2 The Tipasjärvi greenstone belt

The Tipasjärvi greenstone belt forms a southern part of the Tipasjärvi-Kuhmo-Suomussalmi greenstone complex (Figs. 1, 2). The stratigraphy of the Tipasjärvi greenstone belt has been divided by different authors (Papunen et al., 2009, Huhma et al., 2012, Lindborg et al., 2015, and Lehtonen, 2016) into five lithological units (Fig. 4). The lowermost unit, named the Koivumäki Formation (2.80 Ga), is mostly composed of felsic- and intermediate volcanic rocks. It is overlain by the Vuoriniemi Formation, whose composition is more heterogeneous, varying from dacitic and tholeiitic metatuffs to BIF,

mafic metalavas and black schists. Komatiitic lavas from the Kallio Formation, overlie the Vuoriniemi Formation.

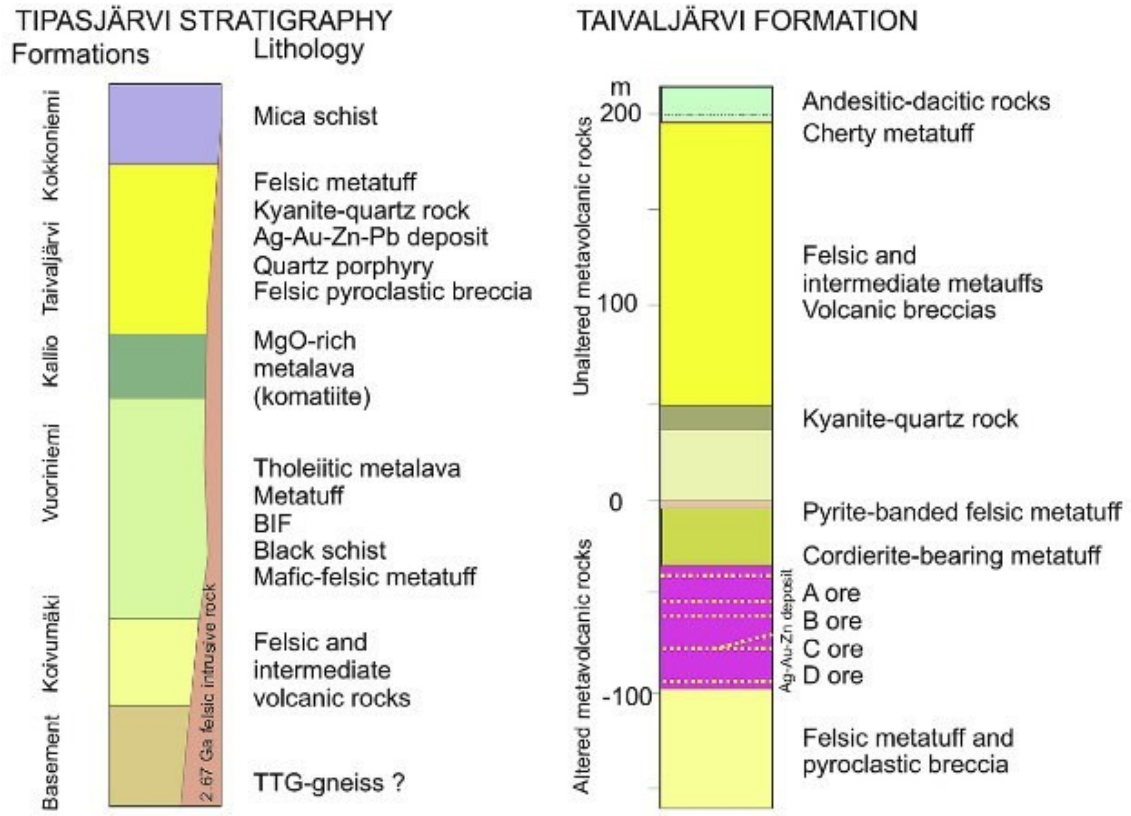

Figure 4. Stratigraphical cross-section of the supracrustal formations in the Tipasjärvi area. (Lindborg et al., 2015). Published with permission of Elsevier.

The Taivaljärvi Formation is composed commonly by quartz porphyries, volcanic breccias, tuffites and felsic tuffs (Lindborg et al., 2015), indicating a shallow-water to subaerial environment of formation (Taipale, 1983). Huhma et al. (2012), placed it on top of the Kallio Formation using radiometric ages (TIMS, U-Pb from zircons). Upper contact of the Taivaljärvi Formation is tectonic and intensive isoclinal folding and overthrusting have brought the older units into the upper contact of the succession (Lindborg et al., 2015). The youngest unit, the Kokkoniemi Formation, is composed of mica schists, which are thought to represent weathering products of the older volcanic rocks. The maximum age of deposition of the Kokkoniemi Formation was determined by Huhma et al. (2012) from the Aarreniemi greywacke (2.75 Ga).

In one of the most recent chronological studies carried by Lehtonen and Käpyaho (2016), new U-Pb helped to reinterpret the evolution of the Archaean TGB. Felsic-intermediate

metavolcanics rocks of at least three different age groups were obtained: 2.84 Ga, 2.82 Ga, and 2.80 Ga. These rocks fall into three units which the author calls the Talassuo unit, the Hietajärvi unit, and the Koivumäki unit respectively. Volcanism in the TGB partly coevaled with the volcanism in the Kuhmo and Suomussalmi greenstone belts. The metavolcanics rocks of ca. 2.84 Ga of the Talassuo unit formed contemporaneously with the oldest volcanic rocks in the Kuhmo greenstone belt. The Hietajärvi dacite with an age of ca. 2.82 Ga formed contemporaneously with the youngest volcanic rocks in the Suomussalmi greenstone belt and agrees with some zircon ages from the Kuhmo greenstone belt (Lehtonen and Käpyaho, 2016).

3.3 Mineral deposits and targets in the Tipasjärvi greenstone belt

The Taivaljärvi Ag-Zn-Pb-Au deposit is currently the only economic mineralization found in the Tipasjärvi greenstone belt. However, the TGB is highly prospective for finding new Ag-Zn-Pb-Au deposits hosted by acid volcanic rocks. (Papunen and Parkkinen, 2011). An area of over 400 km^2 has been covered with low-altitude airborne geophysical survey flown by the Geological Survey of Finland at 100 meters' line spacing which allowed to identify some other anomalies along the Koivumäki Formation as later on discussed. The gold and nickel potential seem to be distinctly weaker than in the Kuhmo- and Suomussalmi greenstone belts, generally because of the large volume of felsic rocks in spite of the showings found (Pietikäinen et al., 2008).

Geological Survey of Finland (GTK) conducted a research program in the Tipasjärvi belt in 2005-2007, indicating that there are several promising exploration targets throughout the belt (Pietikäinen et al., 2008). The work included bedrock mapping, soil sampling and core drilling (more than 9 km.). The western part of the belt has been (to some extent) prospected for Taivaljärvi-type deposits but, for the time being, without notable discoveries. Geophysical surveys indicate that the most promising targets seem to be the Kokkokorpi Au-As indications and a zinc-bearing zone in the eastern part of the Tipasjärvi greenstone belt (Pietikäinen et al., 2008). Kyanite quartzites of the area have been investigated for potential industrial mineral deposits (Kopperoinen and Tuokko, 1988, Tuokko and Kopperoinen, 1989). Pyrite and BIF deposits of the belt have been prospected over the years (Papunen et al., 1989). These units have also been used as marker horizons in the stratigraphy between the volcanic units of the area (Kopperoinen and Tuokko, 1988).

Interesting geophysical anomalies have been detected in a study carried out by Leväniemi (2018) as part of an internal report for Sotkamo Silver Oy, from which some of the targets were selected and assessed geochemically for this research project, specifically in the Lapasuo and Kivisuo-Talassuo areas.

3.4 The Taivaljärvi Ag-Zn-Pb-Au deposit

3.4.1 General features

The Taivaljärvi Ag-Zn-Pb-Au deposit is located in the central part of the Tipasjärvi greenstone belt (Fig. 3). The ore deposit is hosted by felsic volcanic rocks in the upper part of the Koivumäki Formation. The orebody crops out at the surface in an area having an average size of 40x400 m. The orebody has a lens-shaped structure. It dips 65° to southeast, plunges 60° to south-southwest and extends at least to a depth of 600 m (Papunen et al., 1989), though geophysical "Sampo" surveys indicate that the mineralized zone may even go down to a depth of 2 km (Lindborg et al., 2015). As part of the Koivumäki Formation, the Taivaljärvi deposit has been interpreted to belong to an isoclinally folded antiform structure, lying in the eastern flank of the antiform. With a cut-off grade 30 g/t Ag, the current resource estimate amounts to what shown in table 2, with 19.3 Moz. Of Ag.

Table 2: Measured, indicated and inferred resource estimates in the Taivaljärvi ore deposit with a cut-off grade of 30 g/t Ag (Sotkamo Silver, Annual report, 2017).

Resource category	Tonnage (ktn)	Ag (g/tn)	Au (g/tn)	Pb (%)	Zn (%)
Measured	2968	88	0.25	0.31	0.66
Indicated	3656	79	0.23	0.29	0.62
M+I	6624	83	0.24	0.3	0.64
Inferred	4298	61	0.17	0.20	0.47

Ore processing is conducted through a conventional flotation circuit on site (Paholski et al., 2017). Three concentrates (Ag-Au-Pb, Zn-Ag and S) are produced.

3.4.2 Geology of the ore deposit

Footwall rocks

The footwall of the deposit is composed of a weakly mineralized, 150-m-thick zone of felsic volcanic rock. The ore zones fade out gradually to the west of the deposit to a homogenous felsic porphyry (Lindborg et al., 2015). The main minerals are quartz, sericite, carbonates, and biotite with thin bands of garnet and tremolite. Ankerite occurs together with sulfides in lesser amounts (1-2%). Chlorite, epidote, cordierite, and rutile can be found as accessory minerals. The texture of the rock is porphyritic, and the foliation varies intensively (Papunen et al., 1989).

Hanging-wall rocks

In the hanging wall, the contact between the wall rock and ore is sharp (Papunen et al., 1989). Light porphyritic quartz-sericite rock overlies the contact, and carbonate minerals, which are very typical in the ore zone, are lacking. Lapilli tuff and agglomerate fragments can be seen partially as well as bands of iron sulfides. The termination of the ore zones is indicated by the presence of pinitized cordierite and abundant pyrite (Papunen et al., 1989).

Ore zones

There are several semi-attached ore zones in the Taivaljärvi ore deposit. Four ore zones have been distinguished based on the differences in base and precious metal ratios (Papunen et al., 1989). They are almost aligned with the primary stratigraphic layering (Papunen et al., 2009). Ore zones show similar gangue and ore mineral associations, but their amounts vary. They are not clearly defined as the adjacent zones have no strict borders. Interlayers often contain weak dissemination of ore minerals. The mineralized zones were named by Papunen et al. (1989) as D, C, B and A in the order from the footwall upwards (Fig. 5). The A and B zones are the main mineable units due to their highest valuable metal concentrations.

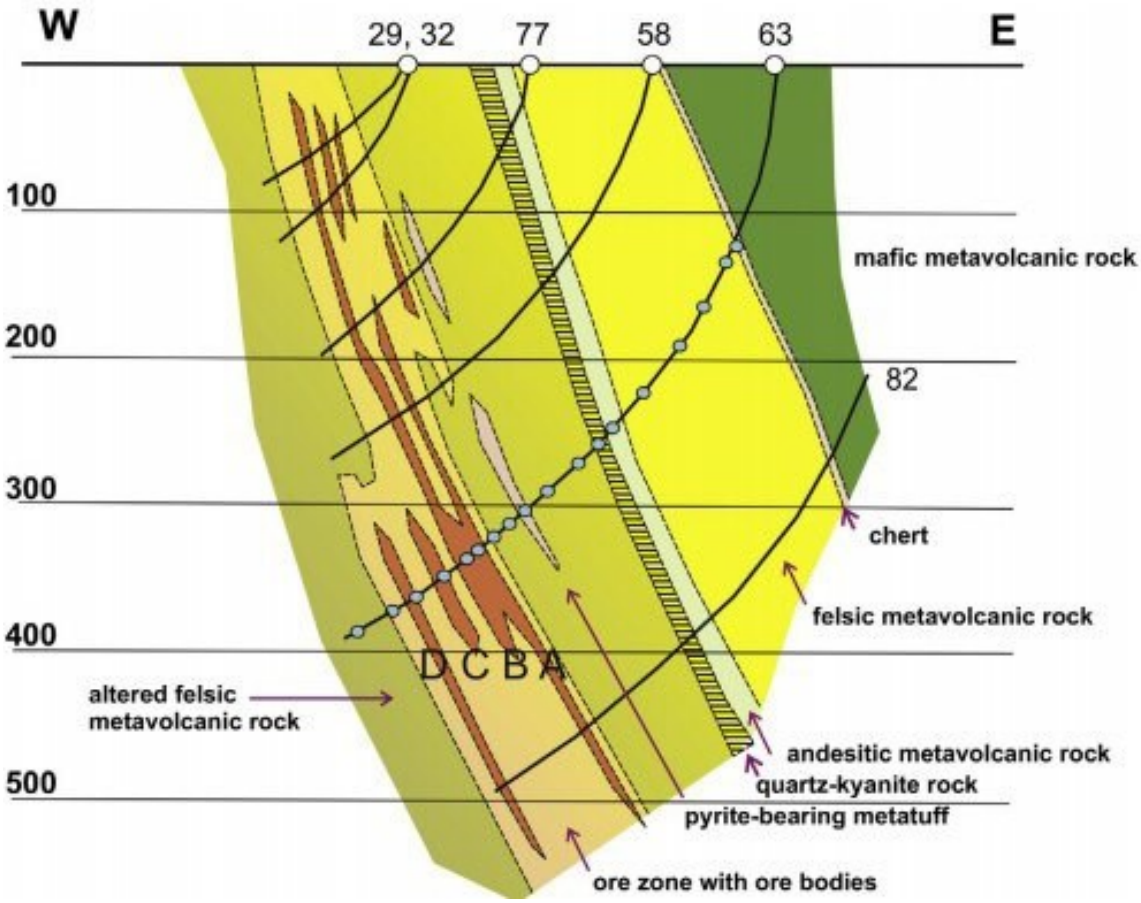

Figure 5. Ore layers and surrounding host rock units after Papunen and Parkkinen (2011). Blue dots in 63 represent old samples taken for that study.

Three terms for the ore types have been used in the previous studies: Ag ore, Ag-Zn-Pb ore, and low-grade footwall mineralization. These types are not restricted to a particular ore zone, and especially the Ag ore and Ag-Zn-Pb ore are mixed within the other zones. In all ore zones A-D, the host rock is quartz-sericite schist with varying amounts of garnet and biotite, with their amount decreasing when approaching the hanging wall. The ore zones are characterized by abundant quartz-carbonate veins. Carbonates have mostly been classified as manganoankerites (3-6 wt% MnO) which together with a MnO enrichment in garnet is a common feature in this kind of deposits (Barrie et al., 1993). The FeO content of manganoankerite is dependent on the zone, increasing from zone A towards the footwall (Papunen et al., 1989). Accessory minerals are chlorite, tourmaline, rutile, barite, epidote, and tremolite (Lindborg et al., 2015).

Ore zone A is the closest one to the hanging wall sequence. Its thickness varies from 4 to even 15 meters. It is discontinuous and has a break at a depth from 150 to 200 meters. The

orebody of this zone is hosted by quartz-sericite schist and has high Ag and modest Zn and Pb values. The zone is characterized by a large number of quartz-ankerite veins.

Ore zone B is 4-8 meters (locally 16 m) in thickness and has a small break at depths between 50-100 m, after which it continues to a depth of 500 meters. The host rock is banded quartz-sericite schist with plentiful quartz-carbonate veins, even 20-30% of the rock volume. Zone C is about 5 meters thick and its ore consists mostly of thin bands of sulfides. The lowermost ore zone D is less than 5 meters thick and characterized by calc-silicate bands and abundant sulfide minerals (Papunen et al. 1989).

Silver occurs mainly as freibergite, dyscrasite, pyrargyrite, native silver, electrum and silver-rich galena. Other Ag-bearing phases such as acanthite, miargyrite, freieslebenite, bournonite are also present in the deposit. The grain size of the Ag-bearing minerals varies from 0.01 to 0.1mm. Galena and the associated Ag minerals are more abundant in the stratigraphically uppermost ore zones, where they occur in quartz-carbonate veins and bands. Silver mineralogy stays basically constant in the whole deposit: over 95% of silver is in sulphides and antimonides, but in silver-rich parts of the ore galena contains ca 0.1% silver and also native silver and silver-gold alloys occur (Lindborg et al., 2015).

Ikäheimo (2018) studied the distribution and characteristics of the gold-bearing phases and observed that they occur in three different vein types: 1) clear quartz veins in fractures created by brittle deformation, associated with galena and native silver, 2) quartz-carbonate veins as heterogeneous grain agglomerations with Ag-minerals and sulfides, and 3) in carbonate vein as small grains of fine dust in carbonate, associated with Ag-minerals and sulfides. The author also found rare Au-bearing silver antimonides such as Au-dyscrasite and Au-allargentum.

4 SAMPLING AND METHODS

4.1 Sampling campaign

A total of 65 samples were selected from 8 profiles across the Tipasjärvi greenstone belt during the summer of 2018 (Fig. 6). These samples were taken from the same stratigraphic unit, the Koivumäki Formation, that hosts the Taivaljärvi deposit.

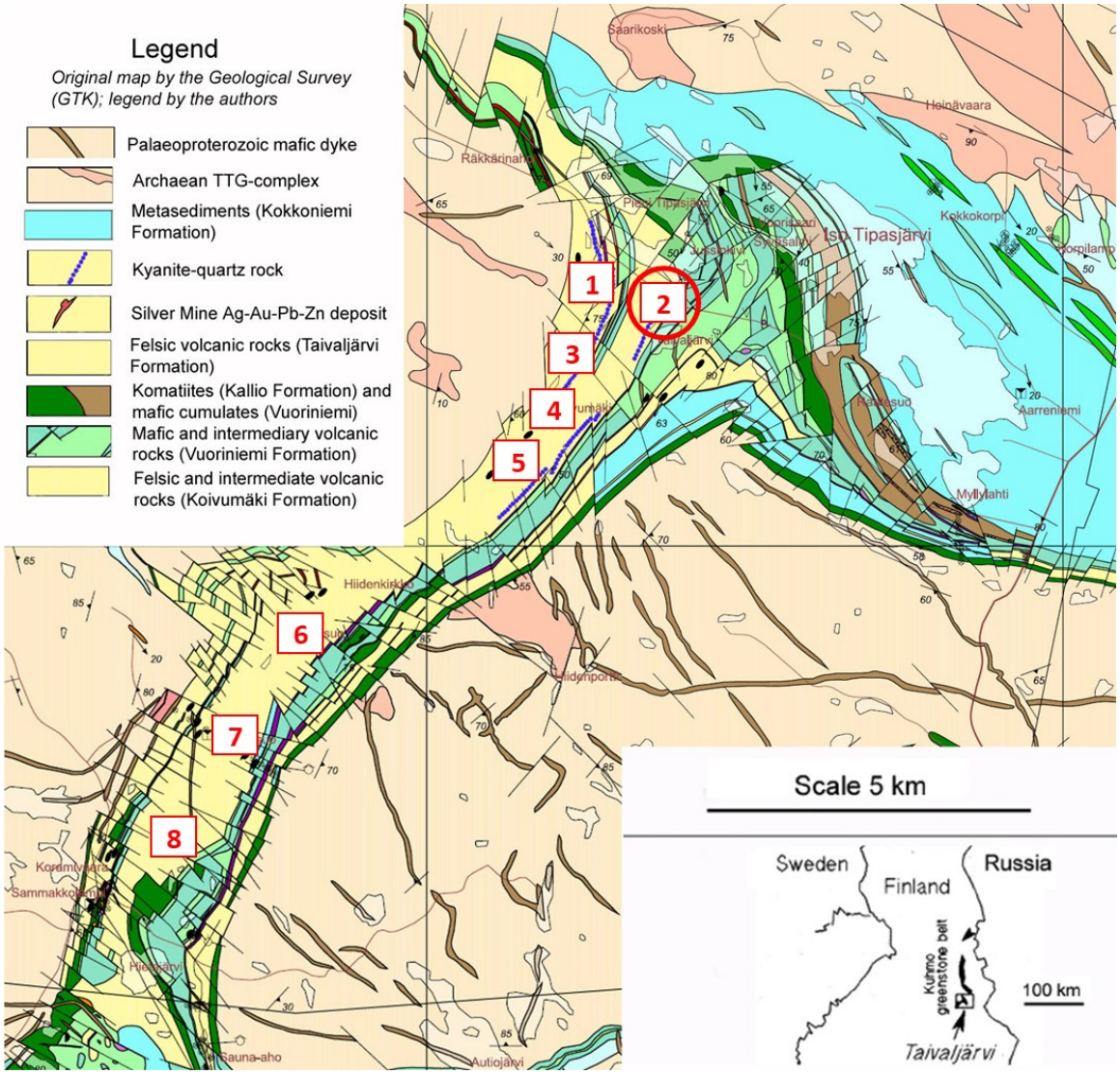

Figure 6. Geological map of the Tipasjärvi greenstone belt after Pietikäinen et al. (2008), as modified by Lindborg et al. (2015) with the location of the main areas of this study added. 1: Koraminvaara. 2: Taivaljärvi Mine. 3: South Jäkäläsuo. 4: Koivumäki. 5: Katajasuo. 6: Kivisuo-Talassuo. 7: Lapasuo. 8: Palovaara. Published with permission of Elsevier.

A considerable number of samples had to be taken with a mini-drill (Fig. 7a) since outcrops were usually polished as a consequence of glaciogenic processes (Figs. 7b, c), resulting in mini-drill core samples (Fig. 7d).

Figure 7. A: Minidrill and hammer used in sampling. B: Polished felsic metavolcanic rock outcropping in the Katajasuo profile. C: Polished outcrop with quartz veins at Koraminvaara. D: Sample from outcrop shown in figure 7c.

Representative samples (Table 3) from the hanging wall (AC-63), mineralized zone (AC-64) and foot wall (AC-65) were selected from core samples of one of the drill holes made by Sotkamo Silver Oy as part of a previous resource delineation campaign (Fig. 8).

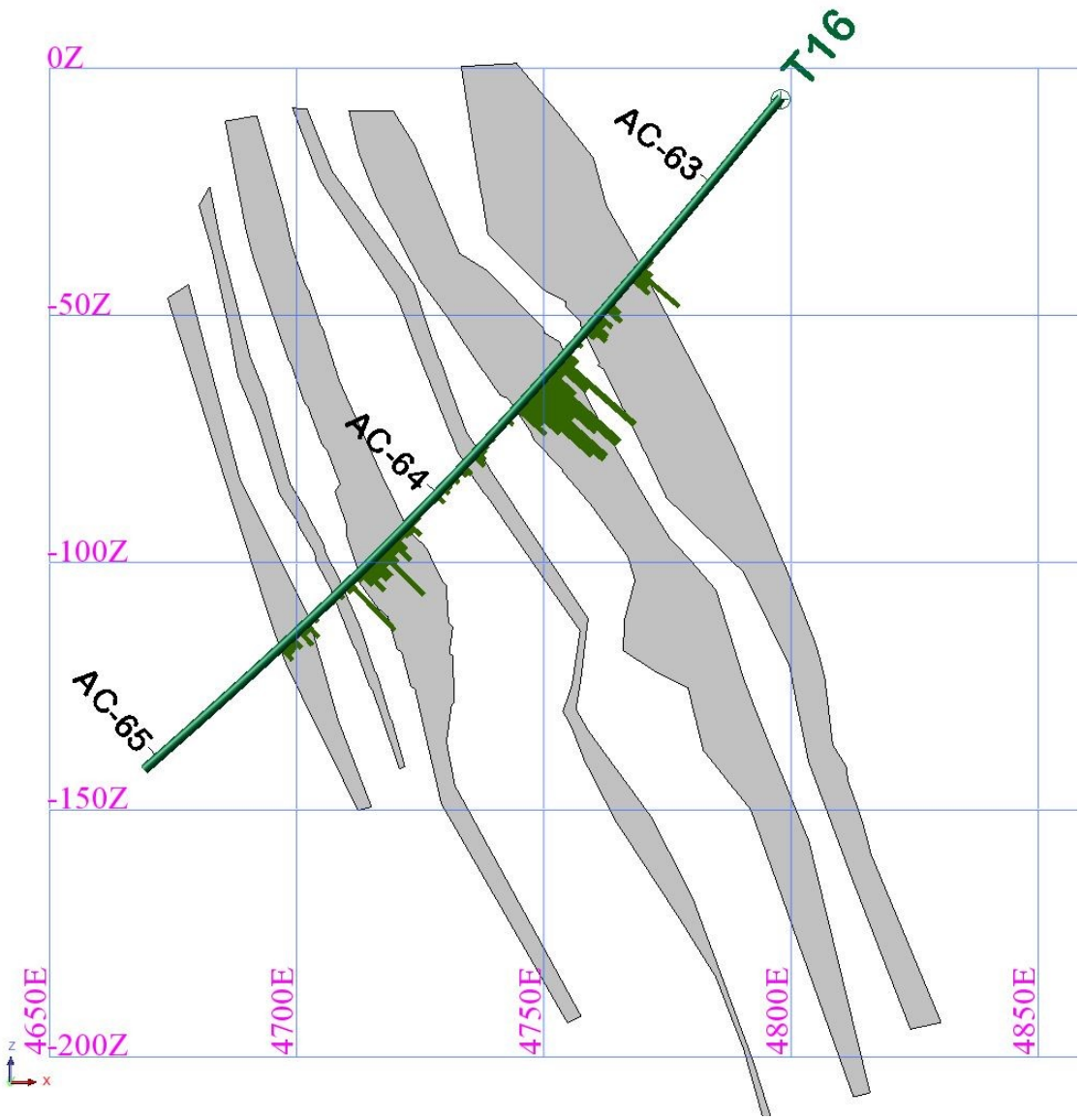

Figure 8. Drill hole T-16 showing the locations of the samples taken from the mine. AC-63: Hangingwall, AC-64: Mineralization zone. AC-65: Footwall.

Petrographic studies were made after selecting 19 of the samples. Thin sections were made at the Lapin AMK facilities in Kemi, Finland and subsequently photographed and studied under polarized optical microscope (Zeiss Axioplan 2) in Oulu Mining School, both under transmitted and reflected light. Observations were focused on alteration and textural features of the selected samples along the belt.

Table 3: Samples selected for whole-rock geochemical analyses and petrographic studies.

Analysis	Thin Section	Area	Analysis	Thin Section	Area	Analysis	Thin Section
AC-1		Kivisuo-Talassuo	AC-23		Lapasuo	AC-45	
AC-2	TSAC-1	Kivisuo-Talassuo	AC-24		Lapasuo	AC-46	
AC-3		Kivisuo-Talassuo	AC-25		Lapasuo	AC-47	TSAC-13
AC-4	TSAC-2	Kivisuo-Talassuo	AC-26		Lapasuo	AC-48	
AC-5		Kivisuo-Talassuo	AC-27		Palovaara	AC-49	
AC-6		Kivisuo-Talassuo	AC-28	TSAC-7	Palovaara	AC-50	
AC-7		Kivisuo-Talassuo	AC-29		Palovaara	AC-51	TSAC-14
AC-8		Kivisuo-Talassuo	AC-30		Palovaara	AC-52	
AC-9	TSAC-3	Kivisuo-Talassuo	AC-31		Palovaara	AC-53	
AC-10		Kivisuo-Talassuo	AC-32		Palovaara	AC-54	
AC-11		Kivisuo-Talassuo	AC-33	TSAC-8	Palovaara	AC-55	
AC-12		Kivisuo-Talassuo	AC-34		Palovaara	AC-56	
AC-13	TSAC-4	Kivisuo-Talassuo	AC-35		Palovaara	AC-57	TSAC-15
AC-14		Kivisuo-Talassuo	AC-36	TSAC-9	Katajasuo	AC-58	
AC-15		Kivisuo-Talassuo	AC-37	TSAC-10	Katajasuo	AC-59	TSAC-16
AC-16		Kivisuo-Talassuo	AC-38		Koraminvaara	AC-60	TSAC-17
AC-17		Lapasuo	AC-39		Koivumäki	AC-61	TSAC-18
AC-18		Lapasuo	AC-40	TSAC-11	Katajasuo	AC-62	TSAC-19
AC-19		Lapasuo	AC-41		Mine (hangingwall)	AC-63	
AC-20	TSAC-5	Lapasuo	AC-42		Mine (minerlization)	AC-64	
AC-21	TSAC-6	Lapasuo	AC-43	TSAC-12	Mine (footwall)	AC-65	

4.2 Analytical methods

4.2.1 Whole-rock analyses

All samples, weighing between 100 and 250 g, were pre-processed at the CRS Laboratories Oy in Kempele, Finland, and analyzed at MS-Analytical Laboratory in Langley, Canada. Preprocessing consisted of crushing the samples to 70% passing 2 mm, splitting 250g with a rotating sample divider and grinding to 85% passing 75 μm.

Samples were analyzed for major element oxides (SiO_2, Al_2O_3, Fe_2O_3, MnO, MgO, CaO, Na_2O, K_2O, TiO_2, P_2O_5, BaO, Cr_2O_3, SrO and LOI) using lithium borate fusion and ICP-AES (Inductively coupled plasma atomic emission spectroscopy). Total C and S were determined directly by induction. For refractory elements and REE's, lithium borate fusion and ICP-MS (Inductively coupled plasma mass spectrometry) were employed while the concentration of additional 7 elements (Ag, Cd, Cu, Mo, Ni, Pb, Zn) were measured by 4-acid digestion and ICP-MS and other 7 elements (As, Au, Bi, Hg, Sb, Se, Tl) by aqua regia digestion and ICP-MS.

4.2.2 Normative mineralogy

Normative mineral calculations from bulk-rock geochemistry were made using SEDMIN, a Microsoft ExcelTm spreadsheet solution developed by Kackstaetter (2014), focusing on sedimentary rocks. However, this spreadsheet was useful since it allowed to calculate weight norms for minerals produced by hydrothermal alteration, such as sericite, chlorite. This made it possible to identify samples that had underwent more or less intensive alteration (critical for the identification of a precursor in the mass-balance exercise).

4.2.3 Mass balance calculations

Mass changes were calculated using the single precursor method outlined by MacLean and Kranidiotis (1987) and Barrett and MacLean (1994). Aluminum was used as the least mobile element for calculating the enrichment factor (EF) defined as:

$$EF = Al_{precursor}/Al_{altered\ sample}$$

The reconstructed composition (RC) of altered samples was calculated from anhydrous values in weight per cent (wt-%) and parts per million (ppm), using total iron FeO_T as 90% of the total Fe_2O_3 provided by the analyses.

$$RC = (EF) \times (wt\ \%\ or\ ppm)_{altered\ sample}$$

The mass change of each element in each sample was then calculated by subtracting the precursor value of that element from the reconstructed composition of the sample:
Mass Change = RC – precursor value.

4.2.4 Softwares

The QGIS™ software was used as the main mapping tool on this research project.
Plots and graphs were made using ioGAS™, Microsoft Excel™ and later on improved using CorelDrawX7™ as the main designing software tool.

5 RESULTS

Considering that the rocks in the TGB underwent several metamorphic events, hydrothermal alteration processes and weathering during their near 2.8 Ga of history, a classification solely relying in major elements should be taken with some caution. Detailed trace element geochemical characterization of the samples was made following the classification scheme described previously in Chapter 2. This chapter also deals with alteration styles, which were critical in choosing of the least altered sample used in mass-balance calculations, leading to the final interpretations.

5.1 Petrography

Rocks studied petrographically range from intermediate to felsic metavolcanic and quartz-kyanite rocks of which the latter are interpreted in previous studies as a metamorphozed bleached lithocap (Papunen et al., 1989).

Felsic metavolcanic rocks show a granolepidoblastic texture (Figs. 9 a, b). and the foliation is not well developed, ranging from rough cleave to massive recrystallized rocks. Some of the rocks show a porphyritic texture (Figs. 9 c, d).

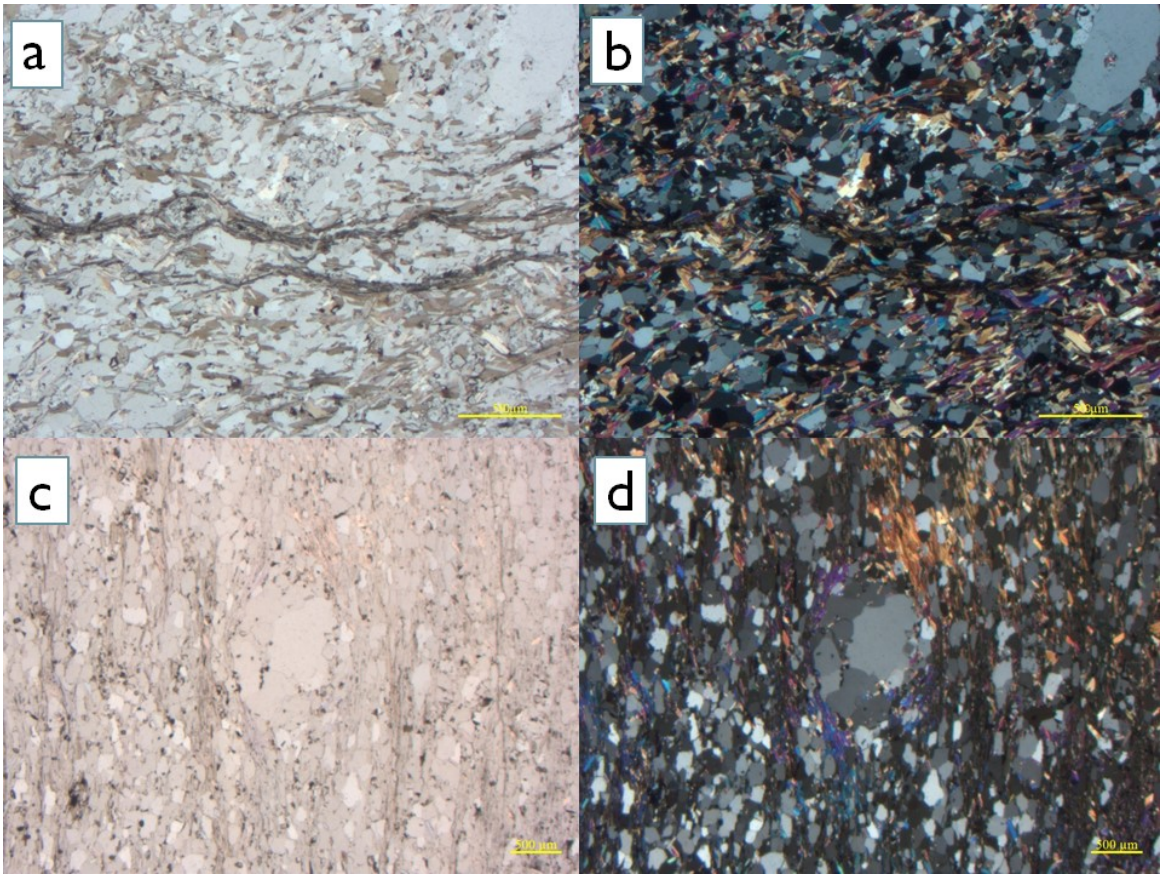

Figure 9. A: Photomicrograph under plane-polarized light (PPL) showing a granolepidoblastic texture with some quartz porphyroblasts up to 1 mm in size. Mica domains are mainly composed by biotite totally or partially sericitized. TSAC-4. B: Idem A., under cross-polarized light (XPL). TSAC-4. C: Photomicrograph under PPL showing granolepidoblastic texture with mica domains dominated by muscovite. Quartz porphyroblasts show recrystallization. TSAC-6. D: Idem C., under XPL. TSAC-6.

Most of the porphyroblasts are represented by quartz and they show evidence for recrystallization, being then made of several quartz blasts. However, in many cases they are made of a single quartz blast ranging from 1 to 1.5 mm (Figs. 10 a-d). There are also biotite porphyroblasts, usually showing evidence for alteration (sericitization) (Figs. 11 a, b).

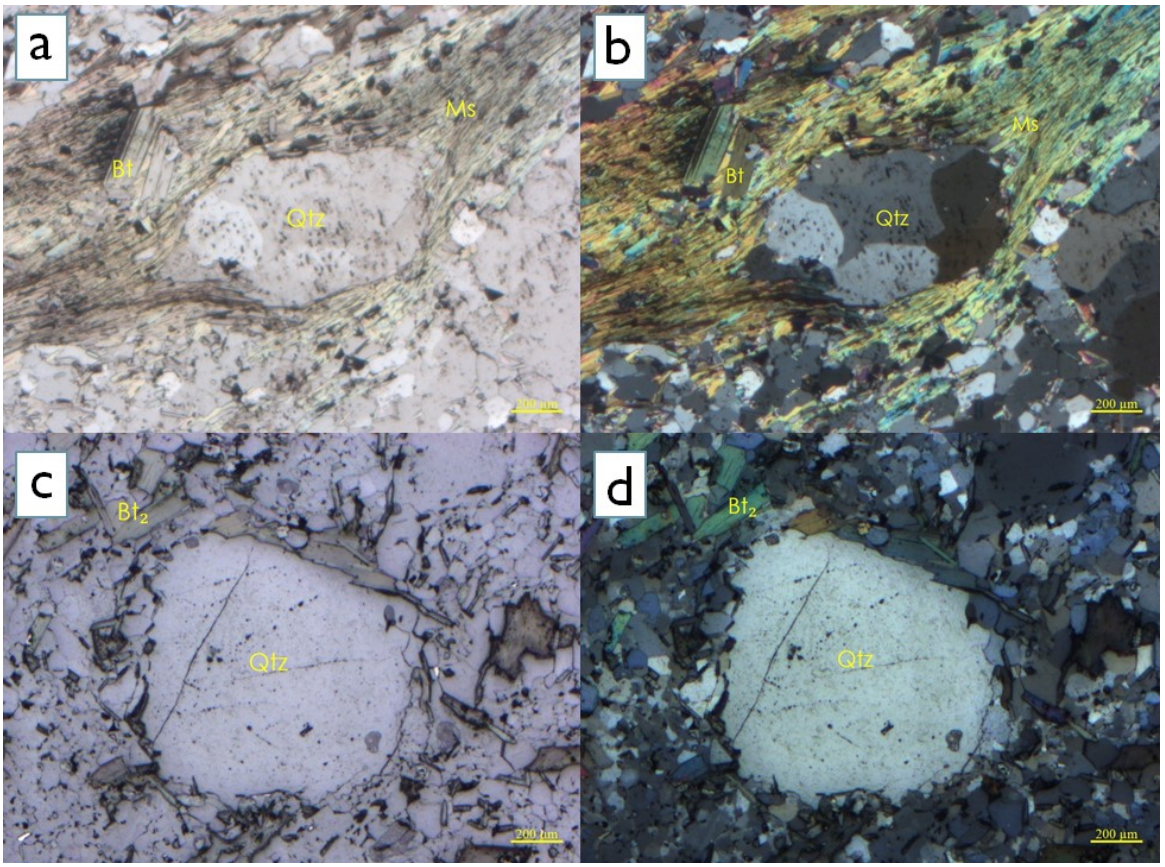

Figure 10. A: Photomicrograph under PPL showing quartz porphyroblast made of several quartz blasts, with metamorphic recrystallization. Muscovite in mica domains showing strain shadows and strain caps. TSAC-6. B: Idem A., under XPL. TSAC-6. C: Photomicrograph under PPL showing a single quartz porphyroblast inside quartz domains of smaller size. TSAC-2. D: Idem C., under XPL. TSAC-2. Qtz = quartz, Ms = muscovite, Bt = biotite.

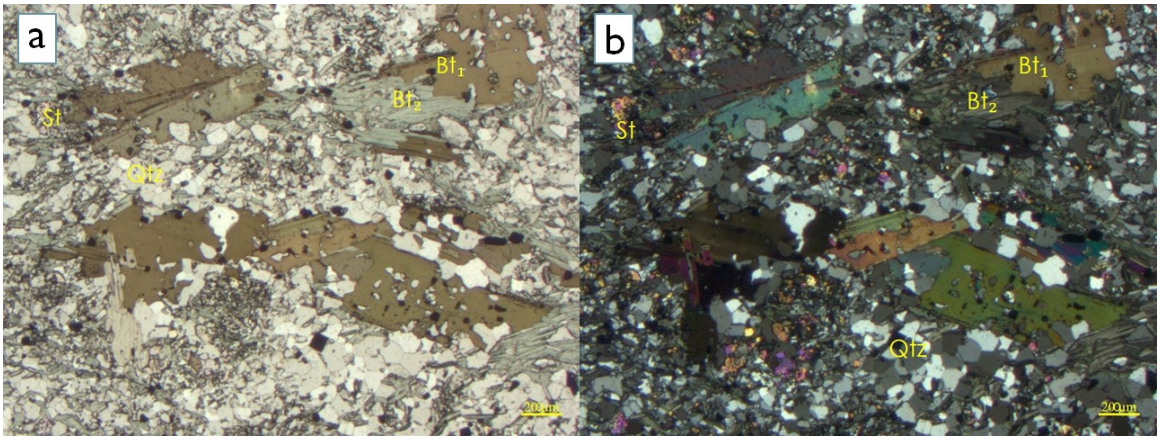

Figure 11. A: Photomicrograph under PPL showing biotite porphyroblasts and quartz inclusions, along a rough cleavage defined by quartz and muscovite domains. TSAC-1. B: Idem A., under XPL. TSAC-1. Qtz = quartz, St = staurolite, Bt = biotite.

Quartz domains along foliation show a mosaic texture with triple contacts of 120º as evidence for metamorphic recrystallization, while they do not show undulose extinction. Quartz blasts in the matrix are usually subhedral and have grain sizes from 0.02 to 0.05 mm. Mica domains are made of biotite and muscovite, being muscovite in some cases a result of alteration of previous biotites grains (Figs. 12 a, b).

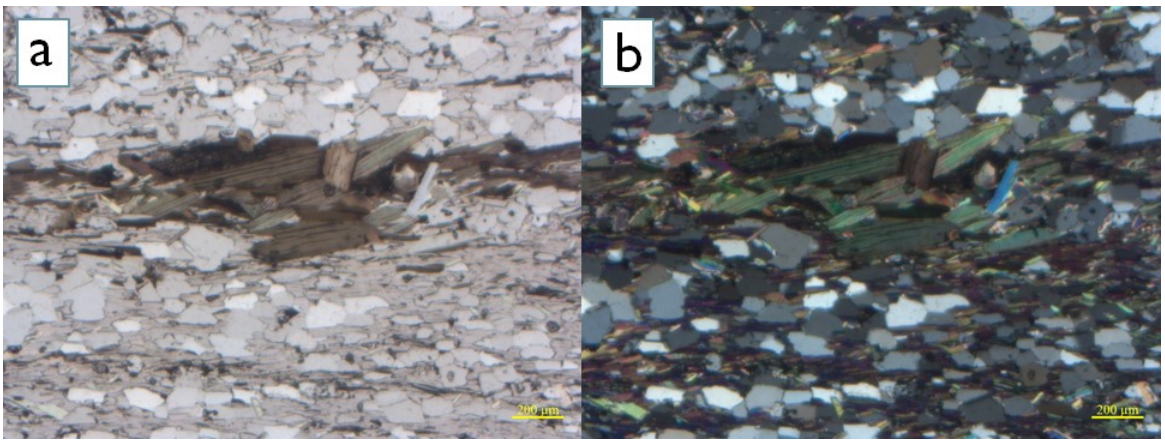

Figure 12. A: Photomicrograph under PPL showing biotite grains showing incipient alteration to muscovite. TSAC-6 B: Idem A., under XPL. TSAC-6.

Some of the secondary biotite is brownish in PPL but show interference colors of the second order in XPL (probably phengitic in composition). Altered biotite shows Fe oxides in cleavage planes due to sericitization (Figs. 13 a, b).

Another alteration style shown by biotite is chloritization, which has resulted in chlorite grains up to 1 mm in size, showing clear pleochroism in PPL from pale to strong green and

anomalous interference colors (Berlin blue) (Figs. 13 c, d).

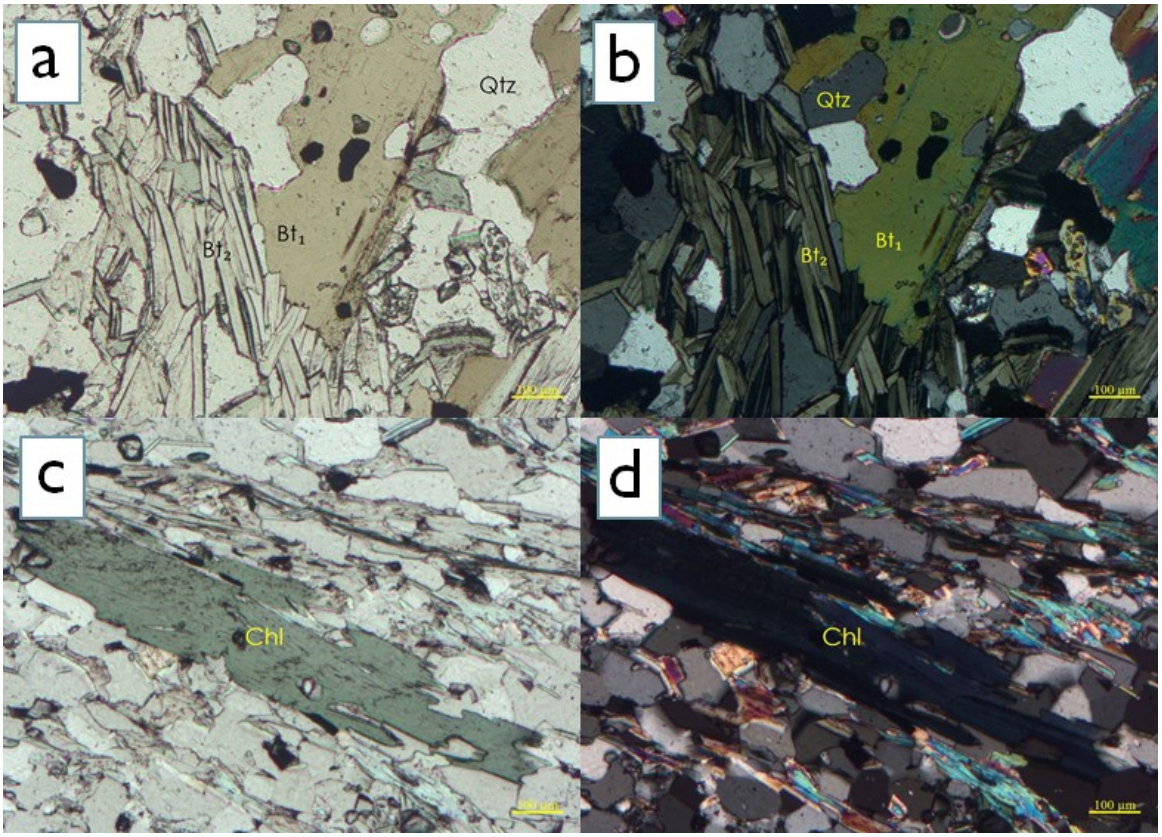

Figure 13. A: Photomicrograph under PPL showing different generations of biotite. Bt_1 represented by unaltered porphyroblasts, usually showing a big amount of quartz and zircon inclusions, strong pleochroism and masked interference colors (B). Second generation biotite (Bt_2) showing sericitization. TSAC-1. B: Idem A., under XPL. TSAC-1. C: PPL. Photomicrograph under PPL showing chlorite crystal, subhedral and near 1 mm in size. It shows characteristic green shades and strong pleochroism. TSAC-5. D: Idem C., under XPL. Anomalous interference colours characteristics of chlorite (Berlin Blue) are observed. TSAC-5. Qtz = quartz, Chl = chlorite, Bt = biotite.

Quartz-kyanite rocks have a rather irregular foliation, in some cases developing a rough cleavage. Quartz and aluminosilicates such as kyanite, staurolite and chloritoid follow this foliation (Figs. 14 a, b*)*. These rocks in general lack mafic phases and besides metamorphic blastesis and deformation one can see silicification as the main alteration phenomenon.

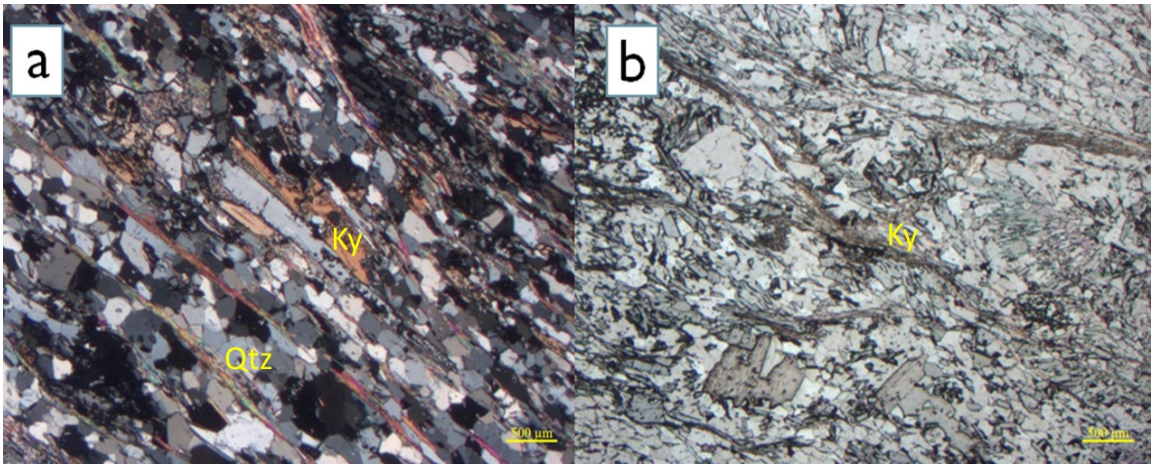

Figure 14. A: Photomicrograph under XPL showin granolepidoblastic texture displayed by quartz and kyanite domains showing a rough cleavage. B: Photomicrograph under PPL showing Irregular foliation, quartz, kyanite, staurolite and chloritoid as main mineralogic species. TSAC-8. Qtz = quartz, Ky = kyanite.

Felsic metavolcanic rocks close to Jäkäläsuo contain some kyanite and staurolite as accessory phases in some occasions. In the quartz-kyanite rock next to this area, these phases together with chloritoid are conspicuous (Figs. 15 a-f).

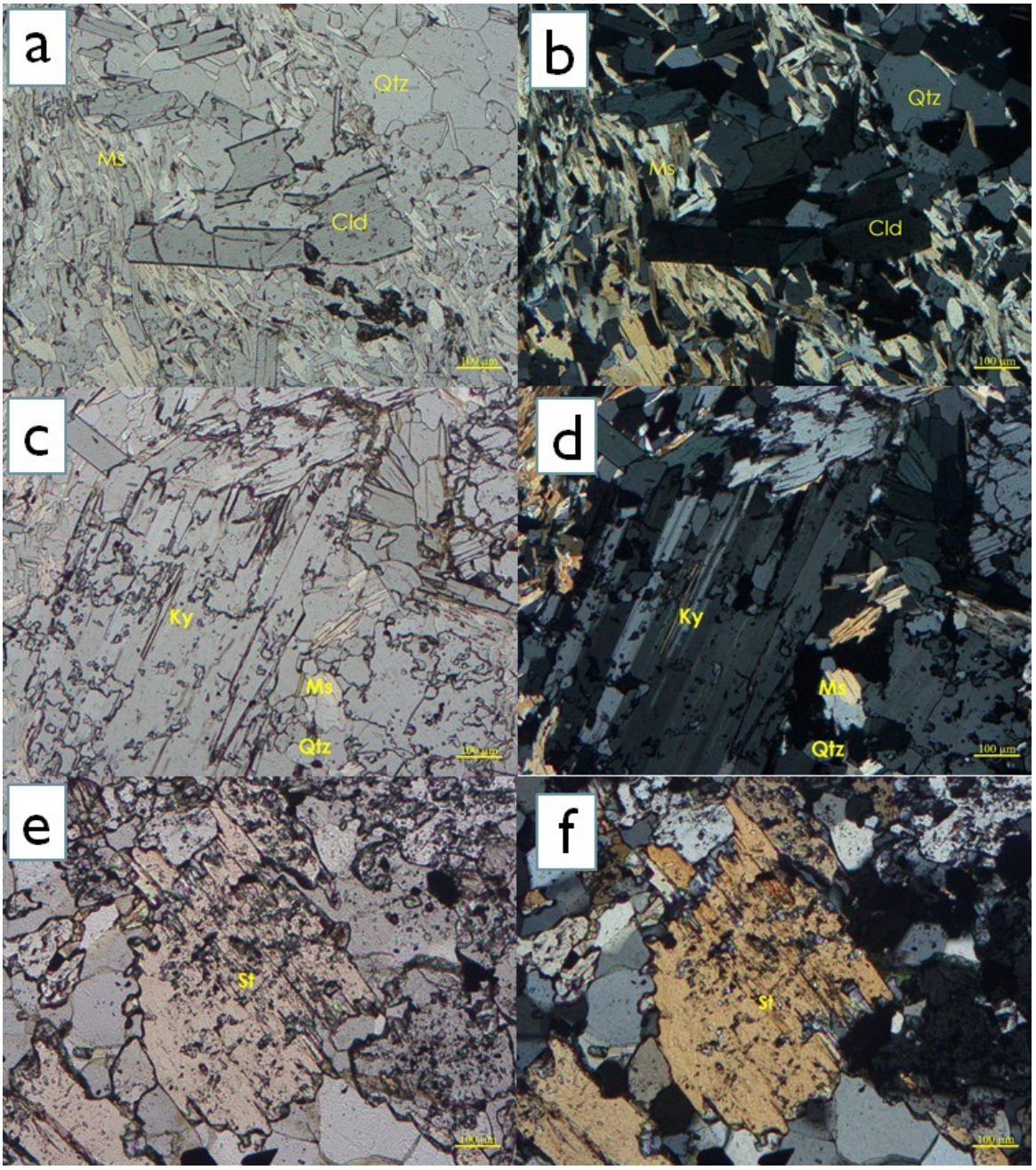

Figure 15. Photomicrographs from sample TSAC-17. A: Chloritoid under PPL along with quartz and muscovite. B: Chloritoid under XPL. C: Kyanite under PPL. D: Kyanite under XPL showing lamellar twinning. E: Poikilitic staurolite porphyroblasts close to quartz and kyanite under PPL. F: Idem E., under XPL. Qtz = quartz, Ms = muscovite, St = staurolite, Ky = kyanite, Cld = chloritoid.

Garnet is a common accessory phase in some of the samples, usually as euhedral poikilitic porphyroblasts showing several inclusions of quartz and in some cases mica. The porphyroblast range from 0.5 to 0.2 mm in size (Figs. 16 a, b).

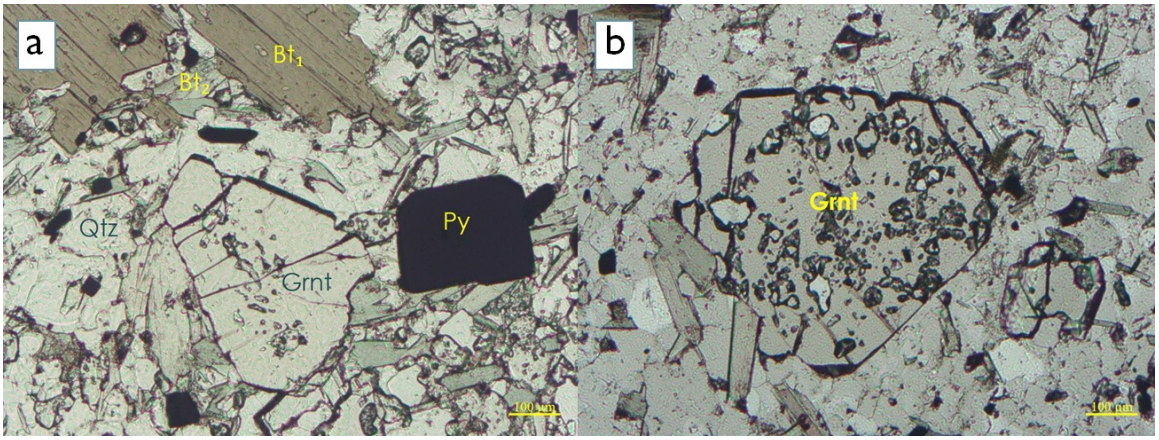

Figure 16. A: Photomicrograph under PPL showing garnet accessory mineral along with euhedral pyrite and different generations of biotite and quartz. TSAC-1. B: Photomicrograph under PPL showing poikilitic garnet porphyroblast showing several inclusions of quartz and micas. TSAC-19. Qtz = quartz, Grnt = garnet, Bt = biotite, Py = pyrite.

Zircon inclusions are present in biotite grains, evidenced by pleochroic halos in the hosting phases, product of metamictization (Fig. 17).

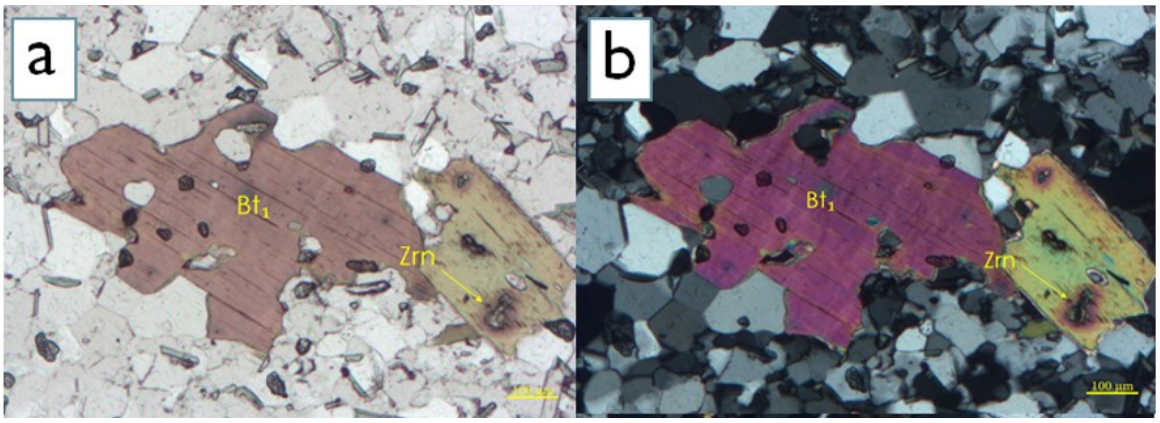

Figure 17. A: Photomicrograph under PPL showing biotite porphyroblasts showing pleochroic halos, product of zircon inclusion and metamictization. TSAC-2. B: Idem A., under XPL. TSAC-2. Bt = biotite, Zrn = zircon.

Most of the felsic metavolcanic rocks share the same petrographic characteristics. However, there is a higher abundance of sulfides in the Koivumäki and Koraminvaara profiles (Fig. 18 a). They are mainly pyrite, although in some occasions, pyrite is associated with pyrrhotite and chalcopyrite (Figs. 18 c, d). There are some iron oxide/hydroxide grains in the samples although it is not a common feature, nor they are significant in amount. (Figs. 18 a, d).

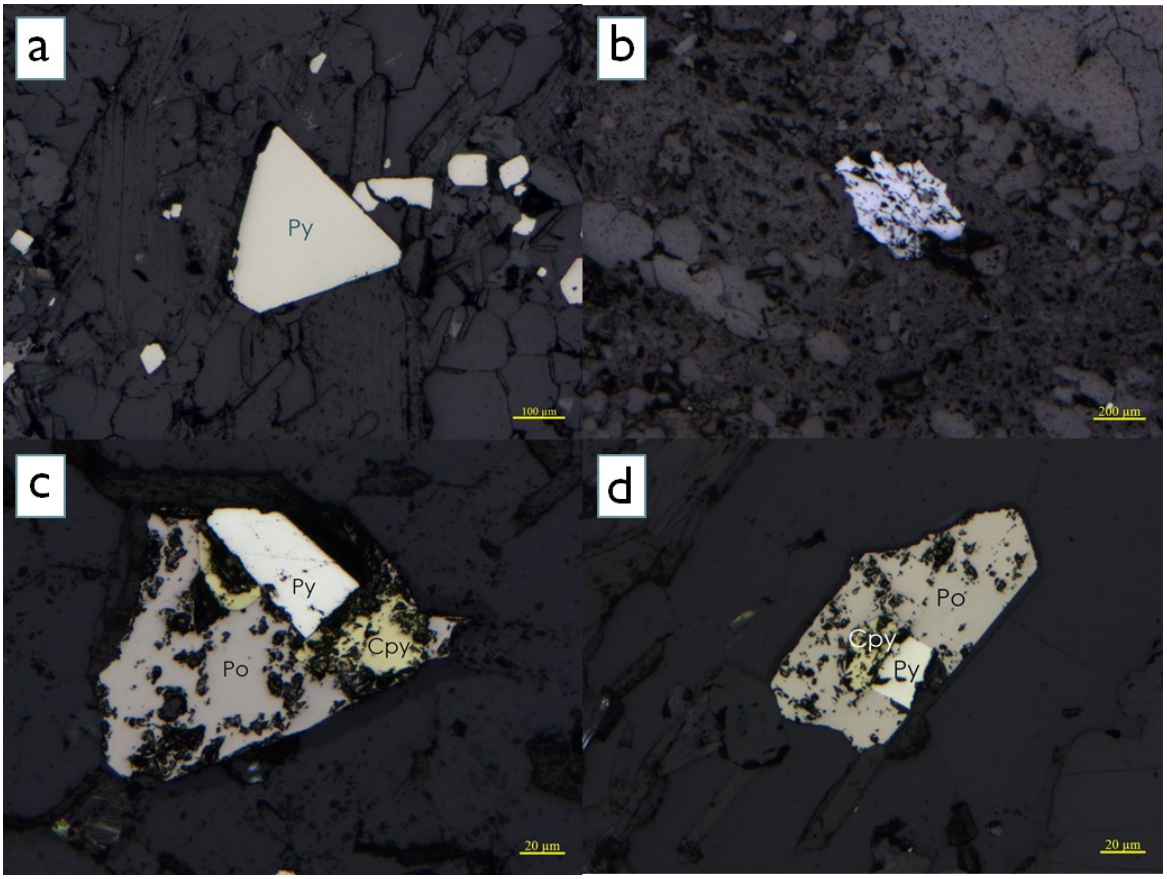

Figure 18. Photomicrographs of opaque phases under reflected light. A: Euhedral pyrite, conspicuous in sample close to Jäkäläsuo. TSAC-1. B: Unidentified oxide phase. TSAC-12. C: Pyrite, Pyrrhotite and chalcopyrite. TSAC-3. D: Idem C., TSAC-4. Py = pyrite, Cpy = chalcopyrite, Po = pyrrhotite.

5.2 Lithogeochemistry

The Jensen cation plot illustrated in Fig. 19 shows a geochemical trend that ranges from basalts to rhyolites. However, Mg is a moderately mobile element (Rollinson, 1993) and should be treated carefully when dealing with units that have undergone chloritization, where this cation is rather mobile.

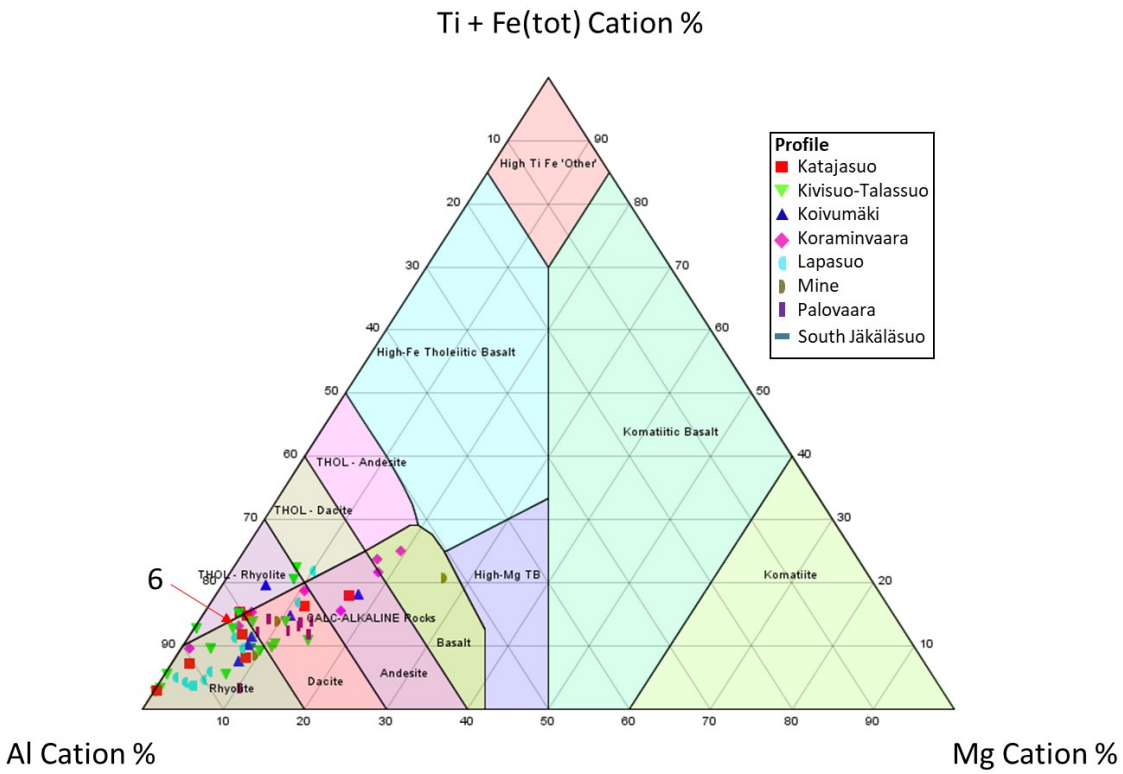

Figure 19. Jensen cation plot after Jensen (1976). Sample 6, which is later used as a precursor in mass-balance calculations, is indicated by a red arrow.

The Zr/Ti vs Nb/Y classification diagram by Winchester and Floyd (1977), as modified later by Paulick et al. (2001) (Fig. 20), shows that samples from the Mine as well as most of the samples from the Kivisuo-Talassuo and Lapasuo profiles are rhyolites, whereas samples from Koraminvaara, Katajasuo and Palovaara are slightly less evolved and plot in the rhyodacite/dacite fields. In the Koivumäki + South Jäkäläsuo profiles both rock types are observed.

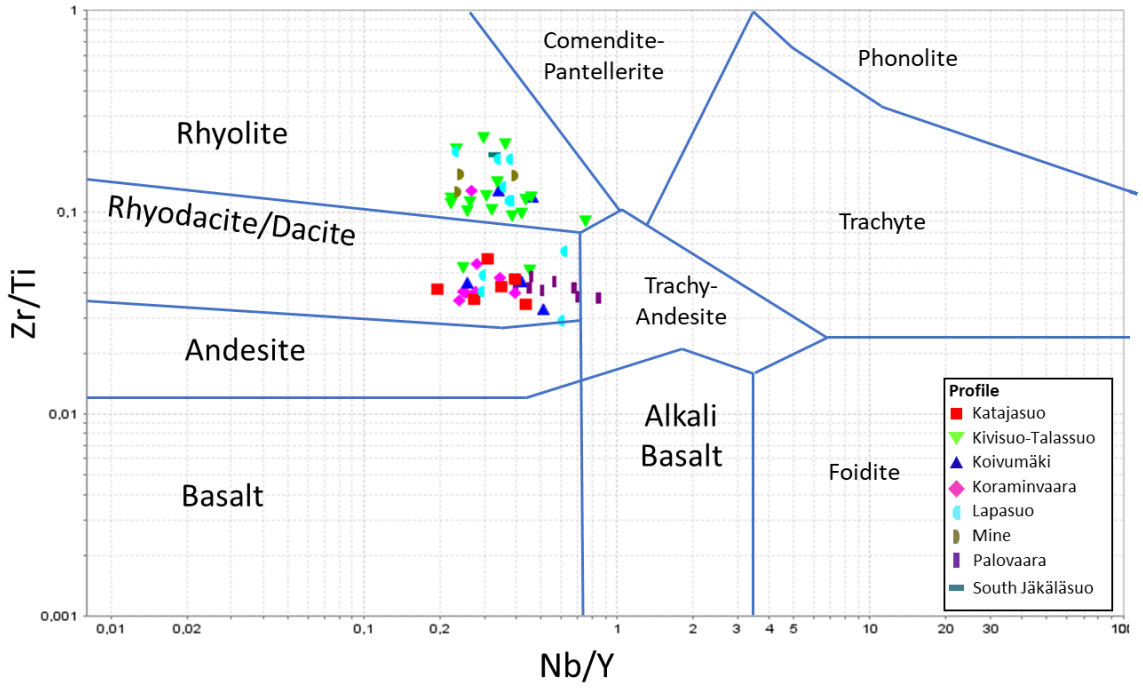

Figure 20. Zr/Ti vs Nb/Y discrimination diagram after Winchester and Floyd (1977) modified by Paulick et al. (2001).

On the Th/Yb vs Nb/Yb plot (Pearce, 2008) (Fig. 21), it can be observed that most of the samples are located in the continental arc partly overlapping the field of oceanic arc basalts. These rocks exhibit a calc-alkaline to transitional series trend (Fig. 22). The mine sample plotting in the tholeiitic field displays an enrichment in Y that can be explained by mobility of this element in scenarios of intense hydrothermal alteration (MacLean, 1988).

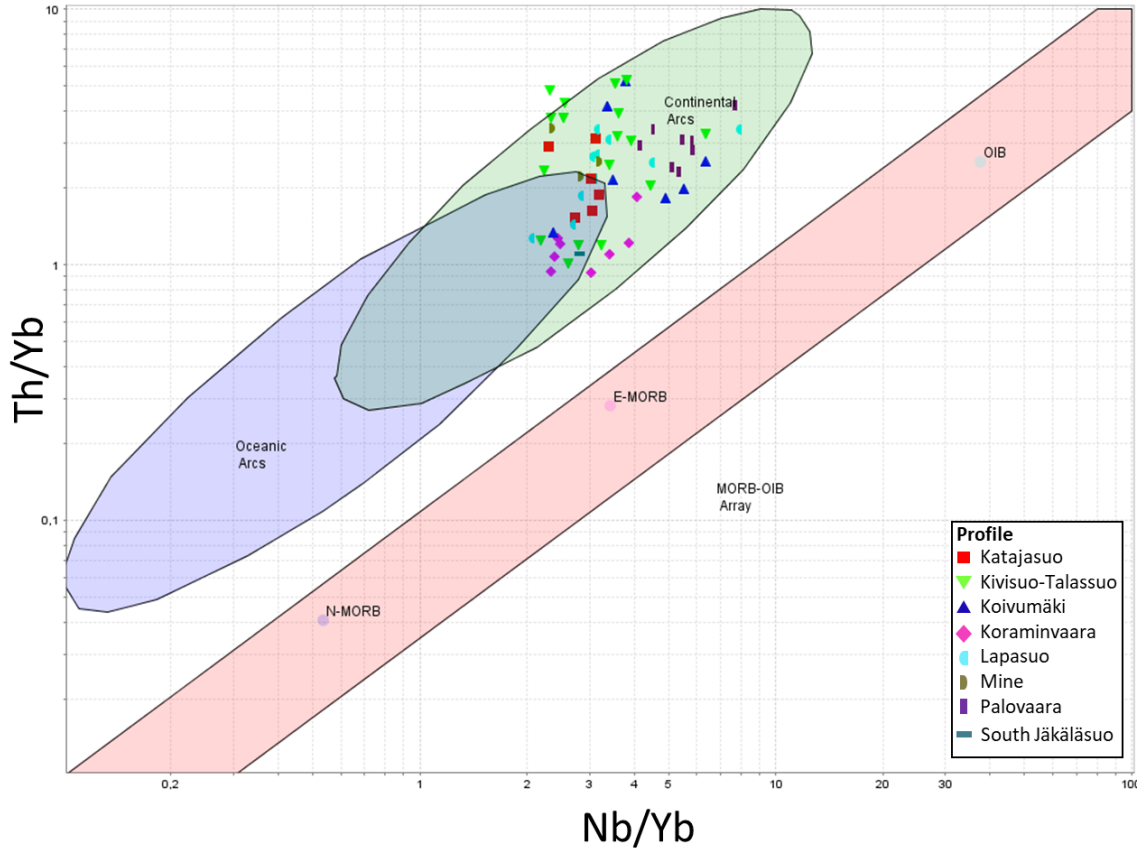

Figure 21. Basalt Th/Yb vs Nb/Yb (Pearce, 2008). TGB felsic volcanics range from continental arcs to transitional.

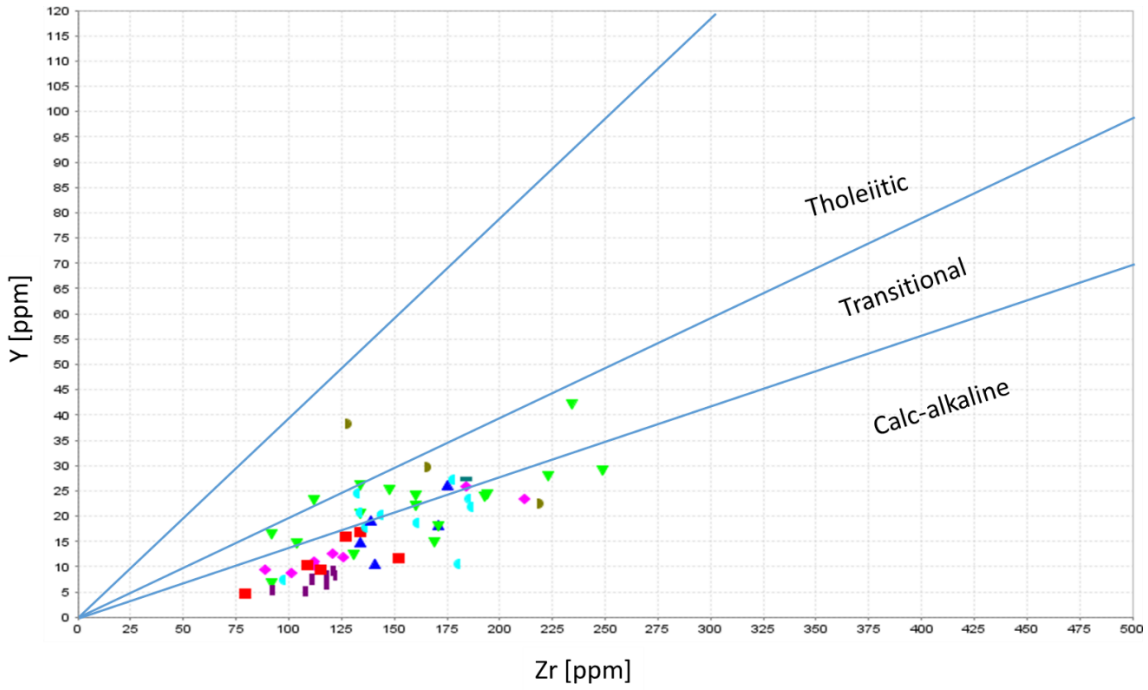

Figure 22. Y vs Zr [ppm] magmatic affinity plot after Ross and Bedard (2009).

It has been previously interpreted by Luukkonen (1991) and Papunen et al. (2009) that the TGB fits with a continental rift setting. Lehtonen (2016) proposed that the most probable setting for the formation of the volcanic rocks with ages of ca. 2.84-2.79 Ga was a continental rift environment with continental and oceanic lithosphere. These interpretations match with the results presented here.

5.3 Alteration

Most of quartz-porphyry schists show a high degree of alteration, with the most common style of alteration being sericitization (Figs. 12a, b). A few show samples display evidences for chloritization (Figs. 13 c, d). Moreover, when heading eastwards, samples start showing strong silicification as well as Al-bearing phases, such as staurolite, kyanite, garnet and no mafic phases (Figs. 14 a, f).

On the Na/Al vs K/Al molar ratio diagram (Fig. 23) developed by Davies and Whitehead (2006), most of the samples follow a sericitization trend and few are relatively unaltered (e.g., sample 6). This is also evidenced in thin sections by the lack of feldspars.

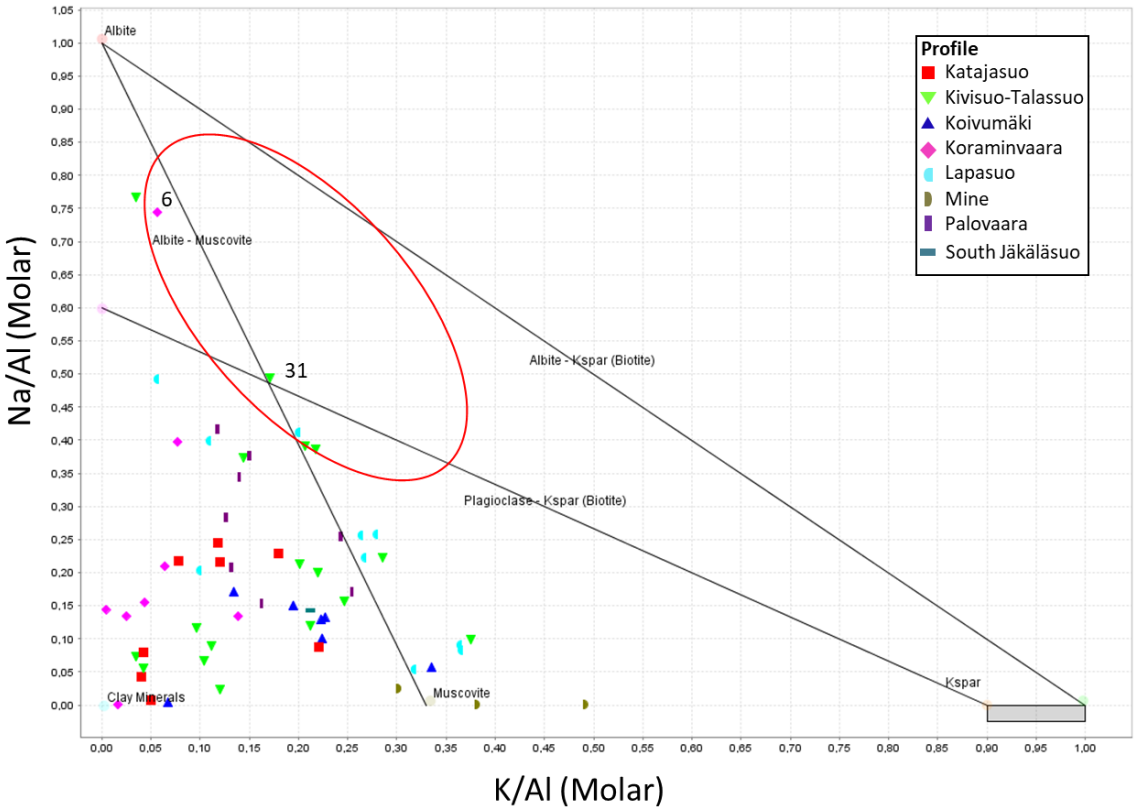

Figure 23. Na/Al vs K/Al molar ratio diagram (modified after Davies and Whitehead, 2006). Circled area represents the least altered zone.

Normative alteration mineralogy was calculated using the program developed by Kackstaetter (2014) and then used to construct ternary diagrams to assess the potential operation of alteration processes, such as sericitization, chloritization and silicification (Figs. 24 a-c). Samples closer to the albite (Ab) tip of the ternary diagrams represent the least altered compositions. When albite is not represented on the ternary plots, the ones closer to quartz (Qtz) behave on the same manner. However, samples which their modal composition have over 70-80% of normative quartz, might probably be affected silicification processes.

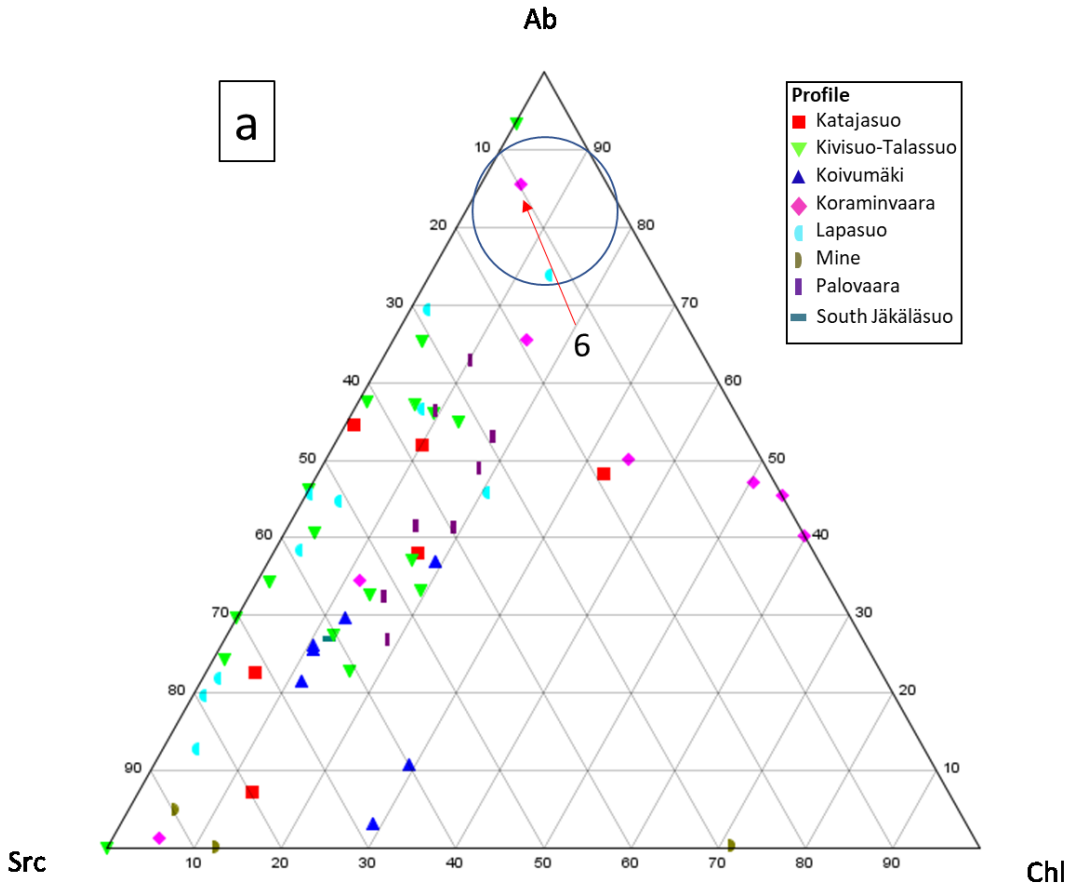

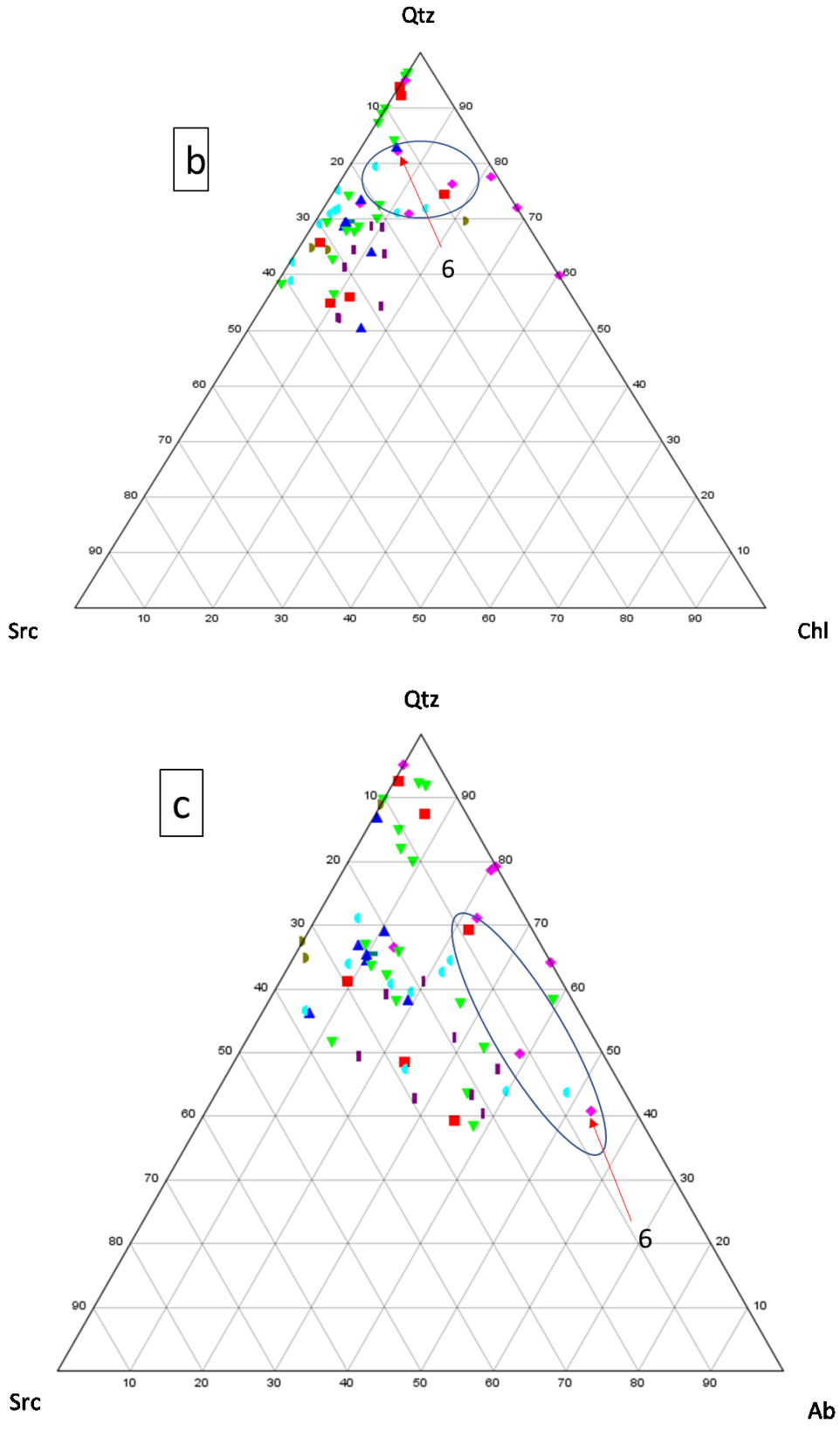

Figure 24. a: Ab-Src-Chl ternary plot based on normative mineralogy that shows sericitization and chloritization processes. c: Qtz-Src-Chl integrated plot that shows silicification, sericitization and chloritization processes. c: Qtz-Src-Ab ternary plot that shows sericitizacion and silicification processes. Circled areas represent those of relatively less alteration and the relatively least altered sample (6) is indicated in a red arrow. Ab = albite, Qtz = quartz, Src = sericite, Chl = chlorite.

Besides identifying the most common alteration processes, combining petrographic studies and alteration diagrams allowed to recognize the relatively least altered sample (AC-6), later on used as most non-altered the precursor composition for mass-balance calculations.

5.4 Trace element geochemistry and fertility evaluation

5.4.1 REE patterns

Figure 25 shows selected chondrite-normalized rare earth element patterns for samples from the mine area (Fig. 25 i), representing the mineralized zone and the hanging wall and footwall rocks. They show steep LREE, flat HREE and a pronounced Eu anomaly, being similar to the patterns reported from Archean mineralized felsic rocks such as the Wabigoon and Abitibi belts, for example (Lesher et al., 1986). Samples from the Koivumäki (Fig. 25 c, d) and Kivisuo-Talassuo (Fig. 25 b) profiles share a similar REE signature but those from Lapasuo (Fig. 25 e, f) are characterized by flat to slightly LREE-depleted REE patterns and low REE and HFSE abundances. Samples from the Koraminvaara (Fig. 25 g) and Katajasuo (Fig. 25 a) profiles have a lower level of Yb_{CN} than the previous profiles and they do not show a negative Eu anomaly, being in some cases even positive.

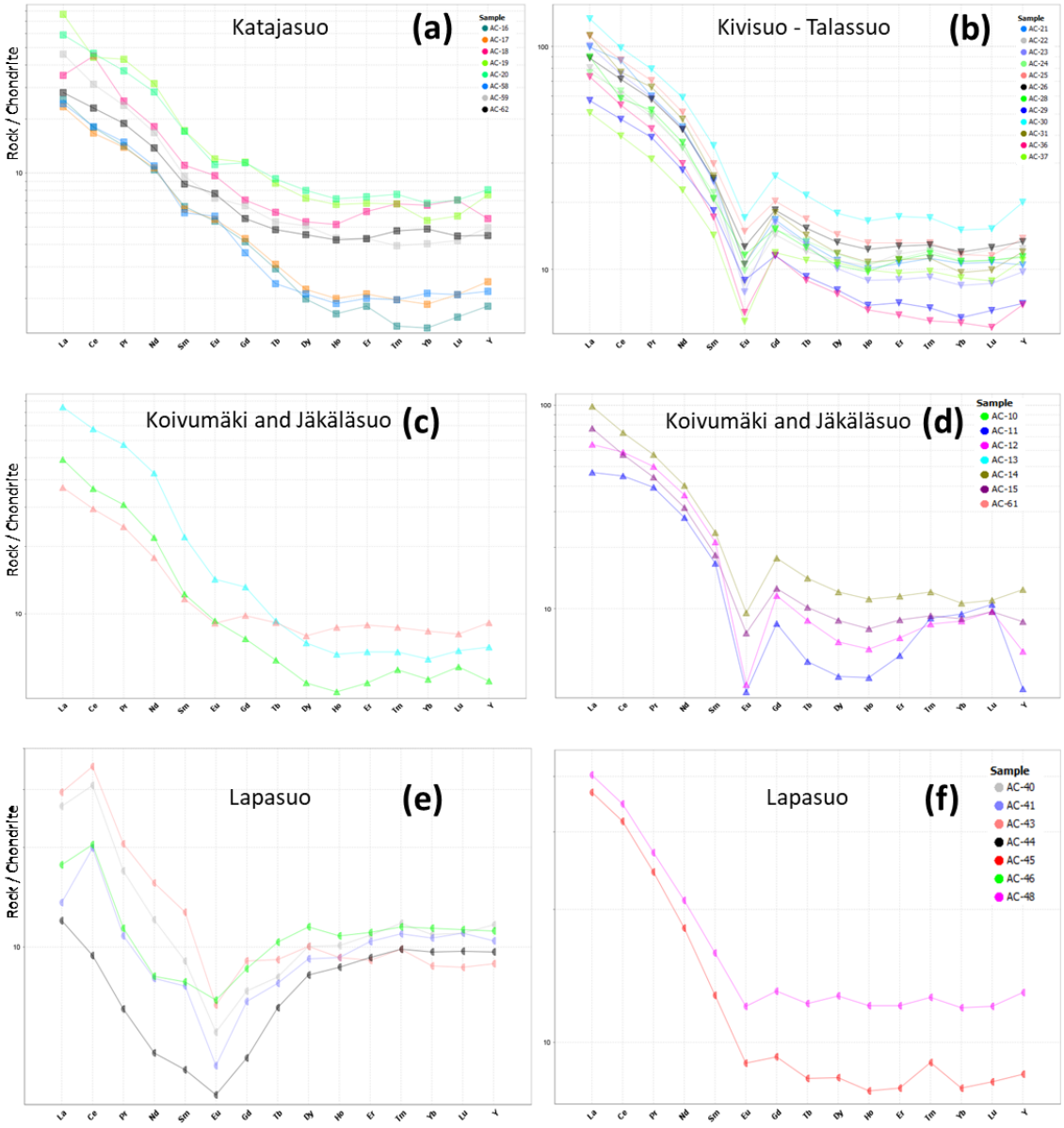
Katajasuo
(a)
Kivisuo - Talassuo
(b)
Koivumäki and Jäkäläsuo
(c)
Koivumäki and Jäkäläsuo
(d)
Lapasuo
(e)
Lapasuo
(f)
Rock / Chondrite
Sample
AC-16
AC-17
AC-18
AC-19
AC-20
AC-58
AC-59
AC-62
AC-21
AC-22
AC-23
AC-24
AC-25
AC-26
AC-28
AC-29
AC-30
AC-31
AC-36
AC-37
AC-10
AC-11
AC-12
AC-13
AC-14
AC-15
AC-61
AC-40
AC-41
AC-43
AC-44
AC-45
AC-46
AC-48
La
Ce
Pr
Nd
Sm
Eu
Gd
Tb
Dy
Ho
Er
Tm
Yb
Lu
Y

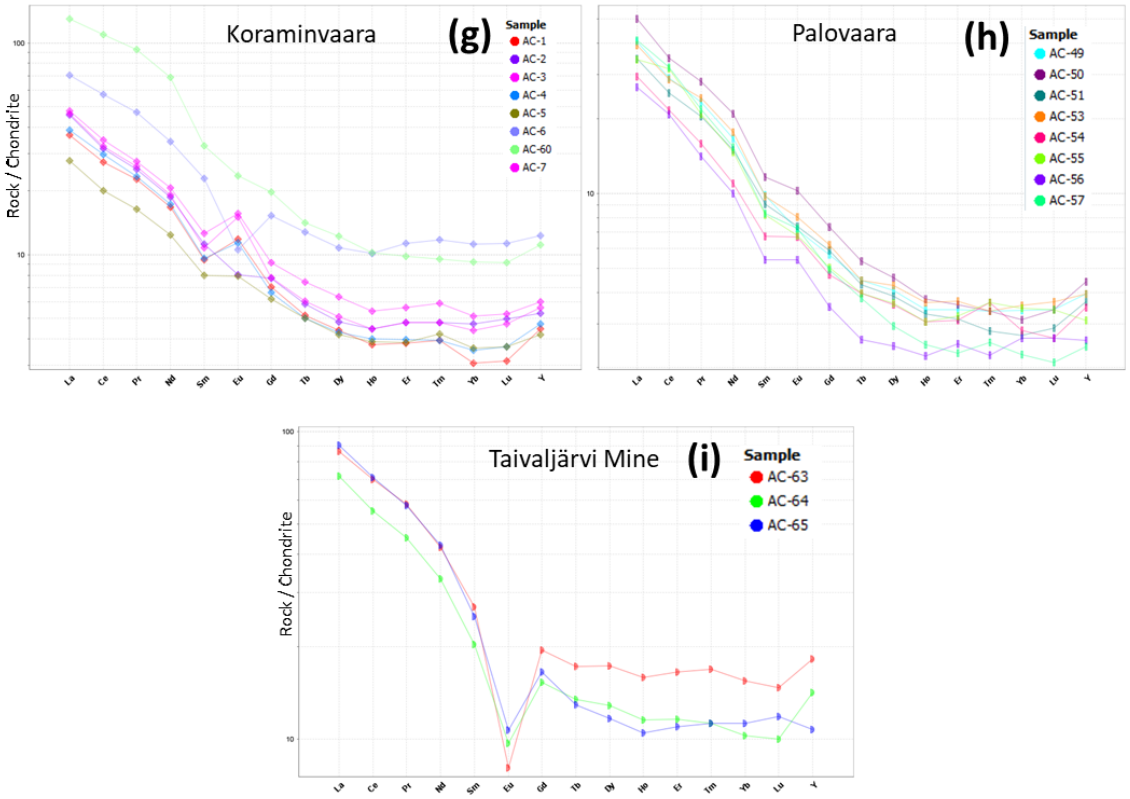

Figure 25. REE profiles. a: Katajasuo. b: Kivisuo-Talassuo. c-d: Koivumäki + Jäkäläsuo. e-f: Lapasuo. g: Koraminvaara. h: Palovaara. i: Mine. Chondrite normalized values after Taylor and McLennan (1985) in Rollinson (1993).

Samples from Palovaara (Fig. 25 h) profile have not only a low level of Yb_{CN}, but also a steep REE pattern, with high La/Yb_{CN} and depletion in HREE.

According to MacLean and Hoy (1991) some alteration processes might affect the distribution and concentration of REE. For instance, chloritization may cause the rocks to lose REE and sericitization to gain REE. This is because REE are leached by hot (>250ºC) hydrothermal fluids in high-temperature Fe-rich chlorite alteration zones and deposited in lower temperature quartz-sericite zones.

Lodders (1996) investigated the effect of partitioning of REE in silicate and sulfide melts as well, resulting in the observation that REE partition coefficients in the FeS/silicate system decrease from light to heavy REE, while the opposite behavior is found for the CaS/silicate system, where partition coefficients increase from light to heavy REE. In both sulfide systems, Eu is preferentially incorporated into the sulfide phases. Both the influence of hydrothermal alteration and sulfide-bearing phases could then explain Eu anomalies in relatively more mineralized felsic metavolcanic rocks. However, since the level of REE in

sulphides is relatively low, the quatitative effects of sulfides in the mobility of REE in deposits of this size is rather small.

5.4.2 Fertility plots

Fertility for massive sulfides mineralization was assessed according to the methodology described in Lesher et al. (1986) and Hart et al. (2004) in which felsic metavolcanic rocks are classified in relation to their trace element geochemistry (HFSE, LILE, REE and Eu/Eu*). Several samples plot in the FII field in the La/Yb_{CN} vs Yb_{CN} plot (Table 1, Fig. 26).

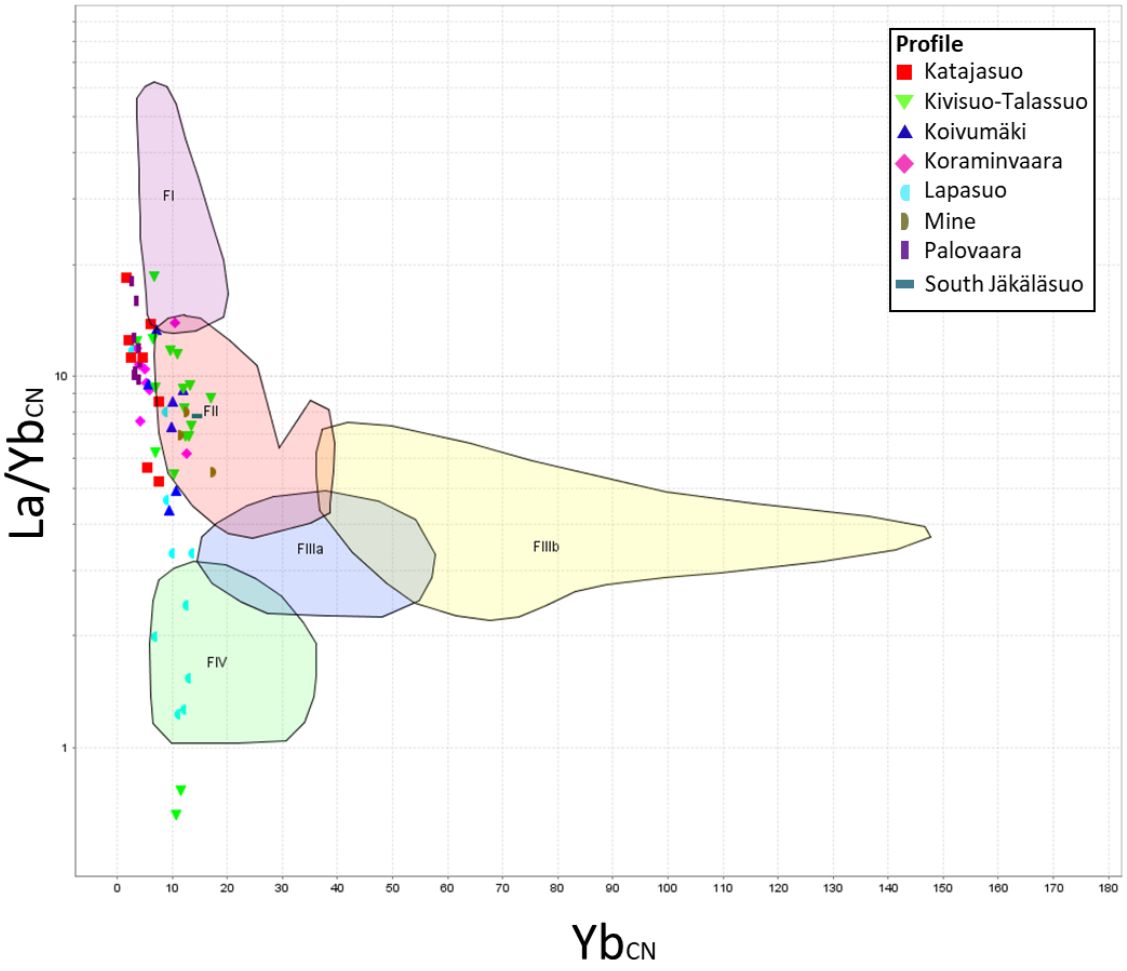

Figure 26. Fertility of felsic volcanic rocks hosting VHMS after Hart et al. (2004).

Footwall, deposit and hangingwall rhyodacite samples all plot in this category, and show moderate Zr/Y values of 3.35-9.73, $[La/Yb]_{CN}$ of 5.5-8, Eu/Eu* of 0.35-0.55 and intermediate HFSE contents. Other areas such as Koivumäki + South Jäkäläsuo, display similar trace element characteristics to those of the mine area. The Kivisuo-Talassuo

samples also show FII trends whereas the Lapasuo samples fall in the FIV category (Table 1), consisting of rhyodacites, rhyolites and high-silica rhyolites characterized by flat to slightly LREE-depleted REE patterns and low REE and HFSE abundances. On the other hand, the Koraminvaara and Katajasuo samples fall near the edge of the FII field but they have a lower level of Yb_{CN} than the previous profiles. The Palovaara samples have not only a small Yb content, but also a steeper REE pattern, with higher La/Yb_{CN} (Table 4).

Table 4: Geochemical characteristics and classification related to VHMS deposits, after Lesher et al. (1986) and Hart et al. (2004).

Profile	N	Felsic volcanic fertility (Hart et al. 2004)	SiO_2 [%]	TiO2 [%]	Y [ppm]	Zr/Y	Yb [ppm]	$[La/Yb]_N$	Eu/Eu*
Koraminvaara	8	FII>0	62-75	0.24-0.89	8.8-25.8	7.13-11.48	0.76-2.78	6.21-13.93	0.56-1.65
Koivumäki – South Jäkäläsuo	8	FII	66-78	0.31-0.68	8.5-27.4	6.7-13-43	1.26-3.19	4.36-13.37	0.27-0.96
Katajasuo	8	FII>FI>0	60-81	0.31-0.72	3.8-16.9	7.93-27.74	0.34-1.68	5.22-18.49	0.8-1.24
Kivisuo-Talassuo	12	FII>FI>0	66-86	0.15-0.55	14.6-42.2	4.85-11.42	1.43-3.74	5.46-12.58	0.39-0.65
Lapasuo	9	FIV>FII	65-81	0.11-0.61	17.8-27.2	5.39-8.56	1.91-2.97	1.23-8.02	0.61-0.84
Palovaara	8	0	65-70	0.4-0.48	5.1-9.3	13.01-21.18	0.56-0.88	9.8-18.03	0.95-1.24
Mine	3	FII	69-73	0.17-0.24	22.5-38.2	3.35-9.73	2.54-3.83	5.53-7.99	0.35-0.55

As shown in Figs. 27 and 28, there is an increase in Hg/Na_2O and Ba/Sr (together with Zn) in the proximity of the ore. Samples from the mine plot inside the ore proximal field, while some of the samples from the Lapasuo profile are close to it.

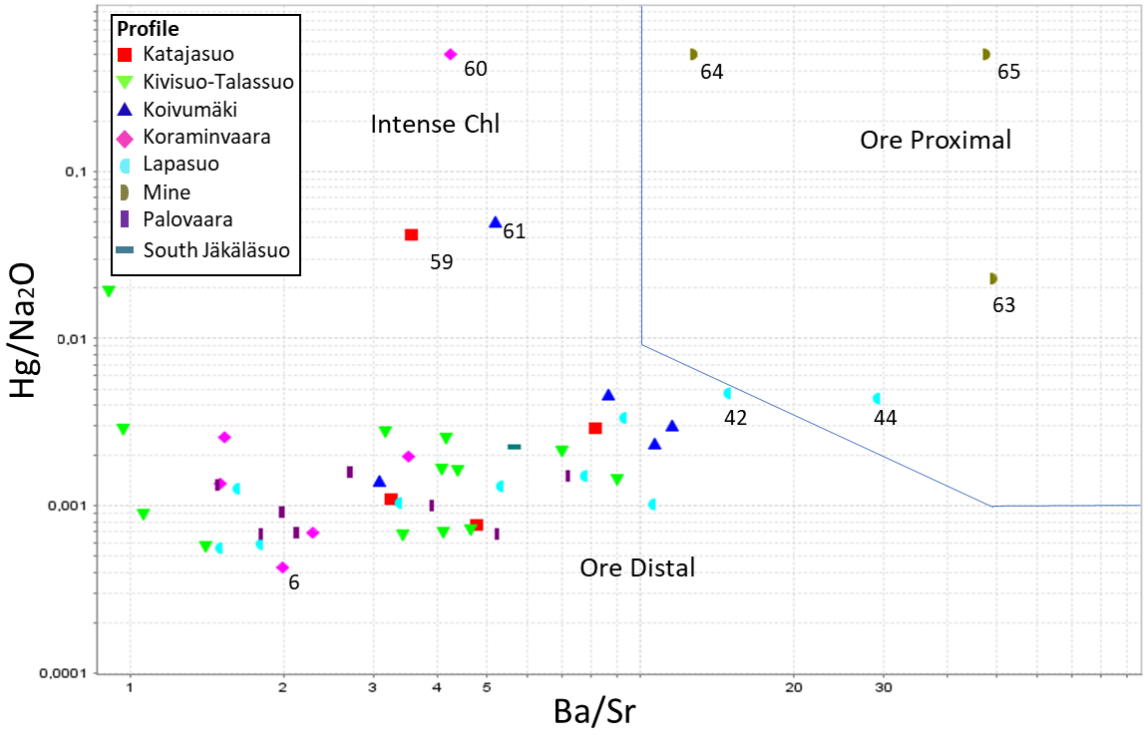

Figure 27. Hg/Na2O vs Ba/Sr plot showing ore distal and ore proximal areas as well as intense chloritization ones (modified after Paulick et al., 2001).

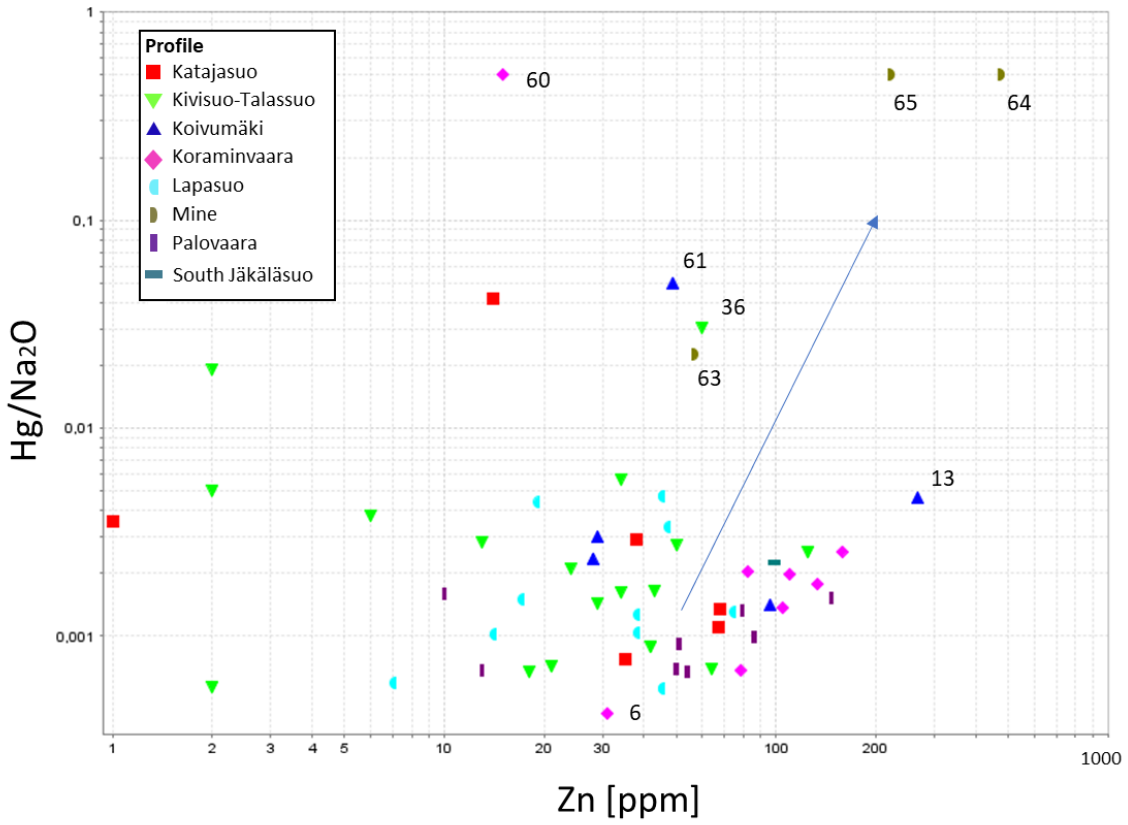

Figure 28. Hg/Na2O vs Zn plot modified after Paulick et al. (2001).

In summary, the Kivisuo-Talassuo and Lapasuo as well as Koraminvaara areas have similar trace-element characteristics to those from the silver mine, representing areas of higher potential for new discoveries.

5.5 Mass balance calculations

In the mass-change calculations, sample AC-6 from the Koraminvaara profile was regarded as the most representative of the original chemical precursor composition for the samples on this work based on petrographic observations, normative alteration mineralogy and major/trace elements geochemical evaluations. Mass changes were calculated using the single precursor method outlined by MacLean and Kranidiotis (1987) and Barrett and MacLean (1994). Aluminum was chosen as the least mobile element for calculation of the enrichment or depletion factors.

Positive ΔK_2O values are clearly highest in the mine area, correlating well with positive ΔZn, ΔAg and ΔMgO values and moderately well with ΔSiO_2 and ΔFeO_T. This area also shows one of the greatest depletions in Na_2O (Fig. 30). The Lapasuo and Kivisuo-Talassuo areas display a similar behavior, which could indicate potential anomalies related to the same type of mineralization.

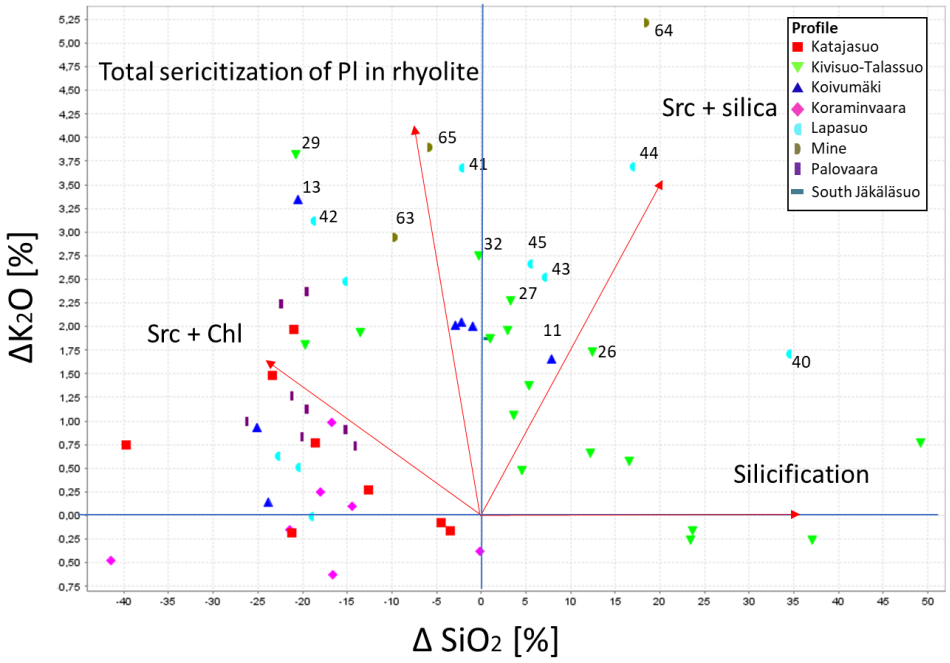

Figure 29. ΔK2O [wt. %] vs ΔSiO2 [wt. %] showing silicification, sericitization + silicification, sericitization + chloritization and total sericitization alteration processes (modified after Buschette and Piercey, 2016).

Some samples from the Lapasuo profile (AC-43, AC-44, AC-45) show a trend towards the same behavior as that of the Taivaljärvi deposit. Furthermore, this behavior is also observed in samples AC-31, AC-26 and AC-27 from the Kivisuo-Talassuo profile.

Gridding plots with mass gain/loss of different elements were constructed to highlight the areas that have undergone major mass changes (Fig. 30). As it can be observed, positive ΔK_2O values are clearly higher in the mine area, correlating well with positive $\Delta FeO_T+\Delta MgO$, ΔLOI (mainly H_2O and CO_2 from carbonates) and metal values (ΔAg+Zn+Pb+Au+Cu) and moderately well with ΔSiO_2. This area also indicates one of the greatest depletions in Na_2O. With this behavior around the mine area as a reference, it can be seen that the Lapasuo and Kivisuo-Talassuo areas have interesting anomalies, correlating rather well with the geophysical responses that were identified in other surveys (Leväniemi, 2018).

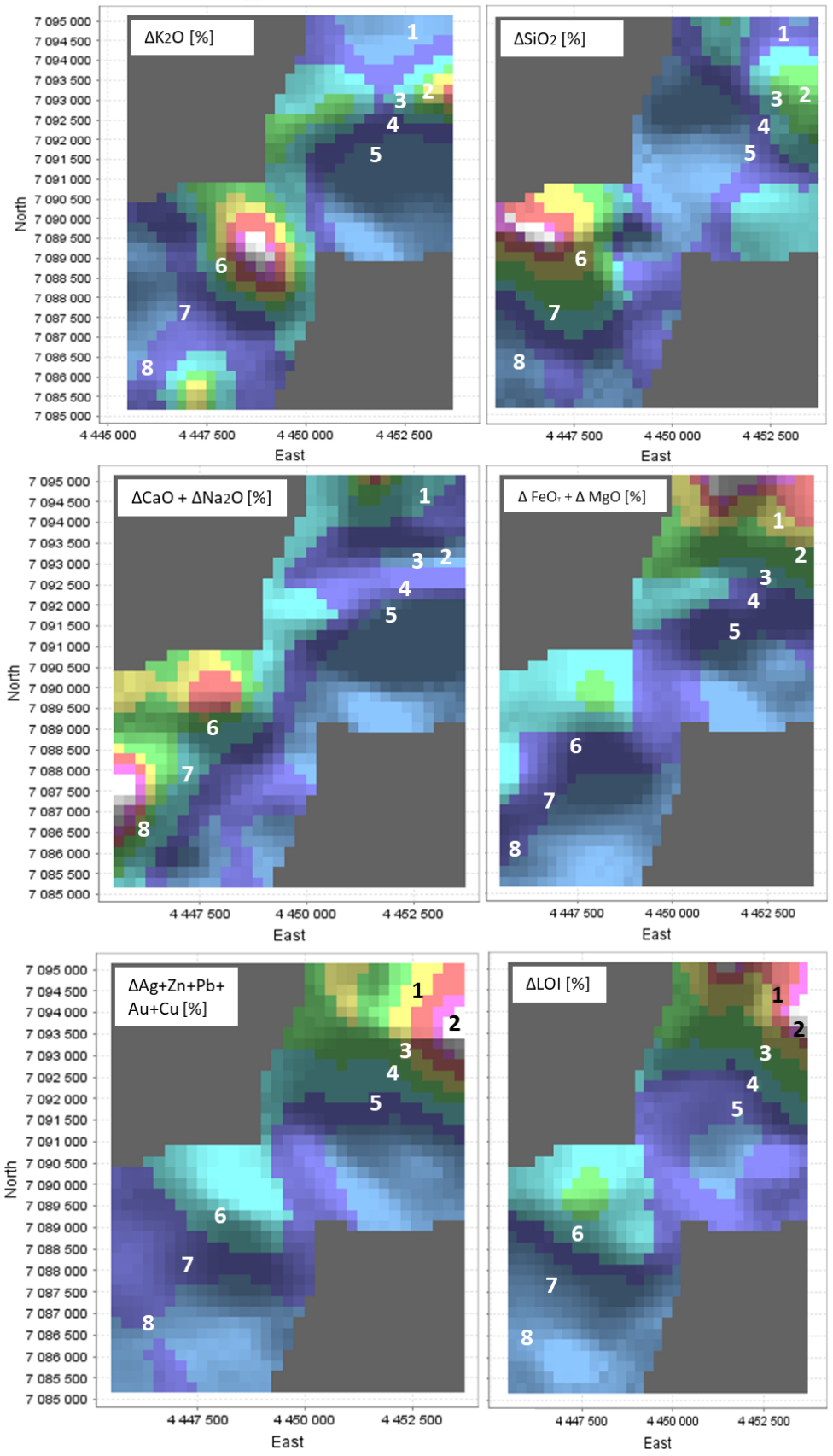

Figure 30. Gridding plots showing spatial gain/loss of major elements and key metals. Warmer colors are higher values of mass change and cooler colours are lower and more negative values. 1: Koraminvaara. 2: Taivaljärvi Mine. 3: South Jäkäläsuo. 4: Koivumäki. 5: Katajasuo. 6: Kivisuo-Talassuo. 7: Lapasuo. 8: Palovaara.

6 EXPLORATION IMPLICATIONS

The geochemical characterization presented in this study, after a careful analyses of alteration styles, major and trace lithogeochemistry, and mass-balance calculations, resulted in useful additional information on the pre-existing targets on the belt. Application of immobile element lithogeochemical methods has proved to be useful to the identification and correlation of anomalies along the Koivumäki Formation, which hosts the Taivaljärvi deposit.

Definition of these pre-existing targets on the belt are of particular importance in further drilling programs in order to assess their potential as well as to add more detailed geochemical data on them, which could lead to a further discovery or in the worst-case scenario assure that they can be dismissed for further surface exploration activities. Moreover, these techniques could be expanded to the Kivisuo-Talassuo and Lapasuo areas in order to lessen the area extension of the anomalies themselves, which would require detailed and probably a grilled sampling campaign in the outcrops nearby that have not been approached. As appreciated during this work, the Kivisuo-Talassuo and Lapasuo areas turned out to be those of most interest and along with the already existing geophysical data, could represent targets that the exploration team should consider for further activities.

7 CONCLUSIONS

The following conclusions can be drawn from this study:

1) Rocks of the Koivumäki Formation range in composition in different areas from intermediate to felsic metavolcanic rocks and quartz-kyanite rocks. They show granolepidoblastic textures with a rough cleavage. Some of the rocks show a porphyritic texture, with quartz porphyroblasts ranging from 1 to 1.5 mm in size.

2) The mineralogy is represented by a quartz-sericite-biotite assemblage with zircon, garnet and sulfides as main accessory phases. Quartz-kyanite rocks also contain staurolite and chloritoid among its Al-rich phases. No apparent connection between quartz-kyanite rocks located in the hanging-wall and the mineralization has been observed.

3) The main alteration processes in the mineralized part of the host unit of the Taivaljärvi deposit are sericitization, chloritization and silicification. These alteration styles are also shown with different degrees of intensity in the Koivumäki Formation along the belt.

4) In terms of Zr/Ti vs Nb/Y ratios, there are two main groups of felsic metavolcanic rocks. In the Mine, and the Kivisuo-Talassuo, Lapasuo and South Jäkäläsuo areas, they are mainly rhyolites whereas samples from the Palovaara and Katajasuo areas and most of the Koraminvaara samples range from rhyodacites to dacites in their composition. All the rocks show a calc-alkaline to transitional affinity with a trace element signature consistent with a continental arc geological setting.

5) The rocks from the mine area are characterized by FII affinities, gently sloping REE patterns with La/Yb_N ratios of 5.5-8, moderate Zr/Y ratios, intermediate HFSE concentrations and negative Eu anomalies (Eu/Eu* 0.35-0.55).

6) They show gains in K_2O, SiO_2, MgO and several metals (e.g., Ag, Pb, Zn, Au), moderate gains in FeO and depletion in Na_2O and CaO. After integrating the trace element geochemical data, alteration indexes and normative alteration mineralogy, and mass-balance calculations, the Lapasuo and Kivisuo-Talassuo areas followed by the Koraminvaara area were identified as those of the highest discovery potential for silver ore.

7) Rocks in the Palovaara, Katajasuo, Koivumäki and South Jäkäläsuo profiles are geochemically less evolved and generally different in terms of their trace element geochemistry, REE patterns, alteration, and mass-gain/loss processes showing less interest from the exploration point of view.

8 ACKNOWLEDGEMENTS

I would first like to thank my supervisor, Eero Hanski, whom I was lucky to have as a professor during my MSc courses. I am grateful to him for offering me a joint project between Oulu Mining School, Sotkamo Silver Oy, and GTK. His expertise and time spent on helping me during this research was invaluable.

I am really thankful to Erkki Kuronen and the exploration team of Sotkamo Silver Oy for giving me the chance to work together both in this project as well as in the company during this time. I would also like to mention Henriikka Ikaheimo, who was my partner during the summer of 2018 and helped me throughout the sampling campaign which served for this project.

I also want to dedicate my gratitude to Dr. Tapio Halkoaho, who was always willing to collaborate and help contributing with his expertise and data.

I would also like to thank all the people at the University who helped me during this research, including Dr. Shenghong Yang, Marko Moilanen and Sari Forss.

Finally, I would like to thank my family without which I would not be able to be where I am now, to my beloved girlfriend Paloma for all the emotional support and love, and to all my friends, the old and the new ones.

9 REFERENCES

Barrett, T.J. and MacLean, W.H. (1994) Chemostratigraphy and hydrothermal alteration in exploration for VHMS deposits in greenstones and younger volcanic rocks, in Lentz, D.R., ed., Alteration and Alteration processes associated with Ore-forming systems: Geological Association of Canada Short Course Notes 11, 433-467.

Barrett, T.J., MacLean, W. H. and Tennant, S.C. (2001). Volcanic sequence and alteration at the parys mountain volcanic-hosted massive sulfide deposit, Wales, United Kingdom: Applications of immobile element lithogeochemistry. Economic Geology 96, 1279-1305.

Barrie, C.T., Ludden, J.N. and Green, A.H. (1993) Geochemistry of Volcanic Rocks associated with Cu-Zn and Ni-Cu deposits in the Abitibi Subprovince: Economic Geology 88, 1341-1358.

Brauhart, C. W., Huston, D. L., Groves, D. I., Mikucki, E. J. and Gardoll, S. J. (2001) Geochemical mass-transfer patterns as indicators of the architecture of a complete volcanic-hosted massive sulfide hydrothermal alteration system, Panorama District, Pilbara, Western Australia. Economic Geology 96, 1263-1278.

Buschette, M. J. and Piercey, S. J. (2016) Hydrothermal alteration and lithogeochemistry of the Boundary volcanogenic massive sulphide deposit, central Newfoundland, Canada. Canadian Journal of Earth Sciences 53, 1-22.

Campbell, I.H., Coad, P., Franklin, J.M., Gorton, M.P., Scott, S.D., Sowa, J. and Thurston, P.C. (1981) Rare earth elements in felsic volcanic rocks associated with Cu-Zn massive sulfide mineralization: Ontario Geological Survey, Miscellaneous Paper 98, 45-53.

Caruso, S., Fiorentini, M.L., Hollis, S.P., LaFlamme, C., Baumgartner, R.J., Steadman, J.A., Savard, D. (2018) The fluid evolution of the Nimbus Ag-Zn-(Au) deposit: An interplay between mantle plume and microbial activity. Precambrian Research 317, 211-229.

Davies, J.F., and Whitehead, R.E. (2006) Alkali-Alumina and MgO-Alumina Molar Ratios of Altered and Unaltered Rhyolites. Exploration and Mining Geology 15, 75-88.

Gaboury, D. and Pearson, V. (2008) Rhyolite geochemical signatures and association with volcanogenic massive sulfide deposits: Examples from the Abitibi Belt, Canada. Economic Geology 103, 1531-1562.

Gaboury, D. (2006) Geochemical approaches in the discrimination of synvolcanic intrusions as a guide for volcanogenic base metal exploration: Example from the Abitibi belt, Canada. Applied Earth Science 115, 71–79.

Hart, T.R., Gibson, H. L. and Lesher, C. M. (2004) Trace element geochemistry and petrogenesis of felsic volcanic rocks associated with volcanogenic massive Cu-Zn-Pb sulfide deposits. Economic Geology 99, 1003-1013.

Hollis, S.P., Mole, D.R., Gillespie, P., Barnes, S.J., Tessalina, S., Cas, R.A.F., Hildrew. C., Pumphrey,

A., Goodz, M.D., Caruso, S., Yeats, C.J., Verbeeten, A., Belford, S.M., Wyche, S., Martin, L.A.J. (2017) 2.7 Ga plume associated VHMS mineralization in the Eastern Goldfields Superterrane, Yilgarn Craton: Insights from the low temperature and shallow water, Ag-Zn-(Au) Nimbus deposit. Precambrian Research 291, 119–142.

Huhma, H., Mänttäri, I., Peltonen, P., Kontinen, A., Halkoaho, T., Hanski, E. Hokkanen, T., Hölttä, P., Juopperi, H., Konnunaho, J., Layahe, Y., Luukkonen. E., Pietikäinen. K., Pulkkinen, A., Sorjonen-Ward, P., Vaasjoki, M. and Whitehouse, M. (2012) The age of the Archaean greenstone belts in Finland. Geological Survey of Finland, Special Paper 54, 74-175.

Ikäheimo, H. (2018) Mineralogical occurrence of gold in the Archean Taivaljärvi Ag-Zn-Pb-Au deposit, Eastern Finland. University of Oulu, Master's thesis, 68 p.

Jensen, L.S. (1976) A new cation plot for classifying subalkalic volcanic rocks; Ontario Div. Mines, MP 66, 22p.

Kackstaetter, U. R. (2014) SEDMIN – Microsoft ExcelTM spreadsheet for calculating fine-grained sedimentary rock mineralogy from bulk geochemical analyses. Central European Journal of Geosciences 6, 170-181.

Kopperoinen, T. and Tuokko, I. (1988) The Ala-Luoma and Taivaljärvi Zn–Pb–Ag–Au deposits, eastern Finland. Geological Survey of Finland, Special Paper 4, 131-144.

Larson, J.E. and Hutchinson, R.W. (1993) The Selbaie Zn-Cu-Ag deposits, Quebec, Canada: an example of evolution from subaqueous to subaerial volcanism and mineralization in an Archaean caldera environment. Economic Geology, 88, 1460-1482.

LaPierre, H., Cabanis, B., Coulon, C., Brouxel, M., and Albarede, F. (1985) Geodynamic setting of early Devonian Kuroko-type sulfide deposits in the eastern Klamath Mountains (northern California) inferred by the petrological and geochemical characteristics of the associated island-arc volcanic rocks. Economic Geology 80, 2100–2113.

Lehtonen, E. (2016) Painting the volcanic landscape of early Fennoscandia-Geochronology of the Meso- and Neoarchaean Suomussalmi-Kuhmo-Tipasjärvi greenstone complex, Karelia Province, Finland. Unigrafia, Helsinki, Academic dissertation, 40 p.

Lehtonen, E. and Käpyaho, A. (2016) A small Archean belt – diverse age ensemble: A U-Pb study of the Tipasjärvi greenstone belt, Karelia Province, central Fennoscandian Shield, Finland. Lithos 246-247, 31-47.

Lentz, D.R., (1996) Trace element systematics of felsic volcanic rocks associated with massive sulfide deposits in the Bathurst mining camp: Petrogenetic, tectonic and chemostratigraphic implications for VMS exploration. Geological Association of Canada Short Course Notes 12, 359–402.

Lesher, C.M., Goodwin, A.M., Campbell, I.H. and Gorton, M.P. (1986) Trace element geochemistry of ore-associated and barren felsic metavolcanics rocks in the Superior Province, Canada. Canadian Journal of Earth Science 23, 222-237.

Leväniemi, H. (2018) Tipasjärven tihennyslentoalueen aineistokäsittely ja -tulkinta. Unpublished

report. Sotkamo Silver Oy, 28p.

Lindborg, T., Papunen, H., Parkkinen, T. and Tuokko, I. (2015) The Taivaljärvi Ag-Au-Zn deposits in the Archean Tipasjärvi greenstone belt, eastern Finland. In: Maier, W., Lahtinen, R. And O'Brien, H. (Eds.), Mineral Deposits of Finland, Elsevier, Amsterdam, p. 633-657.

Lodders, K. (1996) An experimental and theoretical study of rare-earth-element partitioning between sulfides (FeS, CaS) and silicate and applications to enstatite achondrites. Meteoritics and Planetary Science 31, 749-766.

Luukkonen, E. J. (1988) The structure and stratigraphy of the northern part of the late Archaean Kuhmo greenstone belt, eastern Finland. Geological Survey of Finland, Special Paper 4, 71-96.

Luukkonen, E. J. (1991) Late Archaean and Early Proterozoic structural evolution in the Kuhmo-Suomussalmi Terrain, eastern Finland. Annales Universitatis Turkuensis, Ser. A. II 78, 1–37.

MacLean, W. H. and Kranidiotis, P. (1987) Immobile elements as monitors of mass transfer in hydrothermal alteration: Phelps Dodge massive sulfide deposit, Matagami, Quebec. Economic Geology 82, 951-962.

MacLean, W.H. (1988) Rare earth element mobility at constant inter-REE ratios I the alteration zone at the Phelps Dodge massive sulfide deposit, Matagami, Quebec. Mineralium Deposita 23, 231–238.

MacLean, W.H., and Hoy, L.D. (1991) Geochemistry of hydrothermally altered rocks at the Horne mine, Noranda, Quebec. Economic Geology 86, 506–528.

Maier, W. D., Peltonen, P., Halkoaho, T. and Hanski, E. (2013) Geochemistry of komatiites from the Tipasjärvi, Kuhmo, Suomussalmi, Ilomantsi and Tulppio greenstone belts, Finland: implications for tectonic setting and Ni sulfide prospectivity. Precambrian Research, 228, 63-84.

Mäki, T., Kousa, J., Luukas, J. (2015) The Vihanti-Pyhäsalmi VMS belt. In: Maier, W., Lahtinen, R., O'Brien, H. (Eds.), Mineral Deposits of Finland, Elsevier, Amsterdam, 508-530.

Mitjavila, J.M., Marti, J., and Soriano, C. (1997) Magmatic evolution and tectonic setting of the Iberian pyrite belt volcanism. Journal of Petrology 38, 728–755.

Ohmoto, H. (1996) Formation of volcanogenic massive sulfide deposits: The Kuroko perspective. Ore Geology Reviews 10, 135-177.

Paholski, G., Kuronen, E., Kankkunen, J., Lovén, P., Hindström, S., Ohtonen, A., Niemelä, J., Seppälä, J. and Veisto, P. (2017) Sotkamo Silver Oy Technical Report 2017, 313 p.

Papunen H. and Parkkinen, J. (2011) Exploration potential combined with the Sotkamo Silver Mine. Research report, 58 p.

Papunen, H., Halkoaho, T. and Luukkonen, E. (2009) Archaean evolution of the Tipasjärvi-Kuhmo-Suomussalmi Greenstone Complex, Finland. Geological Survey of Finland, Bulletin 403, 68 pp.

Papunen, H., Kopperoinen, T. and Tuokko, I. (1989) The Taivaljärvi Ag-Zn deposit in the Archean greenstone belt, eastern Finland. Economic Geology 84, 1262-1276.

Paulick, H., Hermann, W. and Gemmell, J. B. (2001) Alteration of felsic volcanics hosting the Thalanga massive sulfide deposit (Northern Queensland, Australia) and geochemical proximity

indicators to ore. Economic Geology 96, 1175-1200.

Pearce, J.A. (2008) Geochemical Fingerprinting of Oceanic Basalts with Applications to Ophiolite Classification and the Search for Archean Oceanic Crust. Lithos 100, 14-48.

Piercey, S. (2009) Lithogeochemistry of volcanic rocks associated with volcanogenic massive sulfide (VMS) deposits and applications to exploration. In B. Cousens and S.J. Piercey (Eds.) Submarine Volcanism and Mineralization: Modern Through Ancient, Geological Association of Canada, Short Course, 29-30 May 2008, Quebec City, Canada, p. 15-40.

Pietikäinen, K., Halkoaho, T., Hartikainen, A. and Niskanen, M. (2008) Tipasjärven vihreäkivivyöhykkeen malmivarojen kartoitushankkeen (2901006) toiminta vuosina 2005-2007 Sotkamon, Valtimon, Kuhmon ja Nurmeksen alueilla. Geologian Tutkimuskeskus, Itä-Suomen Yksikkö, 62 p.

Piirainen, T. (1988) The geology of the Archaean greenstone–granitoid terrain in Kuhmo, eastern Finland. Archean geology of the Fennoscandian Shield. Geological Survey of Finland, Special Paper 4, 39-51.

Prior, G.J., Gibson, H.L., Watkinson, D.H., Cook, R.E., and Hannington, M.D. (1999) Rare earth and high field strength element geochemistry of the Kidd Creek rhyolites, Abitibi greenstone belt, Canada: Evidence for Archean felsic volcanism and massive sulfide ore formation in an Icelandic style rift environment. Economic Geology Monograph 10, 457–484.

Rollinson, H., (1993) Using Geochemical Data: Evaluation, Presentation, Interpretation. Longman Scientific and Technical, Harlow, 352p.

Ross, P. S., and Bedard, J.H. (2009) Magmatic affinity of modern and ancient subalkaline volcanic rocks determined from trace-element discriminant diagrams. Canadian Journal of Earth Sciences 46, 823–839.

Sorjonen-Ward, P. and Luukkonen, E. J. (2005) Archean rocks. In: Lehtinen, M., Nurmi, P.A., and Rämö, O.T. (Eds.), Precambrian Geology of Finland – Key to the Evolution of the Fennoscandian Shield. Amsterdam, Elsevier B.V., p. 19–99.

Sotkamo Silver Oy (2017) Årsredovisning 2017. Annual Report, 76 p.

Syme, E.C., 1998, Ore-associated and barren rhyolites in the Central Flin Flon belt: Case study of the Flin Flon mine sequence. Manitoba Energy and Mines Geological Services Open File Report OF98-9, 26 p.

Taipale, K. (1983) The geology and geochemistry of the Archaean Kuhmo greenstone-granite terrain in the Tipasjärvi area, eastern Finland. University of Oulu, Master's thesis, 46 p.

Tuokko, I. and Kopperoinen, T. (1989) Tutkimustyöseloste valtaukselta Kivimaisema (kaivosrek.no 3543/1) Sotkamon kunnassa., Yhtyneet paperitehtaat Oy, Kajaani.

Weihed, J.B., Bergstrom, U., Billstrom, K., and Weihed, P. (1996) Geology, tectonic setting, and origin of the Paleoproterozoic Boliden Au-Cu-As deposit, Skellefte district, northern Sweden. Economic Geology 91, 1073–1097.

Winchester, J.A. and Floyd, P.A. (1977) Geochemical discrimination of different magma series and their differentiation products using immobile elements. Chemical Geology 20, 325-343.

Wright-Holfeld, A., Mercier-Langevin, P., and Dubé, B. (2011) Mass changes and element mobility associated with the Westwood deposit ore zones, Doyon-Bousquet-LaRonde mining camp, Abitibi, Quebec. Geological Survey of Canada, Current Research 2011-8, 15p.

APPENDICES

Appendix 1. Whole-rock geochemistry

Sample	AC-1	AC-2	AC-3	AC-4	AC-5	AC-6	AC-7	AC-8	AC-9	AC-10
Profile	Koraminvaara	Koraminvaara	Koraminvaara	Koraminvaara	Koraminvaara	Koraminvaara	Koraminvaara	South Jäkäläsuo	South Jäkäläsuo	Koivumäki
[%]										
SiO_2	69.8	62.55	63.84	67.88	67.22	75.67	70.16	75.49	42.07	66.62
TiO_2	0.37	0.47	0.38	0.4	0.46	0.24	0.5	0.16	0.83	0.52
Al_2O_3	11.97	14.94	13.99	14.36	15.1	12.95	15.41	12.79	20.1	17.06
Fe_2O_3	8.08	8.9	7.52	4.75	5.82	3.03	4.18	2.29	12.28	4.79
MnO	0.24	0.22	0.12	0.11	0.12	0.03	0.16	0.11	0.37	0.05
MgO	3.29	3.41	3.34	2.8	1.79	0.66	0.91	1.04	7.27	1.95
CaO	3.5	5.32	4.28	4.18	1.52	0.98	5.23	2.15	5.96	4.19
Na_2O	0.98	1.41	1.23	1.83	3.65	5.86	1.26	1.11	0.65	1.78
K_2O	0.27	0.6	0.05	0.85	1.07	0.67	1.97	2.51	4.67	2.11
BaO	0.01	<0.01	<0.01	0.01	0.02	0.02	0.03	0.04	0.01	0.03
P_2O_5	0.07	0.08	0.08	0.09	0.08	0.03	0.08	0.01	0.26	0.12
Cr_2O_3	<0.01	<0.01	<0.01	<0.01	<0.01	<0.01	<0.01	<0.01	<0.01	<0.01
SrO	<0.01	0.01	<0.01	0.01	<0.01	0.01	<0.01	<0.01	<0.01	<0.01
LOI	3.25	3.51	3.42	1.9	2.22	0.53	1.79	1.8	4.32	1.46
TC	<0.01	<0.01	<0.01	<0.01	0.02	0.02	0.02	<0.01	0.01	0.02
TS	1.77	1.61	0.98	<0.01	0.01	0.06	0.24	0.24	3.31	<0.01
Total	101.84	101.41	98.25	99.16	99.08	100.67	101.69	99.5	98.78	100.67
[ppm]										
Ba	96	53.1	9.9	114.3	162.8	149.7	254.2	368.2	117.9	218
Sr	62.7	92.4	75.6	76.1	71.5	75	72.4	65.1	44.4	70.9
Rb	11.9	28.6	2	31.9	32.2	17.1	68.4	77.1	198.6	100.5
Cs	0.5	1.5	0.09	2.65	1.54	0.42	2.59	1.97	4.02	2.42
Ga	15.7	18.8	17.6	13.3	17.2	20.3	18.1	18.3	26.5	18.3
Y	9.4	11.1	11.8	9.9	8.8	25.8	12.6	27.4	34	10.5
Zr	89	112	126	113	101	184	121	184	171	141
Hf	2.2	3	3	2.9	2.5	5.1	3	5.4	4.6	3.7
V	60	79	56	42	65	16	76	<10	114	72
Hg	<0.005	<0.005	<0.005	<0.005	<0.005	<0.005	<0.005	<0.005	<0.005	<0.005
Cr	24	27	21	24	14	<10	27	<10	60	31
Ni	16.3	16.4	5.8	3.8	10.6	3.1	12.8	1.1	50.7	10.8
Cu	46.9	3.8	8.2	2.7	13	5.9	28.3	10.8	49.6	1.5
Zn	158	133	82	105	78	31	110	99	425	96
As	3	7.8	2.8	0.6	0.5	1	0.7	1.4	4.3	0.9
Se	0.2	0.2	0.4	<0.2	<0.2	<0.2	<0.2	<0.2	<0.2	<0.2
Mo	2.03	1.57	2.62	3.08	0.85	5.92	1.63	3.19	1.48	2.98
Ag	0.38	0.16	0.08	0.08	0.08	0.12	0.68	0.17	0.5	0.08
Cd	0.11	0.21	0.09	0.05	0.02	0.02	0.18	0.09	0.15	0.32
Sn	<5	<5	<5	<5	<5	<5	<5	<5	<5	<5
Sb	0.1	0.19	0.08	0.06	<0.05	0.05	0.08	<0.05	0.08	<0.05
W	1	<1	<1	<1	<1	<1	<1	1	<1	<1
Pb	10	14.7	10.2	9.6	4.3	4.6	49.8	18.3	28.6	25.7
Bi	0.33	2.18	0.28	0.15	0.13	0.1	0.34	0.11	0.14	0.09
Au	0.0035	0.004	0.0007	<0.0005	<0.0005	0.0006	0.001	0.0007	0.0013	<0.0005
Tl	0.12	0.21	<0.02	0.25	0.43	0.08	0.33	0.29	1.3	0.58
Nb	2.6	2.8	3.3	3.4	2.1	6.9	3.1	9	7.1	4.4
U	0.42	0.75	0.68	0.59	0.42	2.65	0.89	2.17	2	1.8
Th	0.84	1.26	1.02	1.07	0.85	3.37	1.61	3.54	3.83	2.7
Ta	0.9	1	1	1	1	1.1	1.2	1.1	1	1
REE [ppm]										
La	13.5	16.8	17	14.2	10.2	25.8	17.5	37.3	29.5	18
Ce	26.2	30.3	31.1	28.4	19.2	54.7	33.3	75.9	64.1	34.8
Pr	3.12	3.47	3.58	3.2	2.25	6.45	3.77	8.72	7.73	4.23
Nd	11.9	13.3	13.6	12.3	8.8	24.3	14.7	33.4	31.1	15.6
Sm	2.19	2.59	2.49	2.22	1.85	5.3	2.92	6.36	6.06	2.83
Eu	1.03	0.7	1.31	0.99	0.69	0.92	1.36	1.02	1.76	0.81
Gd	2.15	2.37	2.38	2.03	1.89	4.68	2.81	5.59	6.31	2.36
Tb	0.3	0.34	0.35	0.29	0.29	0.74	0.43	0.9	1.03	0.36
Dy	1.68	1.83	1.94	1.64	1.6	4.1	2.41	5.14	5.96	1.87
Ho	0.32	0.38	0.38	0.34	0.33	0.86	0.46	1.06	1.24	0.38
Er	0.95	1.19	1.19	0.99	0.96	2.82	1.4	3.28	3.83	1.22
Tm	0.14	0.17	0.17	0.14	0.15	0.42	0.21	0.51	0.55	0.2
Yb	0.76	1.17	1.09	0.88	0.9	2.78	1.27	3.19	3.4	1.26
Lu	0.12	0.19	0.18	0.14	0.14	0.43	0.2	0.5	0.54	0.22

Sample	AC-11	AC-12	AC-13	AC-14	AC-15	AC-16	AC-17	AC-18	AC-19	AC-20
Profile	Koivumäki	Koivumäki	Koivumäki	Koivumäki	Koivumäki	Katajasuo	Katajasuo	Katajasuo	Katajasuo	Katajasuo
[%]										
SiO_2	78.72	75.49	66.01	74.72	75.77	71.47	70.12	60.32	66.23	68.66
TiO_2	0.07	0.08	0.68	0.23	0.24	0.44	0.35	0.72	0.51	0.6
Al_2O_3	12.2	13.09	15.49	13.18	13.48	16.97	15.91	21.73	16.38	16.26
Fe_2O_3	1.79	1.77	6.18	2.68	2.37	4.49	2.07	4.2	5.32	4.23
MnO	0.06	0.03	0.21	0.04	0.03	0.22	0.05	0.15	0.09	0.09
MgO	1	0.98	3.33	0.99	1.03	0.91	1.32	1.33	2.11	0.7
CaO	1.73	1.61	1.83	2.02	1.56	0.14	4.87	3.91	3.39	2.46
Na_2O	1.12	1.03	0.54	1.06	0.83	0.44	2.09	3.24	2.28	0.86
K_2O	2.19	2.7	4.8	2.76	2.79	0.63	1.76	2.37	2.72	3.31
BaO	0.04	0.05	0.04	0.04	0.04	<0.01	0.02	0.07	0.04	0.04
P_2O_5	<0.01	<0.01	0.21	0.03	0.03	0.07	0.06	0.14	0.09	0.14
Cr_2O_3	<0.01	<0.01	<0.01	<0.01	<0.01	<0.01	<0.01	<0.01	<0.01	<0.01
SrO	<0.01	<0.01	<0.01	<0.01	<0.01	<0.01	0.03	0.02	0.01	<0.01
LOI	1.68	1.89	2.36	1.94	2.28	2.63	1.32	2.55	1.29	2.27
TC	0.02	0.02	0.01	0.01	0.01	<0.01	0.01	<0.01	<0.01	<0.01
TS	<0.01	0.12	0.27	1.04	0.56	0.07	<0.01	<0.01	<0.01	<0.01
Total	100.6	98.73	101.68	99.69	100.45	98.41	99.98	100.74	100.45	99.62
[ppm]										
Ba	319.4	399.9	338.7	382.5	323.2	54.1	164.4	611.3	304.9	373
Sr	38	34.8	39.1	35.9	28	19.7	202.6	127.7	94	45.7
Rb	63.6	75.9	146.4	79.2	65.6	13.6	34.7	33.7	73.8	85.7
Cs	0.89	1.31	2.39	1.29	0.91	0.28	2.2	0.72	3.68	2.26
Ga	17.8	19.3	18.2	19.1	20	25.4	18	24.8	18.5	20
Y	8.5	13	14.9	26.1	18.2	3.8	5.2	11.7	15.9	16.9
Zr	100	103	134	175	171	113	92	152	127	134
Hf	3.7	3.8	3.8	5.1	5.1	2.8	2.4	4.5	3.3	3.4
V	<10	<10	88	13	13	62	41	118	84	107
Hg	<0.005	<0.005	<0.005	<0.005	<0.005	<0.005	<0.005	<0.005	<0.005	<0.005
Cr	<10	<10	38	<10	<10	30	26	30	27	44
Ni	1.9	1.3	14.8	2	2.1	16.9	18.7	8.2	16.8	12.3
Cu	3.5	8.7	24.9	3.8	1.4	8.7	1.7	1.3	4.2	4.2
Zn	39	47	267	28	29	43	27	35	67	38
As	0.9	1.2	1.3	5.8	5.1	0.4	0.4	0.6	0.9	0.8
Se	<0.2	<0.2	<0.2	<0.2	<0.2	<0.2	<0.2	<0.2	<0.2	<0.2
Mo	2.51	3.73	1.42	3.16	3.66	2.03	1.34	0.78	0.73	1.87
Ag	0.13	0.3	0.25	0.18	0.15	0.07	0.04	0.1	0.06	0.08
Cd	0.06	0.06	0.11	0.03	0.03	0.02	0.03	0.06	0.04	0.1
Sn	<5	<5	<5	<5	<5	<5	<5	<5	<5	<5
Sb	<0.05	0.06	0.06	0.07	0.05	<0.05	<0.05	<0.05	0.06	<0.05
W	<1	<1	<1	2	3	<1	<1	4	<1	6
Pb	18.2	15.3	16.3	15.3	13.3	3.3	5.4	9.3	8.4	12.3
Bi	0.07	0.08	0.07	0.3	0.32	0.09	0.04	0.04	0.06	0.05
Au	<0.0005	0.001	0.0016	0.0017	0.0022	0.0005	<0.0005	0.0013	0.001	<0.0005
Tl	0.17	0.23	0.69	0.21	0.11	0.03	0.11	0.06	0.29	0.21
Nb	12.9	13.7	7.6	8.9	8.4	<0.1	<0.1	5.1	3.1	4.6
U	1.48	3.13	1.9	2.93	2.15	0.69	0.36	0.75	1.21	0.96
Th	4.65	5.47	2.84	11.06	11.64	0.47	0.43	5.13	3.93	2.57
Ta	1.3	1.2	1	1.1	1.2	0.8	0.7	1.1	1	1
REE [ppm]										
La	17.2	23.6	31	36.3	28.3	9.4	8.6	12.8	28	21.5
Ce	43.1	56.3	64.5	70.2	54.7	17.2	16	42.9	42.2	44.5
Pr	5.43	6.86	7.84	7.84	6.07	1.94	1.91	3.44	5.87	5.07
Nd	20	25.7	30.4	28.7	22.3	7.4	7.6	12.9	22.4	20.1
Sm	3.87	4.91	5.1	5.46	4.25	1.5	1.45	2.55	3.97	3.93
Eu	0.34	0.37	1.24	0.83	0.66	0.47	0.48	0.84	1.04	0.97
Gd	2.59	3.55	4.03	5.42	3.85	1.27	1.32	2.16	3.51	3.48
Tb	0.32	0.51	0.54	0.82	0.59	0.17	0.18	0.35	0.51	0.54
Dy	1.77	2.62	2.82	4.6	3.35	0.76	0.86	2.04	2.76	3.04
Ho	0.39	0.54	0.56	0.95	0.68	0.14	0.17	0.44	0.57	0.61
Er	1.47	1.79	1.68	2.87	2.2	0.45	0.53	1.52	1.69	1.84
Tm	0.32	0.3	0.24	0.43	0.33	0.05	0.07	0.24	0.24	0.27
Yb	2.34	2.16	1.55	2.64	2.22	0.34	0.46	1.64	1.35	1.68
Lu	0.4	0.37	0.26	0.42	0.37	0.06	0.08	0.27	0.22	0.27

Sample	AC-21	AC-22	AC-23	AC-24	AC-25	AC-26	AC-27	AC-28	AC-29	AC-30
Profile	Kivisuo-Talassuo	Kivisuo-Talassuo	Kivisuo-Talassuo	Kivisuo-Talassuo	Kivisuo-Talassuo	Kivisuo-Talassuo	Kivisuo-Talassuo	Kivisuo-Talassuo	Kivisuo-Talassuo	Kivisuo-Talassuo
[%]										
SiO_2	73.67	77.04	86.67	71.67	77.15	79.26	75.58	65.93	69.6	76.27
TiO_2	0.22	0.22	0.2	0.28	0.19	0.16	0.23	0.5	0.55	0.19
Al_2O_3	12.45	12.43	11.33	14.93	12.7	11.65	12.4	15.24	16.42	12.45
Fe_2O_3	3.36	3.19	0.31	1.2	2.26	2.5	1.96	6.4	4.26	2.39
MnO	0.06	0.08	<0.01	0.01	0.03	0.02	0.02	0.12	0.06	0.03
MgO	1.4	0.82	0.02	1.03	1.4	1.87	1.2	1.41	0.71	1.4
CaO	2.59	0.17	0.08	0.7	0.34	0.37	0.68	1.97	0.95	0.99
Na_2O	0.91	0.88	0.5	3.51	1.54	1.51	1.18	3.62	0.99	2.83
K_2O	2.44	1.1	0.36	3	2.58	2.16	2.82	2.91	5.69	1.66
BaO	0.03	<0.01	<0.01	0.06	0.04	0.03	0.05	0.06	0.07	0.02
P_2O_5	0.03	0.02	0.03	0.04	<0.01	<0.01	0.02	0.06	0.08	0.01
Cr_2O_3	<0.01	<0.01	<0.01	<0.01	<0.01	<0.01	<0.01	<0.01	<0.01	<0.01
SrO	0.01	0.01	<0.01	0.01	0.01	<0.01	<0.01	0.02	0.02	0.02
LOI	1.61	1.94	1.47	1.56	2.01	2.07	1.94	1.18	2.45	1.53
TC	<0.01	<0.01	<0.01	<0.01	0.02	<0.01	0.02	0.03	0.02	0.03
TS	<0.01	<0.01	<0.01	<0.01	<0.01	<0.01	<0.01	<0.01	0.28	<0.01
Total	98.76	97.92	100.98	98.01	100.24	101.61	98.08	99.42	101.86	99.77
[ppm]										
Ba	276.2	89.9	16.9	533.6	343.1	276.2	423.8	557.2	585.5	146
Sr	87.3	92.7	40.1	114.9	78.4	67.7	60.5	135.6	141	137.6
Rb	98.1	39.2	8.5	120.6	129.5	92.5	71.6	65.4	121.1	107.1
Cs	2.1	0.42	0.14	3.27	1.25	1.1	2.46	1.55	1.23	1.5
Ga	17.8	17.4	17.7	23.8	19	17.3	18.9	18.5	22	17.7
Y	22	26.1	20.5	23.8	29	28	24.3	24	14.8	42.2
Zr	160	134	134	193	249	223	194	160	169	234
Hf	4.9	4.1	3.9	5.9	6.7	6.2	5.9	4.4	4.4	6.1
V	11	24	13	13	<10	<10	<10	62	51	<10
Hg	<0.005	<0.005	<0.005	<0.005	<0.005	<0.005	<0.005	<0.005	<0.005	<0.005
Cr	<10	<10	13	<10	21	14	17	25	35	<10
Ni	4.1	4.8	1.2	6.4	1.7	1.3	8.9	30.3	26.2	2
Cu	2.3	1.7	1.9	9.3	2.3	3.2	3.6	3.8	56	16.4
Zn	50	13	2	21	34	43	24	64	125	42
As	1.2	0.9	1.1	1	1.2	1	0.3	1	0.8	1.4
Se	<0.2	<0.2	<0.2	<0.2	<0.2	<0.2	<0.2	<0.2	<0.2	<0.2
Mo	2.46	3.37	3.17	1.39	5.02	1.84	4.53	1.92	1.31	2.39
Ag	0.07	0.07	0.03	0.1	0.08	0.07	0.06	0.07	0.14	0.08
Cd	0.09	0.03	<0.02	<0.02	<0.02	<0.02	<0.02	0.02	0.05	0.02
Sn	<5	<5	<5	<5	<5	<5	<5	<5	<5	<5
Sb	<0.05	<0.05	<0.05	<0.05	<0.05	<0.05	<0.05	<0.05	<0.05	<0.05
W	<1	<1	<1	<1	<1	<1	<1	<1	<1	<1
Pb	10.6	7	6.6	7.6	5.8	5.5	4.7	6.1	13.7	9
Bi	0.09	0.03	1.6	0.12	0.05	0.07	0.39	0.2	0.17	0.2
Au	<0.0005	0.0022	<0.0005	<0.0005	<0.0005	<0.0005	<0.0005	<0.0005	<0.0005	0.0005
Tl	0.36	0.03	<0.02	0.23	0.22	0.16	0.14	0.21	0.15	0.24
Nb	6.7	6.7	5.4	10.4	10.5	8.3	8.2	5.9	6.7	9.8
U	2.25	1.75	3.28	3.33	2.54	2.73	2.19	1.27	1.63	3.01
Th	9.95	10.79	9.09	14.34	11.42	3.54	3.05	3.35	3.09	3.78
Ta	1.1	1.1	1.2	1.3	1.5	1.2	1.1	1	1.1	1.2
REE [ppm]										
La	36.6	29.5	37	28.1	41	32.6	2.9	33	21.1	48.9
Ce	83	58.3	72.1	60.5	83.4	68.5	17.2	56	45.1	94.4
Pr	8.22	6.63	8.1	6.82	9.65	7.96	0.98	7.12	5.37	10.9
Nd	31	25.1	30.4	25.1	36.1	30.2	4.3	26.4	19.9	42
Sm	5.82	4.75	5.74	5.12	6.88	5.94	2.27	4.82	4.25	8.32
Eu	0.92	0.76	0.69	0.86	1.29	1.1	0.66	1.01	0.78	1.49
Gd	5.13	4.41	4.98	4.6	6.2	5.67	3.04	4.66	3.54	8.05
Tb	0.77	0.7	0.75	0.78	0.98	0.89	0.62	0.73	0.54	1.25
Dy	4.2	4.16	3.84	4.49	5.47	5.05	4.02	3.98	3.09	6.83
Ho	0.86	0.89	0.76	0.9	1.12	1.05	0.87	0.83	0.59	1.41
Er	2.66	2.94	2.25	2.77	3.29	3.18	2.73	2.75	1.77	4.3
Tm	0.4	0.44	0.33	0.43	0.47	0.46	0.41	0.42	0.24	0.61
Yb	2.65	2.86	2.11	2.72	2.9	2.97	2.54	2.69	1.51	3.74
Lu	0.41	0.47	0.33	0.42	0.44	0.48	0.39	0.42	0.25	0.58

Sample	AC-31	AC-32	AC-33	AC-34	AC-35	AC-36	AC-37	AC-38	AC-39	AC-40
Profile	Kivisuo-Talassuo	Kivisuo-Talassuo	Kivisuo-Talassuo	Kivisuo-Talassuo	Kivisuo-Talassuo	Kivisuo-Talassuo	Kivisuo-Talassuo	Kivisuo-Talassuo	Lapasuo	Lapasuo
[%]										
SiO_2	77.47	74.63	81.92	29.86	86.64	82.58	77.06	82.33	70.95	81.62
TiO_2	0.21	0.24	0.22	0.23	0.17	0.18	0.17	0.15	0.56	0.11
Al_2O_3	12.38	12.82	12.07	4.44	8.99	10.77	10.82	9.46	17.37	9.6
Fe_2O_3	1.91	2.88	0.42	12.52	0.25	2.3	5.25	0.71	0.89	1.61
MnO	0.03	0.03	<0.01	0.19	<0.01	<0.01	0.03	<0.01	0.03	0.03
MgO	0.42	0.58	0.06	29.62	0.02	0.02	0.96	0.02	0.24	0.69
CaO	1.53	0.67	0.11	1.85	<0.01	0.04	0.08	0.48	2.54	0.88
Na_2O	3.72	1.74	0.66	<0.01	0.13	0.36	0.44	4.41	4.21	2.4
K_2O	1.95	3.38	1.24	0.01	1	0.42	1.04	0.3	1.74	1.76
BaO	0.05	0.06	<0.01	<0.01	<0.01	<0.01	<0.01	<0.01	0.06	0.02
P_2O_5	0.02	0.03	<0.01	<0.01	<0.01	0.04	0.04	0.06	0.13	0.02
Cr_2O_3	<0.01	<0.01	<0.01	0.49	<0.01	<0.01	<0.01	<0.01	<0.01	<0.01
SrO	0.02	<0.01	<0.01	<0.01	<0.01	<0.01	<0.01	<0.01	0.04	<0.01
LOI	0.82	1.94	2.1	20.23	1.14	2.06	2.28	0.57	1.08	0.74
TC	0.02	0.08	<0.01	4.48	0.05	<0.01	<0.01	0.13	0.02	<0.01
TS	<0.01	0.01	<0.01	0.1	<0.01	1.61	1.36	<0.01	<0.01	<0.01
Total	100.55	99.01	98.8	99.43	98.34	98.78	98.17	98.48	99.83	99.47
[ppm]										
Ba	495.3	515.1	34.7	2.2	12.2	29.7	18.4	47.2	520.3	161.4
Sr	144.4	57.1	71.1	15.4	13.4	54.2	49.8	33.6	289.8	48.1
Rb	64.5	121.5	40.9	0.5	25	12.2	44.6	7.5	40.3	60.9
Cs	1.69	2.01	0.65	0.04	0.17	0.22	0.54	0.07	0.38	1.98
Ga	16.9	20.8	15.7	5.1	13.2	14.1	19	8	19.9	11.7
Y	25.2	18	12.4	2.4	6.8	14.6	23.1	16.5	7.5	24.5
Zr	148	171	131	11	92	104	112	92	97	132
Hf	4.4	5.2	3.8	<0.2	3	3.2	3.3	3	3.1	3.9
V	10	14	13	110	<10	<10	12	<10	72	<10
Hg	<0.005	<0.005	<0.005	<0.005	<0.005	0.011	<0.005	<0.005	<0.005	<0.005
Cr	<10	<10	<10	4905	<10	<10	<10	<10	25	<10
Ni	3.5	1.3	6.9	1241.1	1.7	59.5	20	1.2	3.2	1.2
Cu	4.3	12.7	0.8	63	1.1	1	26.9	4.8	4.8	6.3
Zn	18	29	6	105	2	60	34	2	7	38
As	1.2	0.3	0.5	0.5	0.5	56.4	0.7	1.1	0.4	0.4
Se	<0.2	<0.2	<0.2	<0.2	<0.2	<0.2	<0.2	<0.2	<0.2	<0.2
Mo	1.31	1.55	1.45	0.13	1.8	4.25	2.44	1.89	0.73	2.27
Ag	0.06	0.11	0.04	0.03	0.03	0.05	0.09	0.05	0.04	0.18
Cd	<0.02	<0.02	<0.02	0.07	<0.02	0.18	<0.02	<0.02	<0.02	0.02
Sn	<5	<5	<5	<5	<5	<5	<5	<5	<5	<5
Sb	<0.05	<0.05	<0.05	<0.05	<0.05	0.09	<0.05	<0.05	<0.05	<0.05
W	<1	2	<1	<1	1	2	1	<1	1	<1
Pb	8.3	8.2	8	1.2	3	11.8	9.8	7.9	5	9.2
Bi	0.31	0.4	0.01	0.35	0.04	1.12	0.91	0.1	0.03	0.54
Au	<0.0005	<0.0005	<0.0005	0.0047	<0.0005	0.0022	0.0024	<0.0005	0.0006	0.0006
Tl	0.14	0.13	<0.02	<0.02	<0.02	<0.02	0.08	<0.02	<0.02	0.15
Nb	5.6	8.3	5.2	<0.1	5.1	5.6	5.1	5.3	4.5	5.6
U	1.68	3.29	3.13	<0.05	1.53	2.32	2.39	2.04	0.67	1.39
Th	11.62	11.98	3.78	0.31	2.61	4.38	5.35	4.74	1.93	3.45
Ta	1.3	1.3	1.1	0.8	1	1.1	1	1	0.9	1
REE [ppm]										
La	41.3	2.3	14.3	0.3	14.9	26.9	18.6	41	10	9.8
Ce	73.4	6	28.4	1.2	31	52.5	38.1	77.2	34.4	29.5
Pr	9.01	0.7	3.3	0.14	3.51	5.88	4.3	8.55	2.45	2.33
Nd	33.7	2.8	12.3	0.7	13.1	21.3	16.2	31.3	9.3	8.6
Sm	6.07	1.09	2.28	0.23	2.44	3.98	3.3	6.1	2.13	2.09
Eu	0.92	0.34	0.31	0.09	0.34	0.56	0.51	0.97	0.72	0.48
Gd	5.53	1.52	2.09	0.31	2	3.55	3.65	5.33	1.98	2.25
Tb	0.83	0.4	0.34	0.06	0.26	0.52	0.64	0.75	0.28	0.47
Dy	4.51	2.92	2.03	0.4	1.42	2.96	4.09	4.06	1.62	3.82
Ho	0.92	0.66	0.44	0.09	0.27	0.56	0.85	0.72	0.29	0.86
Er	2.76	2.17	1.45	0.28	0.77	1.56	2.4	1.85	0.77	2.7
Tm	0.4	0.34	0.24	0.04	0.11	0.21	0.35	0.24	0.09	0.42
Yb	2.41	2.34	1.53	0.34	0.8	1.43	2.28	1.48	0.57	2.71
Lu	0.38	0.37	0.26	0.06	0.13	0.21	0.34	0.21	0.09	0.42

Sample	AC-41	AC-42	AC-43	AC-44	AC-45	AC-46	AC-47	AC-48	AC-49	AC-50	AC-51	AC-52
Profile	Lapasuo	Lapasuo	Lapasuo	Lapasuo	Lapasuo	Lapasuo	Lapasuo	Lapasuo	Palovaara	Palovaara	Palovaara	Palovaara
[%]												
SiO_2	77.63	70.87	78.66	81.1	76.71	73.46	65.56	67.75	69.45	66.59	68.99	49.26
TiO_2	0.17	0.47	0.2	0.13	0.2	0.27	0.55	0.61	0.41	0.48	0.45	1.11
Al_2O_3	13.69	16.15	12.31	11.34	12.25	15.75	14.98	15.89	16.02	16.19	14.51	15.01
Fe_2O_3	1.26	2.97	0.57	0.59	0.78	0.86	4.91	7.37	3.42	4.25	3.72	13.6
MnO	0.01	0.03	<0.01	<0.01	0.02	<0.01	0.09	0.11	0.03	0.09	0.06	0.25
MgO	0.64	0.86	0.43	0.44	0.57	0.41	1.75	1.86	1.29	2.19	1.25	7.07
CaO	0.42	1.14	0.75	0.26	1.42	0.83	4.02	3.11	2.84	2.06	3.35	11.13
Na_2O	0.75	0.53	1.67	0.57	1.92	2.46	4.48	1.97	3.67	2.51	3.68	1.48
K_2O	4.59	4.72	3.03	3.82	3.15	3.82	0.76	1.45	2.22	3.63	1.57	0.42
BaO	0.04	0.09	0.06	0.09	0.05	0.08	0.04	0.03	0.06	0.06	0.03	<0.01
P_2O_5	0.01	0.11	0.02	0.02	0.02	0.04	0.17	0.13	0.09	0.11	0.11	0.09
Cr_2O_3	<0.01	<0.01	<0.01	<0.01	<0.01	<0.01	<0.01	<0.01	<0.01	<0.01	<0.01	0.03
SrO	<0.01	<0.01	<0.01	<0.01	0.01	<0.01	0.03	0.02	0.01	0.02	0.02	0.02
LOI	1.95	2.59	1.51	1.58	1.4	1.53	0.84	1.63	1.22	1.58	1.6	0.58
TC	0.07	0.09	0.03	0.01	0.13	0.04	0.02	0.05	0.03	<0.01	0.24	<0.01
TS	<0.01	<0.01	<0.01	<0.01	0.02	<0.01	<0.01	<0.01	<0.01	0.05	<0.01	0.05
Total	101.16	100.53	99.21	99.94	98.51	99.51	98.19	101.93	100.74	99.76	99.34	100.05
[ppm]												
Ba	400.9	850.9	584.8	837.4	460.6	736.5	345.3	260.8	555.7	551.9	267.6	47.6
Sr	43.4	57.6	75.7	28.9	87	69.9	231	161.3	106.2	141.4	148.2	130.4
Rb	117	149.7	97.3	122.3	109.1	118.5	21.4	37.7	56.3	90.8	42.6	6.5
Cs	1.72	3.27	1.13	1.36	1.67	1.63	0.54	1.23	2.24	1.55	1.19	0.3
Ga	18.1	19.1	15.9	15.2	17.3	23.2	14.8	19.8	18.3	19	16.3	17.5
Y	21.9	10.5	18.7	20.3	17.8	23.5	20.8	27.2	8.3	9.3	7.7	21.4
Zr	186	180	160	143	136	185	133	177	118	121	111	56
Hf	5.8	5	4.8	4.4	4.3	6	3.8	5.3	3.3	3.3	3	1.7
V	<10	48	12	<10	<10	17	78	43	46	62	51	337
Hg	<0.005	<0.005	<0.005	<0.005	<0.005	<0.005	<0.005	<0.005	<0.005	<0.005	<0.005	<0.005
Cr	<10	12	<10	<10	<10	<10	44	16	<10	20	20	230
Ni	1	4.1	1.6	1.7	0.8	0.9	20	9.8	9.9	16.4	9.4	96.3
Cu	7.1	7.5	0.9	0.8	6.7	3	19.7	2.4	2.9	34.4	9.2	111.6
Zn	47	45	17	19	74	14	45	38	13	86	54	97
As	0.3	0.2	0.4	0.2	0.7	0.3	0.8	0.6	0.5	0.5	0.5	0.3
Se	<0.2	<0.2	<0.2	<0.2	<0.2	<0.2	<0.2	<0.2	<0.2	<0.2	<0.2	0.2
Mo	1.24	1.55	1.74	2.49	1.41	1.35	1.45	1.6	1.74	1.9	1.38	0.87
Ag	0.12	0.06	0.07	0.08	0.12	0.11	0.06	0.09	0.05	0.15	0.1	0.16
Cd	<0.02	0.02	<0.02	<0.02	0.19	<0.02	0.06	0.05	0.03	<0.02	0.02	0.16
Sn	<5	<5	<5	<5	<5	<5	<5	<5	<5	<5	<5	33
Sb	<0.05	<0.05	<0.05	<0.05	<0.05	<0.05	<0.05	<0.05	<0.05	<0.05	<0.05	<0.05
W	2	2	2	2	2	2	1	<1	1	1	<1	<1
Pb	21.8	8	7.9	10.5	14.4	8.1	6.9	7.2	4.1	4.6	4.9	4.9
Bi	0.64	0.11	0.05	0.08	0.09	0.12	0.13	0.44	0.14	0.08	0.07	0.05
Au	0.0006	0.0006	<0.0005	<0.0005	<0.0005	0.0006	0.0005	0.0015	0.0005	<0.0005	0.0007	0.0081
Tl	0.08	0.23	0.02	0.03	0.05	<0.02	0.09	0.1	0.22	0.38	0.16	0.03
Nb	8.2	6.5	6.6	6.8	6.6	8.9	6	8	3.8	4.2	3.9	3.8
U	1.71	1.08	3.24	1.73	1.8	2.33	1.75	1.46	0.62	0.85	0.58	0.14
Th	5.76	3.64	5.76	4.48	6.04	9.57	5.16	4.27	2.85	2.38	2.05	0.92
Ta	1.1	1	1.1	1	1.1	1.2	0.9	1.1	0.9	0.9	0.9	0.8
REE [ppm]												
La	5	4.3	10.8	4.4	13.5	6.5	22.9	14.8	14.9	18.4	12.7	3.9
Ce	19.1	9	33.6	9	30.3	19.5	51.1	33.2	27.8	33.3	24.2	9.9
Pr	1.48	1.07	2.81	0.89	3.33	1.56	5.61	3.68	3.18	3.84	2.79	1.53
Nd	5.7	4.1	11.1	3.4	12.9	5.8	20.7	14.9	11.8	14.8	10.6	7.9
Sm	1.76	1.03	2.94	0.98	2.95	1.81	3.59	3.68	2.27	2.69	2.09	2.47
Eu	0.38	0.35	0.58	0.31	0.78	0.6	0.95	1.05	0.62	0.89	0.64	0.93
Gd	2.09	1	2.78	1.41	2.84	2.63	3.37	3.99	1.74	2.24	1.81	2.9
Tb	0.45	0.19	0.53	0.38	0.48	0.6	0.53	0.71	0.26	0.31	0.25	0.54
Dy	3.51	1.58	3.82	3.13	3.17	4.39	3.35	4.86	1.55	1.75	1.47	3.7
Ho	0.79	0.38	0.79	0.74	0.66	0.92	0.72	1.03	0.29	0.32	0.28	0.82
Er	2.58	1.31	2.27	2.31	1.96	2.75	2.16	3.01	0.85	0.89	0.78	2.41
Tm	0.39	0.21	0.35	0.35	0.32	0.41	0.29	0.45	0.12	0.12	0.1	0.36
Yb	2.64	1.45	2.17	2.4	1.95	2.83	1.91	2.97	0.84	0.77	0.67	2.3
Lu	0.42	0.24	0.33	0.37	0.31	0.43	0.33	0.46	0.13	0.13	0.11	0.34

Sample	AC-53	AC-54	AC-55	AC-56	AC-57	AC-58	AC-59	AC-60	AC-61	AC-62	AC-63	AC-64	AC-65
Profile	Palovaara	Palovaara	Palovaara	Palovaara	Palovaara	Katajasuo	Katajasuo	Koraminvaara	Koivumäki	Katajasuo	Mine	Mine	Mine
[%]											[Hangingwall]	[Mineralization]	[Footwall]
SiO_2	67.99	68.64	65.52	69.56	70.8	81.01	80.75	66.59	70.12	67.88	72.61	68.73	72.94
TiO_2	0.45	0.43	0.47	0.4	0.48	0.31	0.31	0.89	0.52	0.41	0.17	0.18	0.24
Al_2O_3	15.83	15.84	17.16	14.9	16.83	14.52	14.7	25.16	17.53	13.95	14.23	9.45	13.5
Fe_2O_3	3.92	3.57	4.65	3.39	0.53	0.39	1.51	3.32	6.68	5.58	2.11	5.65	3.62
MnO	0.07	0.07	0.09	0.06	0.01	<0.01	0.02	0.14	0.18	0.13	0.05	0.94	0.11
MgO	2.14	2.48	2.62	1.83	1.58	0.03	0.29	0.24	1	2.77	1.33	3.81	1.36
CaO	3.97	1.72	3.53	3.67	3.43	0.06	0.03	0.43	0.27	3.17	0.39	2.68	0.1
Na_2O	2.73	1.65	3.6	1.89	1.57	0.7	0.06	<0.01	0.05	1.84	0.22	<0.01	<0.01
K_2O	1.84	3.72	2.21	1.81	2.52	0.57	0.67	0.37	1.09	1.01	3.97	4.29	4.76
BaO	0.03	0.06	0.05	0.01	0.05	<0.01	<0.01	<0.01	<0.01	<0.01	0.07	0.04	0.09
P_2O_5	0.12	0.1	0.11	0.08	0.09	0.01	0.05	0.4	0.13	0.09	0.04	0.02	0.04
Cr_2O_3	<0.01	<0.01	<0.01	<0.01	<0.01	<0.01	<0.01	0.01	<0.01	<0.01	<0.01	<0.01	<0.01
SrO	0.02	<0.01	0.03	0.01	0.02	<0.01	<0.01	<0.01	<0.01	<0.01	<0.01	<0.01	<0.01
LOI	1.09	1.87	0.94	0.95	1.96	1.58	1.6	1.6	2.39	1.94	3.15	3.37	2.2
TC	0.03	0.02	<0.01	<0.01	<0.01	0.02	0.03	0.03	0.02	0.04	0.02	0.71	0.02
TS	<0.01	<0.01	<0.01	<0.01	<0.01	<0.01	0.03	0.13	0.08	<0.01	0.92	0.05	0.45
Total	100.21	100.14	100.96	98.58	99.9	99.17	99.99	99.15	99.98	98.77	98.34	99.17	98.96
[ppm]													
Ba	278.9	517.2	429.6	130.1	475.5	37.5	59.7	38.1	87.3	62	667.4	399.1	816.9
Sr	140.6	71.7	202.8	87.8	176.5	45.2	16.8	9	16.8	76	13.6	31.3	17.1
Rb	48	113.8	70	63.5	64.9	9.5	15.2	8.3	27.2	39	133.4	161.7	106.8
Cs	1.68	2.66	1.71	2.08	1.44	0.2	0.3	0.18	0.45	1.39	2.67	3.88	1.59
Ga	18.3	18	18.9	16	19.3	17.3	19.6	21.3	18.8	15.5	20.1	15.2	18.4
Y	8.3	7.3	6.5	5.4	5.1	4.6	10.4	23.4	19.1	9.4	38.2	29.7	22.5
Zr	122	111	118	92	108	79	109	212	139	115	128	166	219
Hf	3.3	2.9	3.4	3	3.4	2.4	3	5.8	3.9	3.5	4.9	4.9	6.8
V	52	45	55	39	56	40	41	114	94	78	<10	<10	<10
Hg	<0.005	<0.005	<0.005	<0.005	<0.005	<0.005	<0.005	<0.005	<0.005	<0.005	0.005	<0.005	<0.005
Cr	24	13	19	12	12	24	30	82	34	34	<10	<10	<10
Ni	21	10	18.6	5.4	2.1	2.1	3.5	2.2	13.9	16	2.7	3.2	2.5
Cu	6.3	2.1	3.5	0.9	1.7	0.7	5	4.6	16.6	3.8	8	1.4	165.6
Zn	51	147	50	79	10	<2	14	15	49	68	57	479	223
As	0.5	0.3	0.5	0.3	0.5	0.3	0.7	5.8	0.7	0.4	16.8	3.5	8.6
Se	<0.2	<0.2	<0.2	<0.2	<0.2	<0.2	<0.2	<0.2	<0.2	<0.2	<0.2	<0.2	0.6
Mo	0.73	1.1	1.24	0.76	1.1	1.5	4.43	3.75	1.65	1.58	3.72	1.49	2.32
Ag	0.08	0.04	0.05	0.07	0.04	0.03	0.25	0.14	0.21	0.07	0.33	5.6	0.43
Cd	0.04	0.04	0.04	0.07	0.02	<0.02	<0.02	<0.02	0.04	0.08	0.15	0.45	0.57
Sn	<5	<5	<5	<5	9	9	<5	<5	<5	<5	<5	<5	<5
Sb	<0.05	<0.05	<0.05	<0.05	<0.05	<0.05	<0.05	0.17	0.08	<0.05	0.26	3.59	0.3
W	<1	1	<1	<1	1	3	4	2	1	<1	2	1	3
Pb	8.6	34.9	5	17.3	8.3	11	5.4	4	9.5	11	12.9	131	43.6
Bi	0.05	0.03	0.03	0.04	0.03	0.01	0.14	0.53	0.04	0.02	0.03	0.02	0.06
Au	0.0007	<0.0005	0.0007	<0.0005	<0.0005	<0.0005	0.001	0.0018	0.0012	<0.0005	0.0014	0.011	0.0216
Tl	0.24	0.52	0.39	0.41	0.14	<0.02	0.02	0.03	0.03	0.08	0.27	1.78	0.38
Nb	4.7	2.9	4.4	3.8	4.3	1.6	3.2	9.3	4.9	3.7	9	7.2	8.9
U	0.9	0.87	0.58	0.62	0.84	0.63	1.32	1.97	0.88	0.73	3.96	2.01	2.89
Th	2.03	2.06	2.08	1.84	2.36	1.15	1.89	4.24	2.78	1.98	13.11	5.66	7.06
Ta	0.8	0.8	0.9	0.9	0.8	0.8	0.9	1.1	1	1.1	1.2	1.2	1.2
REE [ppm]													
La	14.4	10.8	12.6	9.8	15.1	8.9	16.8	47.7	13.5	10.3	31.7	26.3	33.2
Ce	27.4	20.6	30.3	19.8	30.7	17.3	29.9	104.7	28.3	22	66.9	52.9	67.9
Pr	3.3	2.17	2.85	1.93	2.98	2.04	3.26	12.75	3.36	2.59	7.96	6.18	7.89
Nd	12.5	7.8	10.4	7.1	10.9	7.8	11.9	48.9	12.7	9.8	29.9	23.6	30.4
Sm	2.25	1.55	1.89	1.25	1.92	1.39	2.21	7.55	2.69	2	6.21	4.69	5.78
Eu	0.7	0.58	0.59	0.47	0.63	0.5	0.63	2.05	0.79	0.67	0.7	0.84	0.93
Gd	1.9	1.44	1.54	1.07	1.51	1.1	2.01	6.05	3.01	1.71	5.95	4.67	5.05
Tb	0.26	0.23	0.23	0.15	0.22	0.14	0.31	0.82	0.53	0.28	1	0.78	0.75
Dy	1.63	1.36	1.38	0.93	1.12	0.81	1.94	4.67	3.03	1.73	6.57	4.89	4.44
Ho	0.31	0.26	0.26	0.19	0.21	0.16	0.37	0.87	0.74	0.36	1.35	0.98	0.89
Er	0.92	0.77	0.8	0.62	0.57	0.5	1.07	2.44	2.22	1.07	4.1	2.88	2.73
Tm	0.12	0.13	0.13	0.08	0.09	0.07	0.14	0.34	0.31	0.17	0.6	0.4	0.4
Yb	0.88	0.7	0.86	0.65	0.56	0.53	1	2.29	2.07	1.21	3.83	2.54	2.78
Lu	0.14	0.1	0.13	0.1	0.08	0.08	0.16	0.35	0.31	0.17	0.56	0.38	0.45

Appendix 2. Sample locations

Koraminvaara – South Jäkäläsuo – Mine

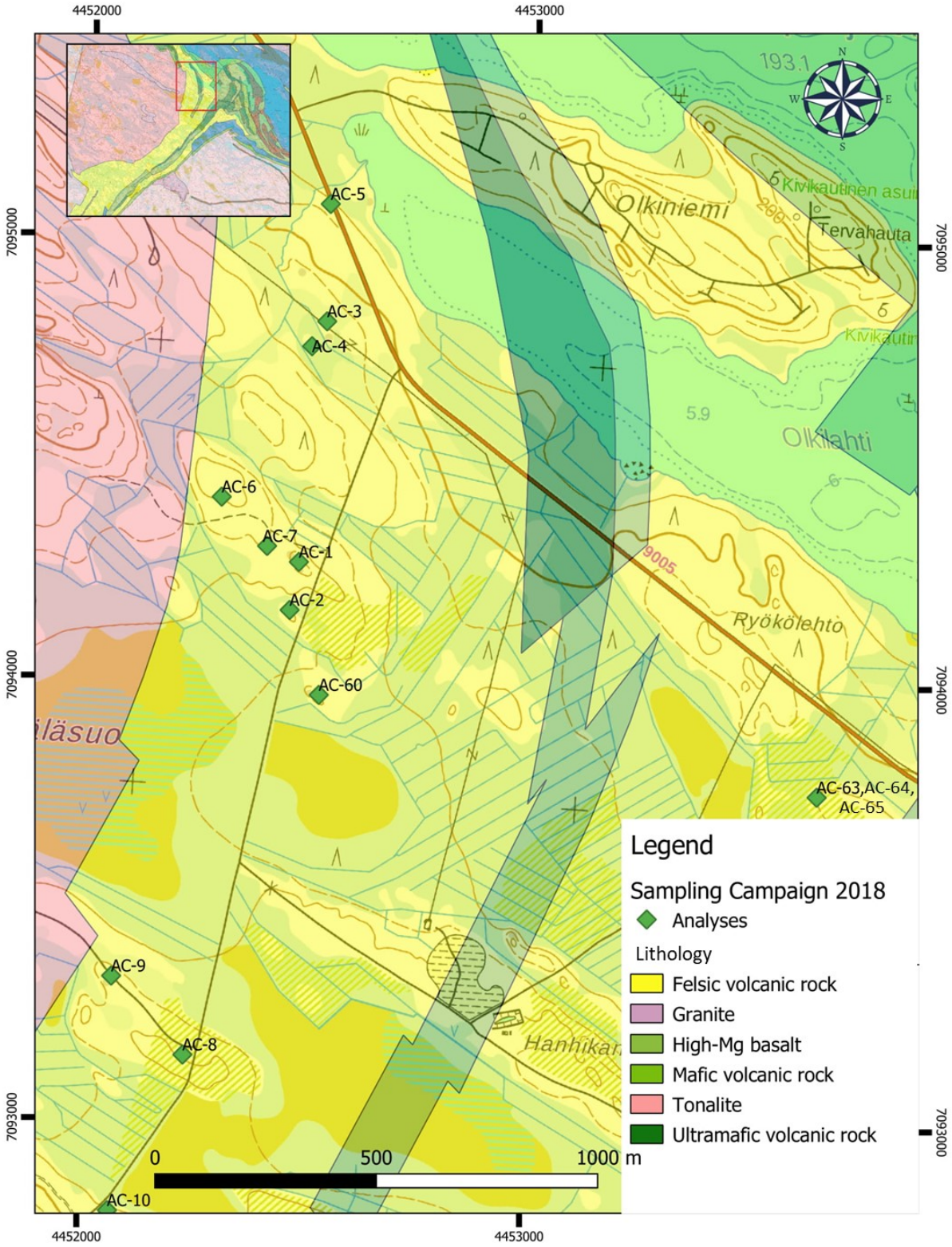

Koivumäki – Katajasuo

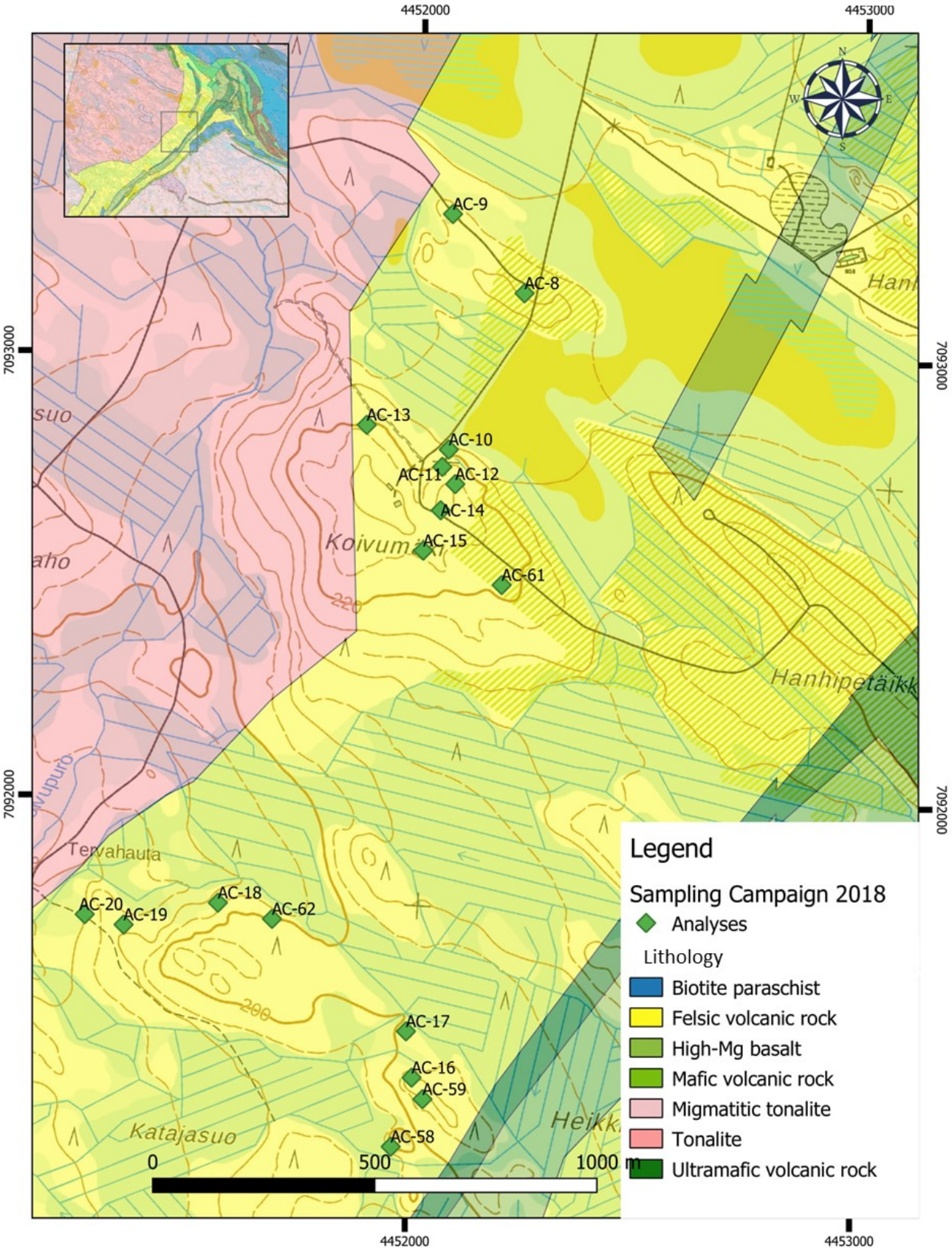

Kivisuo-Talassuo

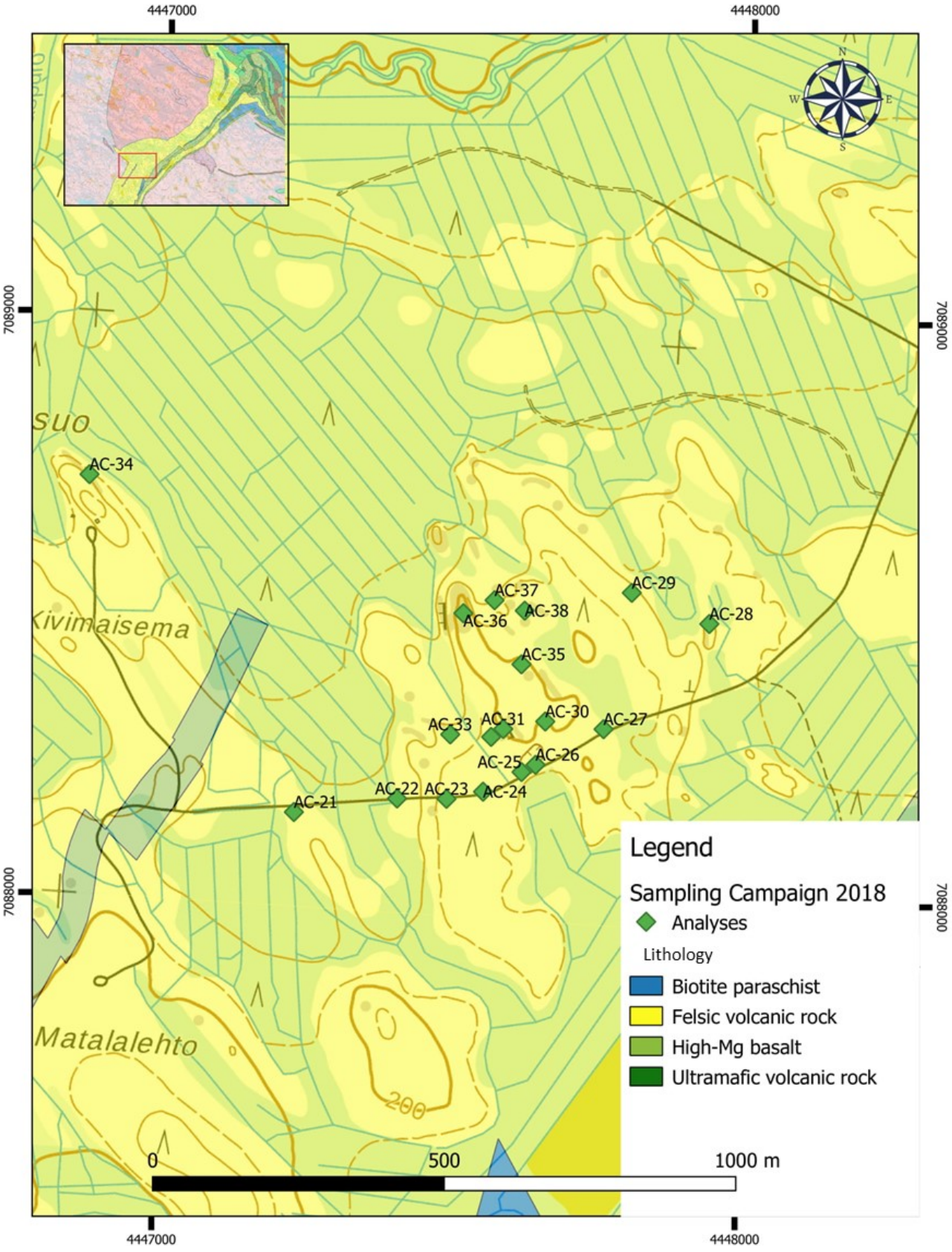

Lapasuo

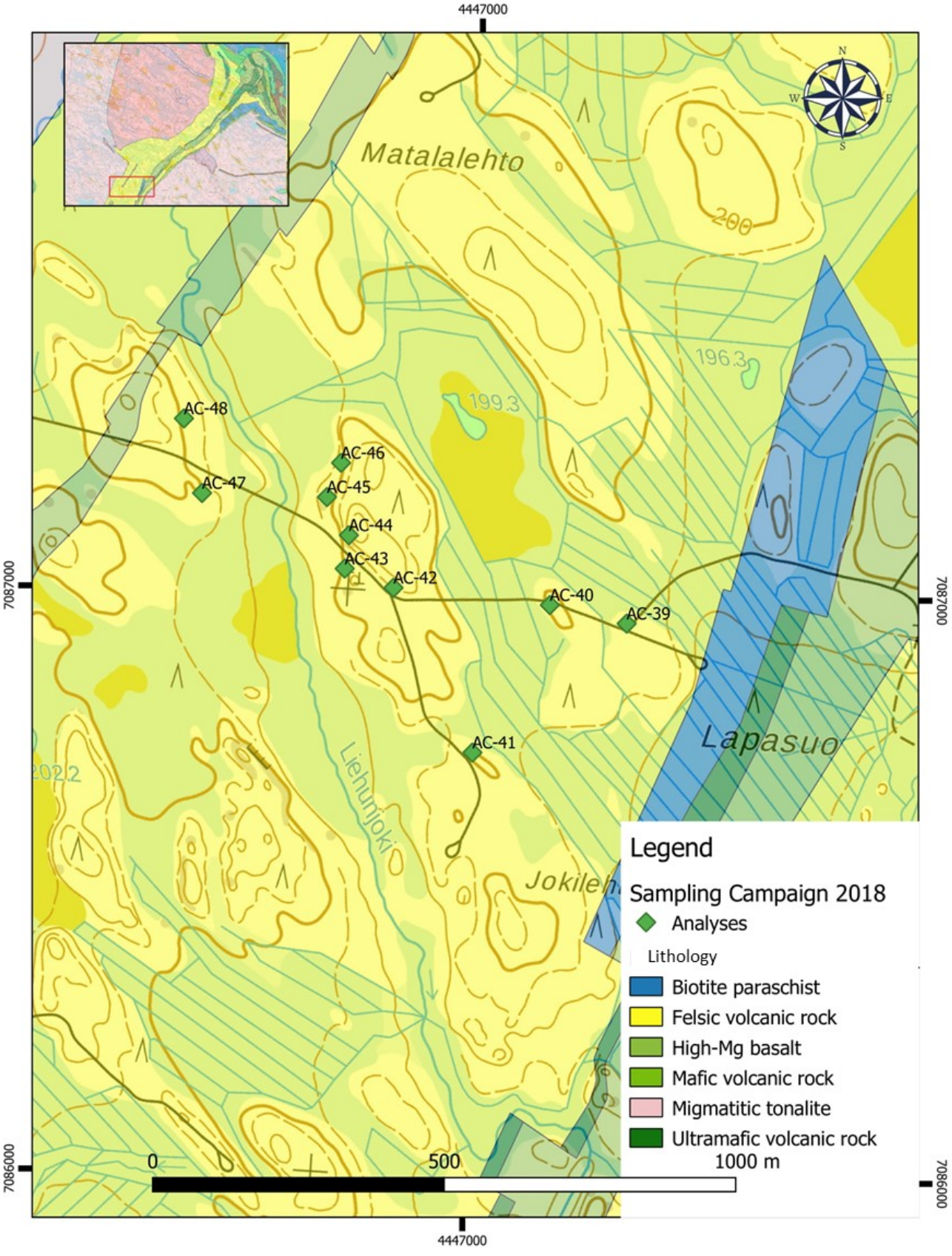
4447000
Matalalehto
200
196.3
199.3
AC-48
AC-47
AC-46
AC-45
AC-44
AC-43
AC-42
AC-40
AC-39
AC-41
Lapasuo
Liehunjoki
Jokileh
202.2
7087000
7086000
0
500
1000 m
Legend
Sampling Campaign 2018
Analyses
Lithology
Biotite paraschist
Felsic volcanic rock
High-Mg basalt
Mafic volcanic rock
Migmatitic tonalite
Ultramafic volcanic rock

Palovaara

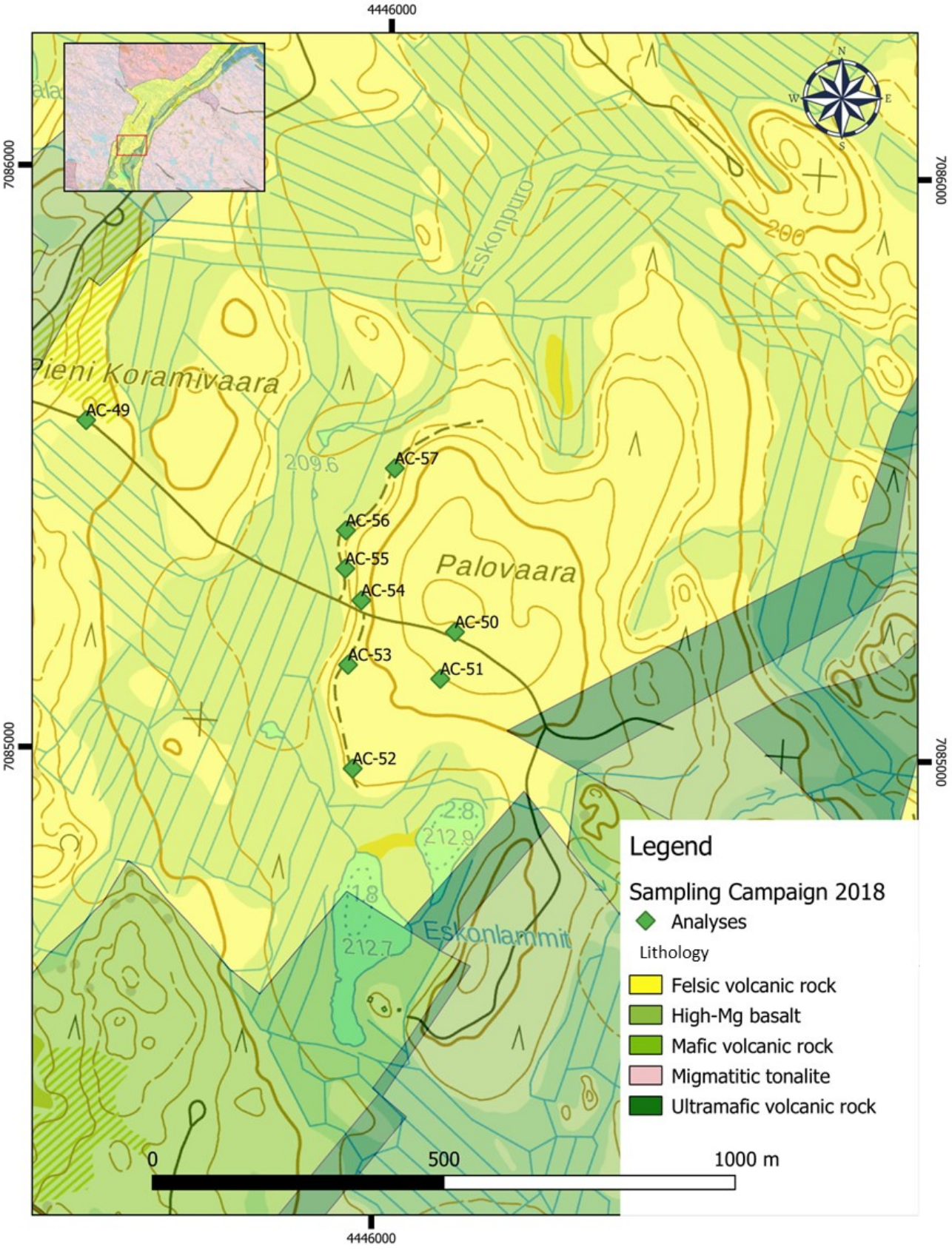
4446000
7086000
7085000
Pieni Koramivaara
Eskonpuro
Palovaara
Eskonlammit
AC-49
AC-57
AC-56
AC-55
AC-54
AC-50
AC-53
AC-51
AC-52
209.6
212.9
212.7
200
N
W
E
S
Legend
Sampling Campaign 2018
Analyses
Lithology
Felsic volcanic rock
High-Mg basalt
Mafic volcanic rock
Migmatitic tonalite
Ultramafic volcanic rock
0
500
1000 m